Lappeenranta
University of Technology

Jaakko Ylätalo

MODEL BASED ANALYSIS OF THE POST-COMBUSTION CALCIUM LOOPING PROCESS FOR CARBON DIOXIDE CAPTURE

Thesis for the degree of Doctor of Science (Technology) to be presented with due permission for public examination and criticism in the Auditorium 1382 at Lappeenranta University of Technology, Lappeenranta, Finland on the 9th of December, 2013, at noon.

Acta Universitatis
Lappeenrantaensis 552

Supervisors Professor Timo Hyppänen
Department of Energy Technology
Faculty of Technology
Lappeenranta University of Technology
Finland

D.Sc. (Tech.) Tero Tynjälä
Department of Energy Technology
Faculty of Technology
Lappeenranta University of Technology
Finland

Reviewers D.Sc. (Tech.) Edward J. Anthony
Reader in Energy
Cranfield University
United Kingdom

Professor Ron Zevenhoven
Department of Chemical Engineering
Thermal and Flow Engineering Laboratory
Åbo Akademi University
Finland

Opponent D.Sc. (Tech.) Edward J. Anthony
Reader in Energy
Cranfield University
United Kingdom

ISBN 978-952-265-520-2
ISBN 978-952-265-521-9 (PDF)
ISSN-L 1456-4491
ISSN 1456-4491
Lappeenrannan teknillinen yliopisto
Yliopistopaino 2013

Abstract

Jaakko Ylätalo
Model based analysis of the post-combustion calcium looping process for carbon dioxide capture
Lappeenranta 2013
106 pages
Acta Universitatis Lappeenrantaensis 552
Diss. Lappeenranta University of Technology
ISBN 978-952-265-520-2, ISBN 978-952-265-521-9 (PDF), ISSN 1456-4491

This thesis presents a one-dimensional, semi-empirical dynamic model for the simulation and analysis of a calcium looping process for post-combustion CO_2 capture.

Reduction of greenhouse emissions from fossil fuel power production requires rapid actions including the development of efficient carbon capture and sequestration technologies. The development of new carbon capture technologies can be expedited by using modelling tools. Techno-economical evaluation of new capture processes can be done quickly and cost-effectively with computational models before building expensive pilot plants.

Post-combustion calcium looping is a developing carbon capture process which utilizes fluidized bed technology with lime as a sorbent. The main objective of this work was to analyse the technological feasibility of the calcium looping process at different scales with a computational model. A one-dimensional dynamic model was applied to the calcium looping process, simulating the behaviour of the interconnected circulating fluidized bed reactors. The model incorporates fundamental mass and energy balance solvers to semi-empirical models describing solid behaviour in a circulating fluidized bed and chemical reactions occurring in the calcium loop. In addition, fluidized bed combustion, heat transfer and core-wall layer effects were modelled.

The calcium looping model framework was successfully applied to a 30 kW_{th} laboratory scale and a pilot scale unit 1.7 MW_{th} and used to design a conceptual 250 MW_{th} industrial scale unit. Valuable information was gathered from the behaviour of a small scale laboratory device. In addition, the interconnected behaviour of pilot plant reactors and the effect of solid fluidization on the thermal and carbon dioxide balances of the system were analysed. The scale-up study provided practical information on the thermal design of an industrial sized unit, selection of particle size and operability in different load scenarios.

Keywords: calcium looping process, modelling, CCS, dynamic, circulating fluidized bed, limestone
UDC 662.96:661.97:552.46:51.001.57

Acknowledgements

This work was carried out in the Department of Energy Technology at Lappeenranta University of Technology, Finland, between 2010 and 2013. The research leading to these results has received funding from the European Community's Seventh Framework Programme (FP7/2007-2013) under GA 241302 "CaOling Project" and from the Carbon Capture and Storage Programme (2011–2015), financed by the Finnish Funding Agency for Technology and Innovation (Tekes) and coordinated by the Finnish Cluster for Energy and Environment (CLEEN Ltd.).

Firstly, I would like express my gratitude to my supervisors Professor Timo Hyppänen and D.Sc. Tero Tynjälä for the guidance and support they provided during this work.

My reviewers D.Sc. Ben Anthony and Professor Ron Zevenhoven I would like thank for the highly valuable and constructive comments that improved the quality of the work significantly.

Several people at LUT and INCAR-CSIC, Spain, deserve acknowledgment due to contribution to this work. D.Sc. Jouni Ritvanen acted as technical support on many occasions, solving many problems of the model. Mr Jarno Parkkinen and Mr Petteri Peltola did parallel research on calcium looping and chemical looping which gave valuable support to my studies. Previous work of D.Sc. Kari Myöhänen was very helpful in the creation of the model framework. D.Sc. Carlos Abanades and D.Sc. Borja Arias provided practical experience and valuable insight on the experimental side of process.

I would also like to thank my colleagues Mr Markku Nikku, Mr Jussi Saari and Mr Lauri Pyy for the constructive discussions during the making of this thesis. Without the discussions, I would have given up a long time ago.

Finally I would like thank my family for their support, especially my dad who encouraged me to continue on this path despite personal doubts.

Jaakko Ylätalo
December 2013
Lappeenranta, Finland

Contents

List of publications supporting the present monograph

The present monograph contains both unpublished material and material which has been published previously by the author elsewhere. A large part of the present monograph is related to the following papers. The rights have been granted by publishers to include the material in the thesis. Jaakko Ylätalo is the principal author and investigator in all of the mentioned papers responsible of the development and application of the model which is the subject of this thesis.

Scientific journal articles

I. Ylätalo, J., Ritvanen, J., Arias, B., Tynjälä, T. and Hyppänen, T. (2012). 1-Dimensional modelling and simulation of the calcium looping process. *International Journal of Greenhouse Gas Control*, 9, pp. 130-135.

The general model framework and balance equations presented in Chapters 3.1, 3.2 and 3.3 are discussed in this article. Chapter 4 is also based on this publication. Borja Arias from INCAR-CSIC, Spain, provided the experimental data for the comparison and analysis of the 30 kW unit.

II. Ylätalo, J., Parkkinen, J., Ritvanen, J., Tynjälä, T. and Hyppänen, T. (2013). Modeling of the oxy-combustion calciner in the post-combustion calcium looping process. *Fuel*, 113, pp. 770-779.

The combustion model in Chapter 3.5.3 and the development done for the calciner model are presented in this publication. Significant results from the publication are presented in Chapter 5. Jarno Parkkinen provided the 3D calciner results applying the model presented by Myöhänen et al. (2011).

III. Ylätalo, J., Ritvanen, J., Tynjälä, T. and Hyppänen, T. (2014). Model based scale-up study of the calcium looping process. *Fuel*, 115, pp. 329-337.

Chapter 6 is based on the results presented in this scientific publication. The most current model framework is discussed in the publication with sulphation modelling and material fraction calculation.

Refereed conference articles

IV. Ylätalo, J., Ritvanen, J., Tynjälä, T. and Hyppänen, T. (2011). Modelling and simulation of the carbonate looping process. *2nd Oxyfuel Combustion Conference, 12.-16.9, Yeppoon, Australia*.

The model framework was first introduced in this peer-reviewed extended abstract.

Nomenclature

In the present work, variables and constants are denoted using *slanted style*, vectors are denoted using **bold regular style**, and abbreviations are denoted using regular style.

Latin alphabet

A	area	m^2
a	decay coefficient for splash zone	1/m
b	experimental coefficient	–
C	molar concentration	$kmol/m^3$
C_D	drag coefficient	–
c_p	specific heat capacity at constant pressure	J/(kgK)
D	diameter in structures	m
D_s	dispersion coefficient	m^2/s
d	particle diameter	m
E	energy	J
f	carrying capacity decay coefficient	–
g	gravitational acceleration constant	m/s^2
H	height	m
h	specific enthalpy	J/kg
K	decay coefficient for transport zone	1/m
k	kinetic coeffcient	$m^3/(kmol\ s)$
L	length	m
M	molar mass	kg/kmol
m	mass	kg
N	number of control volumes	–
n	reaction order	–
P	perimeter	m
p	pressure	Pa
Q_i	reaction enthalpy, heating value	J/kg
q	energy flow rate	J/s
q_m	mass flow rate	kg/s
R	ideal gas constant	J/(mol K)
r	reaction rate	kg/s
T	relative temperature	°C
T^*	absolute temperature	K
t	time	s
$\mathbf{U}$	input vector	–
U	internal energy	J
u	specific internal energy	J/kg
V	volume	m^3
v	velocity magnitude	m/s
W	weight fraction (in solids)	kg/kg
w	weight fraction (in gases)	kg/kg

X	state vector	–
X_r	residual acitivity	–
x	x-coordinate (width)	m
Y	result vector	–
z	z-coordinate (height)	m

Greek alphabet

α	heat transfer coefficient	$W/(m^2K)$
γ	recirculation factor	–
ε	slip coefficient of solids	–
η	core-wall solid flow parameter	–
κ	net mass transfer coefficient	m/s
λ	heat conductivity	W/(mK)
ρ	density	kg/m^3
τ	time constant	s
φ	char-gas contact coefficient	–

Dimensionless numbers

Re	Reynolds number

Superscripts

+	upward flow
″	flux
-	downward flow
0	initial time step

Subscripts

ave	average
c	core
calc	calcination
carb	carbonation
chem	chemical
conv	convectice
daf	dry, ash-free
disp	dispersion
eff	effective
eq	equilibrium
g	gas
ht	heat transfer
i	control volume element index
in	flow in
j	gas fraction index

k	solid fraction index
m	refractory slice index
max	maximum
min	minimum
mp	middle point
out	flow out
p	particle
plainw	plain wall
pn	pneumatic
qms	solid mass flow
ref	refractory
s	solid
s2wl	solid flow to wall layer
sh	super heater/separate heat transfer surface
sulp	sulphation
t	terminal
tot	total
wl	wall layer

Abbreviations

0D	zero dimensional, process scheme
1D	one dimensional
3D	three dimensional
ASU	air separation unit
BFB	bubbling fluidized bed
CCS	carbon capture and sequestration
CFB	circulating fluidized bed
CLC	chemical looping combustion
CV	control volume
IGCC	integrated gasifier combined cycle

1 Introduction

The effects of increasing concentrations of CO_2 in the atmosphere are a growing concern globally. Rapidly developing climate change could have drastic effects on farming areas, population growth and techno-economic development of societies. Governments and scientific entities have agreed globally that anthropogenic greenhouse gas emissions play a key role in the climate change and those emissions should be reduced in the following decades to alleviate the damage done to the planet's biosphere. Power generation is one of the main contributors in global CO_2 emissions, due to the high dependence on fossil fuels. Limiting emissions from power production has also been acknowledged as one of the most efficient and fastest ways to cut down emissions in the current time frame compared, for example, to population control or deliberate slowing economic growth (Metz et al., 2005). Several ways to cut CO_2 emissions in power production have been identified including improved power production efficiency, new methods of power production like fusion, carbon free energy sources like renewables, nuclear power or CO_2 capture from fossil fuels. Currently, all the mitigation methods are being developed simultaneously, each of them having their own advantages and disadvantages.

Carbon capture and sequestration (CCS) means capturing carbon dioxide from fossil fuel combustion directly or indirectly and storing it in the lithosphere or under the ocean floor. The interest towards CCS has increased during previous decades due to the high dependency on fossil fuels in the current power production scheme and the possibility of high emission reductions in a short time frame. However, CCS has several obstacles mainly associated with the power production efficiency penalty and the stability of CO_2 in geological storages. Efforts to overcome these uncertainties have been taken by scientific and corporate entities. Several methods of capturing CO_2 from power production units are being developed simultaneously, each of them having advantages, but the penalty associated with capture seems to be still quite high. A wide industrial CCS is still waiting for corporate motivation which depends on several factors like CO_2 emission trading, legislation and economic penalties.

CCS methods can be crudely divided into pre-combustion capture, oxy-fuel combustion and post-combustion capture. Pre-combustion capture includes methods attempting to refine hydrocarbon fuels into low carbon gaseous fuels before combustion. Integrated gasification combined cycle (IGCC) is a good example of this method refining solid fuel for gas turbine use. Oxy-combustion is a self-explanatory method of CCS, using an atmosphere of recirculated flue gases and oxygen separated from air to combust fossil fuels creating a CO_2 rich flue gas flow suitable for transportation and storage. Post-combustion methods have a lot of variation ranging from chemical treatment of flue gases in amine solutions to mineral sequestration which means storing CO_2 through chemical reactions permanently to abundant minerals. The technical challenges have led to second generation capture technologies utilizing the benefits of existing technologies. Solid looping technologies like calcium looping and chemical looping combustion (CLC) have been in the forefront of the second generation CCS techniques. Calcium

looping is a post-combustion capture technology which attempts to decrease the penalty associated with oxygen production in conventional oxy-combustion. Calcium looping uses two fluidized bed reactors to capture CO_2 from flue gases with lime. In calcium looping the penalties associated with oxy-combustion are smaller because the air separation unit (ASU) is much smaller and the material flows can be integrated with other industries like cement manufacturing.

Novel technologies, although heavily relying on well-known technologies like fluidized bed combustion, pose significant financial risks for power producers struggling with economic uncertainty. This is why a significant research and development effort has to be made before techniques like calcium looping can be utilized in industrial scale. Computational modelling is nowadays a valuable tool in research and development projects. Modelling offers a safe and fairly reliable way to evaluate the operation of novel technical processes. Computational power and resources have increased the possibility of using more complex models which has increased the usability and applicability of the models. The need for constructing costly prototypes has decreased which in terms accelerates the introduction of the technology.

The objective of this thesis is to apply a computational modelling approach to the calcium looping process and to study it at different scales, leading to the most important question whether the technique is feasible at the industrial scale. The modelling approach selected for the task is a 1D dynamic model, incorporating a simple spatial and time discretization. The model framework includes two interconnected reactor models and simple models for the solid return system. Reactor models solve mass and energy balances for solids and gases inside the reactor. Additionally, several submodels have been included in the model in order to describe two-phase flow phenomena and chemical reactions in the system. The model framework combines fundamental continuum equations with semi-empirical models to achieve a compromise between calculation times and the usability of the model compared to accuracy.

The structure of the thesis is the following: Chapter 2 Calcium looping process describes the basics and all the variations and features of the process. In addition, the modelling work done in the field earlier is briefly reviewed. Chapter 3 introduces the model frame and calculation principles. Chapter 4-6 explain the significant results produced during the development of the model and analysis of different modelling cases. A small scale laboratory calcium looping unit is modelled and analysed in Chapter 4. Chapter 5 reports a modelling case studying a pilot scale calciner and the interconnected behaviour of the pilot plant. Chapter 6 presents an attempt to scale-up an industrial calcium looping unit and an analysis of the plant behaviour in different load scenarios. The significant contribution of this work is the application of a multiphysical model framework to a novel CCS technology. Several findings were made during the process studies regarding the behaviour of the interconnected reactor system, including the effect of solid circulation on the capture efficiency and loop energy balance, the behaviour of a pilot plant and issues relating to the calcium looping process scale-up.

2 Calcium looping process

2.1 Concept of the calcium looping process

The ability of calcium oxide to capture and release carbon dioxide has been known for almost two centuries now and utilized in cement manufacturing and chemical processes (du Motay and Maréchal, 1868). However, the concept of using lime to capture CO_2 in a CCS system was only developed during recent decades as a consequence of the increasing need for more efficient capture technologies. Post-combustion calcium looping was first introduced by Shimizu et al. (1999). This technique can capture CO_2 and SO_2 from static sources by utilizing a twin fluidized bed system. Flue gas from a stationary source is processed in a fluidized bed reactor, known as the carbonator. The carbonator captures CO_2 and SO_2 from the flue gas to solid calcium oxide at around 650 ºC. This forms calcium carbonate and calcium sulphate, $CaCO_3$ and $CaSO_4$, which are then transferred to a fluidized bed regenerator, known as the calciner. The calciner regenerates the carbonate back to calcium oxide at around 950 ºC. The regenerated calcium oxide is returned to the carbonator where it resumes capturing CO_2 from the flue gases. The formed calcium sulphate is stable in the loop and will accumulate to the system unless fresh calcium carbonate is fed to the system and the used sorbent is removed at a steady rate. The temperature difference between the reactors can be achieved by many means, burning suitable fuels in the calciner in an atmosphere of oxygen and recirculation gas or from external heat sources. This forms a highly concentrated CO_2 gas flow which can be compressed and transported to a storage site after steam and oxygen removal. As a result of solid fuel combustion, ash accumulates in the system which increases the need of solid purging from the loop. The general layout of the calcium loop is presented in Figure 2.1.

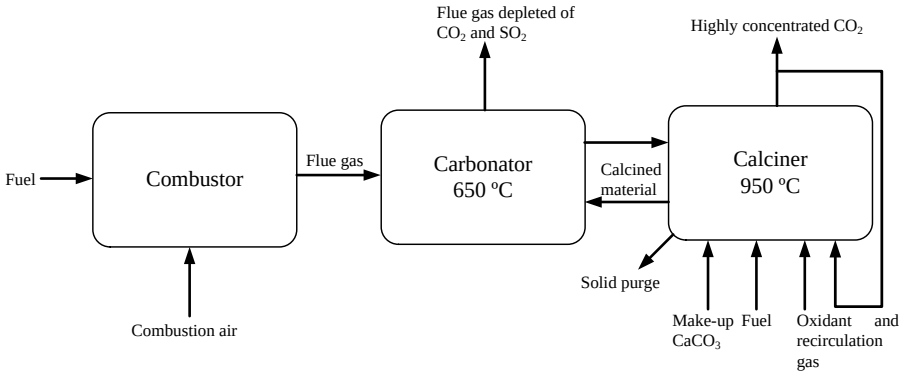

Figure 2.1. General concept of the calcium looping process with the major flows of the system.

The motivation for the post-combustion calcium looping process to capture CO_2 from stationary sources is that it reduces the amount of pure oxygen consumed per produced power compared to the oxy-combustion process. The production of pure oxygen is one of the major expenses for capture units using oxy-combustion. The utilization of the heat from the high temperature the flue gas flows and the exothermic heat from carbonation reaction in a Rankine-cycle ensures that the calcium looping process produces an amount of thermal power that is almost equal to that of the original combustor. In an equivalent oxy-combustion scenario, producing equal power to the calcium loop would require an air separation unit, ASU, double the size of the calcium looping unit ASU (Abanades et al., 2007). Of course the additional limestone flows and construction costs of the calcium loop increase the overall costs of the system, and therefore the overall economic viability is not excessively better than that of an equivalent oxy-combustion unit. The basic calcium looping process is most efficient when retrofitted to an existing plant.

2.1.1 **Carbonator**

The carbonator reactor captures carbon dioxide in fluidized bed of calcium oxide. Shimizu et al. (1999) proposed that a fluidized bed reactor is an effective solution for the calcium looping carbonator because of the ability to handle large amounts of solids and a good gas-solid contact. In addition to that, a fluidized bed reactor configuration secures large enough solid fluxes needed for transporting active calcium oxide between reactors. In this thesis, both reactors, the carbonator and calciner, are assumed to be circulating fluidized bed (CFB) types. The carbonator is fluidized with the incoming flue gas and the gas and solid particles are separated in a cyclone after the reactor. The solids are then transferred along a standpipe to a loop seal. The purpose of this loop seal is to transport a sufficient amount of solids to the regenerator calciner and return the excess back to the carbonator. Figure 2.2 illustrates the general layout of the circulating fluidized bed carbonator.

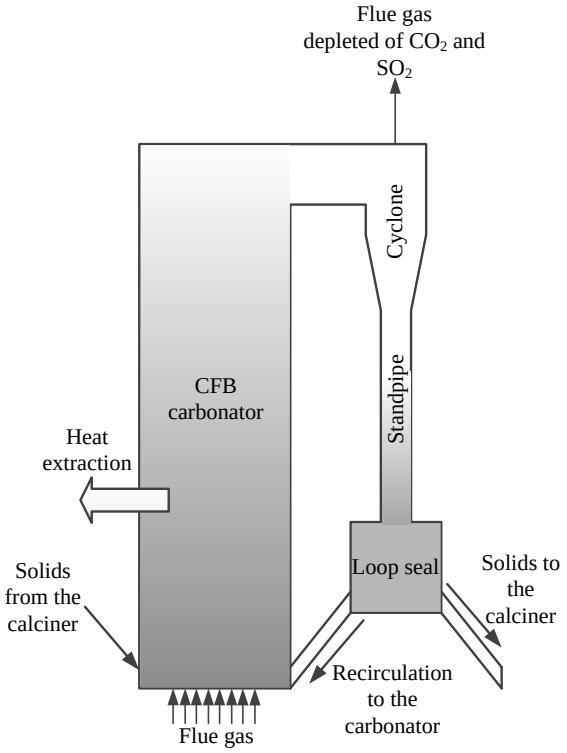

Figure 2.2. The layout of the CFB carbonator reactor.

The carbonation reaction is an exothermic, heterogeneous reaction

$$CaO\ (s) + CO_2\ (g) \leftrightarrow CaCO_3\ (s)\ \Delta H_0 = -178\ \text{kJ/mol} \tag{2.1}$$

The selection of the carbonator operation temperature has to be done as a compromise between the reaction equilibrium and reaction kinetics. Reaction kinetics favour high temperatures but the equilibrium limit of the carbonation reaction is above 750 ºC in CO_2 concentrations commonly found in combustion flue gases, 13-16 vol-% of carbon dioxide. The operation temperature of the carbonator has been selected to be around 650 ºC which means that 1 vol-% concentration of CO_2 is theoretically achievable by capture in the exiting flue gases. The equilibrium curve of the carbonation-calcination reaction has been plotted as a function of temperature in Figure 2.3 using the equation proposed by Silcox et al. (1989)

$$\frac{p_{\mathrm{eq,CO_2}}}{p_\infty} = 4.137 \cdot 10^7 e^{\frac{-20747}{T^*}} \tag{2.2}$$

where $p_{\mathrm{eq,CO2}}$ is the equilibrium partial pressure of carbon dioxide [Pa], p_∞ is atmospheric pressure and T^* represents the ambient absolute temperature [K].

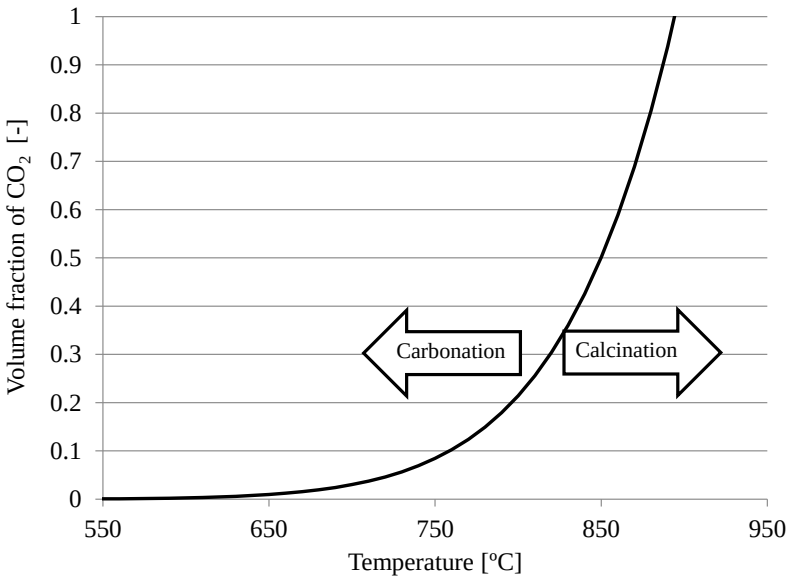

Figure 2.3. The equilibrium curve of carbonation-calcination according to Silcox et al. (1989).

The carbonator reactor has to be fitted with heat extraction because the exothermic reaction produces heat and the hot solids flowing from the calciner bring additional thermal energy to the reactor. The method of cooling the carbonator of large scale units is still under discussion because of the unconventional conditions compared to normal fluidized bed boilers. More analysis of this problem is presented in the results section of this thesis.

In addition to the CO_2 capture, the carbonator will desulphurize the flue gas if any sulphur dioxide remains. Experiments have shown that in the calcium looping process, sulphur capture is very good, above 95 % in normal operation conditions (Sánchez-Biezma et al., 2013). It is unclear what the dominant sulphur capture mechanism in the calcium looping process is but the majority of the material is calcium oxide which supports the indirect sulphation route

$$\begin{aligned} &CaO\ (s) + SO_2\ (g) + ½O_2\ (g) \rightarrow CaSO_4\ (s) \\ &\Delta H_0 = -502.1\ \text{kJ/mol} \end{aligned} \tag{2.3}$$

Direct sulphation is the reaction between calcium carbonate and sulphur dioxide. Direct sulphation could have a role in the calcium looping capture process but the relation of direct and indirect sulphation in calcium looping has not been studied yet.

$$\begin{aligned} &CaCO_3\ (s) + SO_2\ (g) + ½O_2\ (g) \rightarrow CaSO_4\ (s) + CO_2\ (g) \\ &\Delta H_0 = -323.8\ \text{kJ/mol} \end{aligned} \tag{2.4}$$

2.1.2 Calciner

The main purpose of the calciner reactor presented in Figure 2.4 is to regenerate the incoming $CaCO_3$ back to CaO and to generate highly concentrated CO_2 for compression and storage. The highly concentrated CO_2 in the calciner flue gas forces the operation temperature to be around 920–950 ºC in order to stay in the calcination side of the equilibrium curve (Figure 2.3). The high temperature is achieved with oxy-combustion. The calcium looping calciner can utilize various fuels because of the effective combustion in the fluidized bed reactor and the inherent SO_2 capture. Using biofuels could potentially give the system negative CO_2 emissions. To dilute the oxidant and fluidize the bed, flue gas is circulated from the back pass to the primary gas flow. The flue gas recirculation can be wet because of the low SO_2 concentration in the exiting flue gases. The circulating fluidized bed mode has also been chosen for the post-combustion capture calciner because of the good combustion performance and easy connectivity to the carbonator from the solid entrainment point of view. Using bubbling fluidized bed reactors is also a possibility for both the carbonator and the calciner but considering the scale-up and experimental experience, the dual-CFB system seems to be the prevailing technology for retrofitted post-combustion capture calcium looping units (Sánchez-Biezma et al., 2013; Ströhle, 2012). The huge flue gas flow that has to be put in contact with solids suggests that the dual-CFB system would be the most attracting option for the calcium looping process. The interconnection between to circulating fluidized bed reactors is easier to build than between reactors operating in different fluidization modes. The CO_2 flow out of the calciner reactor includes the captured CO_2 from the combustor flue gas, the CO_2 from the calcined make-up and the CO_2 generated from oxy-combustion of fuel.

The make-up flow fed to the calciner serves several purposes. The available reaction surface of the lime decreases with increasing carbonation-calcination cycles which is caused by a change in the porous structure of the lime. This phenomenon is further discussed in the following chapters. The make-up of fresh $CaCO_3$ maintains the average CO_2 carrying capacity of the solids by replacing old cycled material, reducing the need for solid circulation between reactors. Furthermore, the make-up flow serves as

replacement bed material, as the purge removes solids from the calciner bottom area. Without the combination of the purge and make-up, $CaSO_4$ and ash would enrich the bed and decrease the amount of active material circulating between the reactors reducing the efficiency of the system. Installing the purge to the calciner is also beneficial because solid fuels can accumulate ash to the calciner bed.

The calciner reactor itself should be insulated to maintain a sufficient temperature with the minimum fuel and oxygen flow. Heat can be extracted from the high temperature flue gases exiting the reactor.

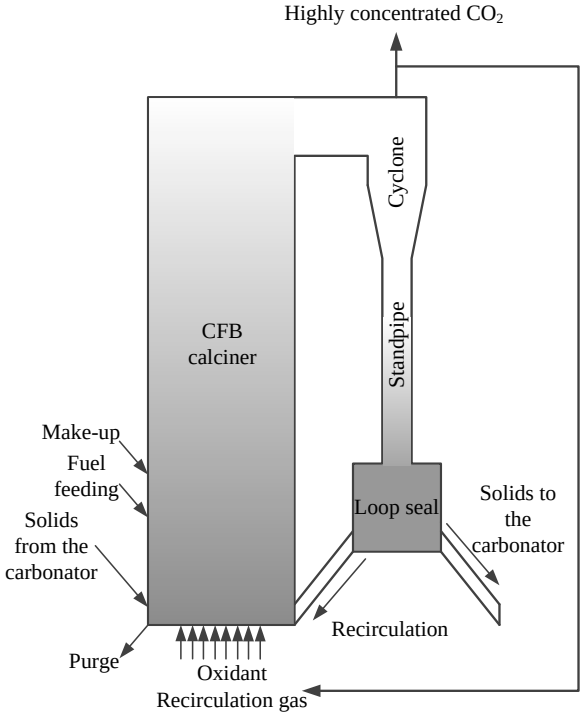

Figure 2.4. The general layout of the CFB calciner reactor.

2.2 Next generation calcium looping process concepts

Alongside the traditional post-combustion calcium looping process, several advanced concepts have emerged. The motivation behind these concepts is to further decrease the penalty caused by the CO_2 capture to the power plant efficiency. There are different options to reduce the penalties associated with capture, mainly reducing the need of heating up the solids by integrating the system with the original combustor or integrating the heat flows inside the calcium looping system. Some of the concepts

allow the abandonment of the ASU which causes high net efficiency losses in oxy-combustion systems. However these concepts are hard to utilize in retrofit capture scenarios because they require such a high level of integration. Other next generation concepts rely on the utilization of existing material flows, like the calcium looping process combined with a cement manufacturing unit.

2.2.1 Solid heat carrier calcium looping unit

The main idea of the solid heat carrier calcium looping process is to replace the oxy-combustion of solid fuels in the calciner by transferring heat alongside a solid flow from a CFB combustor as first introduced by Martínez et al. (2011a). Lime would serve as the primary solid material in the system and combustion in the boiler unit would be normal air-combustion. The system comprises three interconnected fluidized beds illustrated in Figure 2.5.

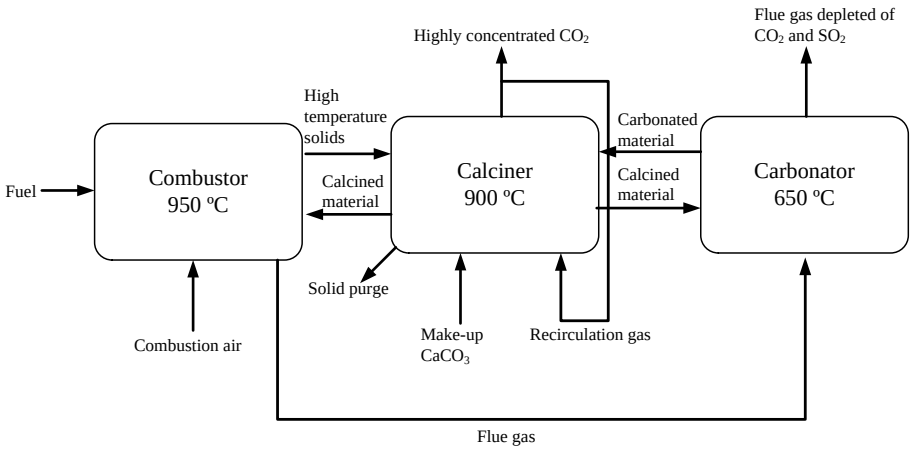

Figure 2.5. Solid heat carrier concept.

The downside of this technique is the increased combustion temperature in the combustor which could lead to increased NO_x emissions. Also the solid flow control and the solid looping ratio is still an uncertainty in this system. However, potentially the net efficiency penalty of this concept could be as low as 4 percentage units (Martínez et al., 2011a) using modern power generation equipment. This is a major improvement over conventional CCS techniques where estimated penalties range from 5-8 percentage units for oxy-combustion and MEA solvents (Vorrias et al., 2013).

2.2.2 Calcium looping units with various heat integrations

The calcium looping process requires heating and cooling of high temperature solid flows which could be potentially exploited by exchanging heat between those flows. Martínez et al. (2012b) presented several different combinations that could result in net efficiency penalties lower than those of the standard calcium loop. The potential number of different combinations is quite high and therefore describing all of them accurately is not essential for this thesis. Most of them utilize a method of pre-heating the solid flow entering the calciner using the high quality heat available in the loop and consequently lowering the required thermal energy in the calciner, Figure 2.6. These techniques will always increase the construction costs of the unit which will in turn increase the costs of the capture process.

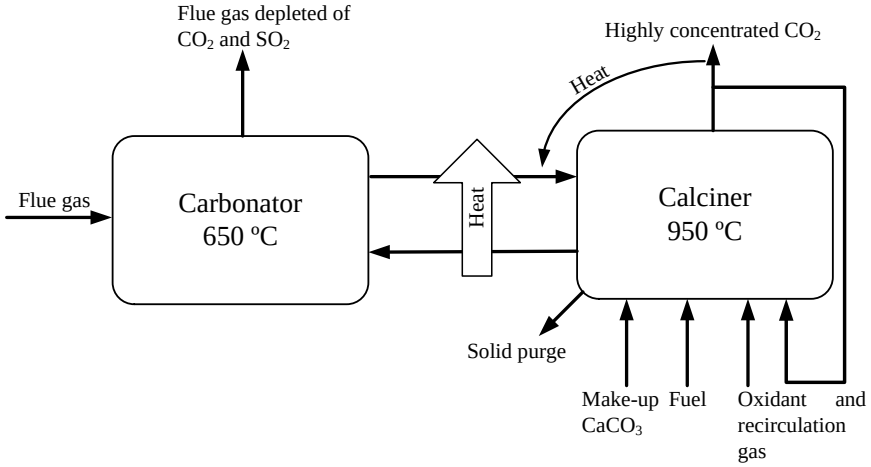

Figure 2.6. Potential heat integration schemes in the calcium looping process. High temperature solids or flue gases can be used to pre-heat the solids entering the calciner.

2.2.3 Chemical looping combustion combined with calcium looping

One interesting carbon capture concept is the combination of chemical looping combustion and the calcium looping process. Chemical looping combustion is a carbon capture process where the combustion oxygen is separated from air by using a metallic solid carrier. This allows the combustion of gaseous fuels in a nitrogen free atmosphere. The chemical looping process incorporates also two reactors, the air reactor which seprates oxygen from the air and the fuel reactor (regenerator) which combust fuel in a high CO_2 atmosphere. By combining these two techniques, the ASU in the calcium looping process becomes obsolete because the chemical looping air reactor provides all the combustion oxygen to the process. This process is a three fluidized bed system, presented in Figure 2.7, including the carbonator which captures CO_2 from a flue gas source, an air reactor which separates oxygen from air with a metallic compound and

feeds it to the calciner/fuel reactor which regenerates both the lime and metallic material (Abanades et al., 2010; Manovic and Anthony, 2011A).

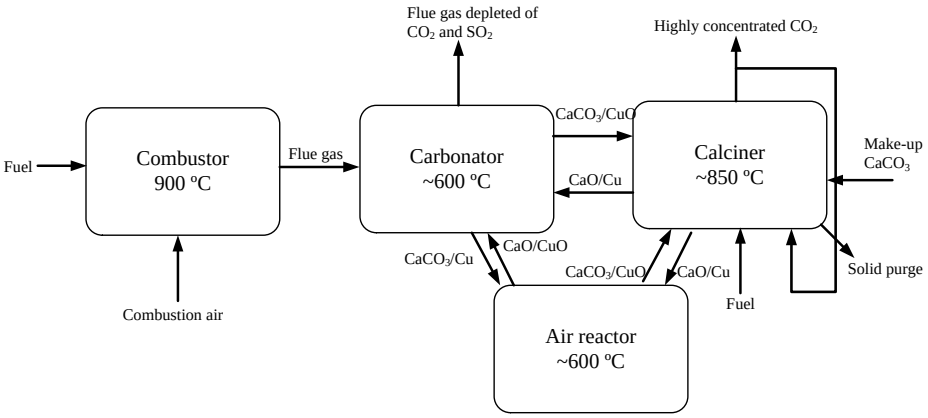

Figure 2.7. Chemical looping combustion combined with calcium looping.

The most interesting feature in this process is the solid material. Because the particles commonly used in chemical looping have quite different fluidization properties compared to common lime particles, there is a risk that the system would not have a homogeneous concentration of each particle type. The solution for this is to coat a metallic particle with lime achieving combined properties of both materials. (Manovic et al., 2011A; Manovic and Anthony, 2011B) Chemical looping combined calcium has not been demonstrated outside laboratory scale.

2.2.4 Calcium looping combined with steam regeneration

Extensive discussion has been going on about the regenerative properties of different steam concentrations on the calcium looping lime during the development of this process ranging from normal flue gas steam concentrations to elevated concentrations 20–60 vol-%. (Arias et al., 2010; Manovic and Anthony, 2010; Arias et al., 2011A; Ramkumar and Fan, 2010; Donat et al., 2010; Wang et al., 2013; Champagne et al., 2013). The mechanism of how steam affects the particles has been researched and the general understanding is that it promotes the diffusion of CO_2 into sintered particles, regenerating some of the lost pore structure. Steam does not have a noticeable effect on the chemical kinetics of carbonation or calcination. It has to be noted that although steam improves the carrying capacity, the effect has a limit and injecting steam from a Rankine process results in process efficiency losses.

2.2.5 Calcium looping applied to industrial processes

Limestone is widely used in industrial processes. An industrial process calcining limestone in high temperatures using fossil fuels could be fitted with a calcium looping unit to reduce the CO_2 emissions of the system. The material flows, end-product and arrangement of the process determine the level of integration but the use of pre-built infrastructure and inherent material flows offer a possibility for low penalty CO_2 emission reduction.

Concrete and cement manufacturing for construction is a significant contributor to the carbon dioxide emissions worldwide. Cement manufacturing plants use fossil fuel fired lime kilns to produce lime for clinker. Combining the calcium looping process with the kiln would reduce the CO_2 emissions of the system and render the plant self-sufficient in electricity if a steam cycle would be fitted to the calcium loop (Rodríguez et al., 2012). Figure 2.8 presents the general layout of a cement manufacturing plant fitted with a calcium loop. The purge of conventional calcium loop is now feeding the rotary kiln of the cement plant.

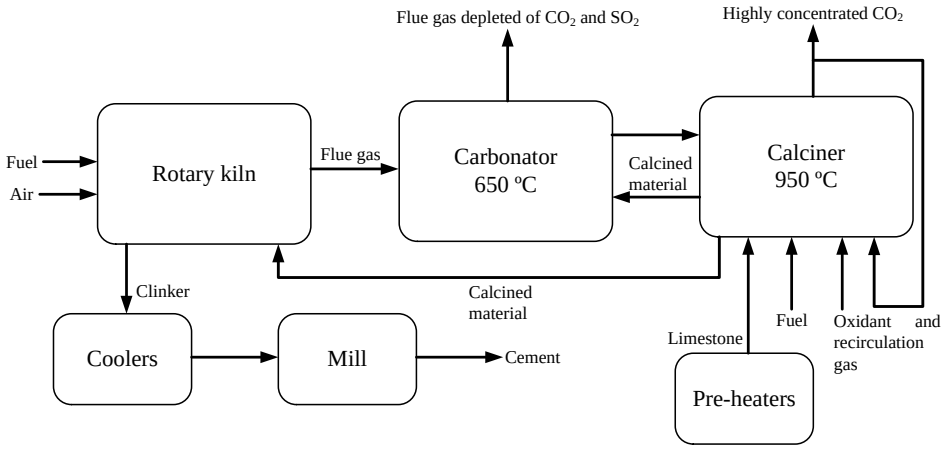

Figure 2.8. Cement manufacturing unit combined with a calcium loop.

Pulp and paper industry are heavy consumers of limestone because it is a critical ingredient in the pulp manufacturing process. Li et al. (2012) and Sun et al. (2013) proposed using purged lime from the pulp cycle in the calcium looping process. The calcium looping cycle could also be used to capture CO_2 from the pulp and paper mill rotary kiln analogically to the cement manufacturing plant.

2.3 Sorbent behaviour in the calcium looping process

Natural lime subjected to cyclic carbonation and calcination undergoes a radical change in physical and chemical properties. Extensive research has been done to understand the behaviour of lime in cyclic carbonation-calcination (Arias et al., 2011; Barker, 1973; Grasa et al., 2009; Stanmore and Gilot, 2005; Wang and Anthony, 2005; Abanades, 2002; Abanades and Alvarez, 2003). The general understanding is that during each high temperature calcination step the porous structure of the lime particle sinters weakening its ability to transfer CO_2 inside the particle. This causes the carbonation step to change from a fast kinetically controlled reaction to a diffusion controlled reaction, which in turn is not very suitable for post-combustion capture purposes. This phenomenon affects the performance of the calcium looping process significantly as shown in Figure 2.9. If one mole of calcium oxide can capture one mole of CO_2 in the first calcination–carbonation cycle, after 20 cycles 10 moles of calcium oxide is needed to capture that one mole of CO_2 in the residence times of a CFB reactor. Therefore, the looping ratio of lime between the reactors has to be 10 times the stoichiometric value or even higher if the unreactive components of the solid material are included. The particle porous structure will regenerate itself slowly if carbonation time is extended (Arias et al., 2011B). Correlations have been devised to predict the loss of activity in cyclic carbonation and calcination (Wang and Anthony, 2005; German and Munir, 1976; Borgwardt, 1989). The most commonly used approach in literature is the one formulated by Grasa and Abanades (2006) in which the maximum carrying capacity reaches a residual value asymptotically as a function of carbonation-calcination cycles

$$X_{\max} = \frac{1}{\frac{1}{1-X_r} + fN} + X_r \tag{2.5}$$

where f represents the carrying capacity decay coefficient [-], N the number of full cycles and X_r the residual activity in molar fractions [-]. Grasa and Abanades (2006) suggested a value of 0.5 for the decay coefficient f. The correlation predicts quite well the maximum CO_2 carrying capacity of natural lime particles. However, particles with enhanced carrying capacity require correlations including the improved residual activity (Valverde, 2013).

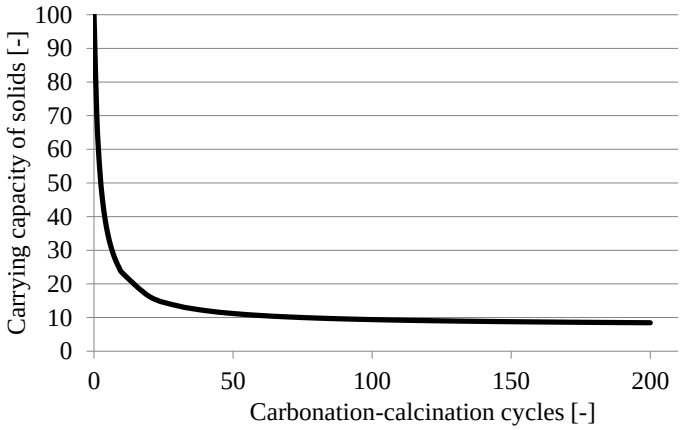

Figure 2.9. Carrying capacity of natural lime as a function of carbonation-calcination cycles plotted with the correlation of Grasa and Abanades (2006). A sharp decrease in CO_2 uptake can be noticed in the first ten cycles.

To compensate for this *l*oss of activity, a make-up flow of fresh limestone has been introduced to the calciner reactor as stated in Chapter 2.1.1. This means that the solid material present in the system will have an age population with different reactive properties.

Alongside the loss of carrying capacity, tests have shown that the limestone particles tend to fragment during the initial calcination steps (Gonzáles et al., 2010). This can be explained by the highly porous structure of the limestone. During the initial calcination, the CO_2 released from the inside of the particle will break down the connections between the micrograins of the particle. This fragmentation of the particle presents some challenges in the design of fluidized bed reactors. If the bed quality changes too much because of the reactions, the fluidization behaviour of solid particles will not match with the designed behaviour. While the calcium looping process is quite sensitive to the solid mass flows rates between reactors because of the high temperature difference, it is important to recognize the particle sizes after fragmentation and use this information to dimension the systems.

2.4 Sorbent enhancement

As in the case of the second generation calcium looping concepts, adding complexity to the process decreases the process efficiency losses caused by the capture. Sorbent enhancement seeks to increase the carrying capacity of lime decreasing the need for solid looping and heating up the solids, which in return would lower the net efficiency

losses caused by the CO_2 capture. Various methods have been devised to improve the CO_2 carrying capacity of natural limestone ranging from chemical enhancement to various physical treatments. All the methods aim at maintaining the porous structure and reactive area of the limestone particles and most of them have been successful at the laboratory scale. However, sorbent enhancement has not been demonstrated at the large scale.

2.4.1 Physical sorbent enhancement

Physical sorbent enhancement means using physical effects to regenerate or sustain the reaction surface area of the sorbent. Various methods have been studied including mechanical pelletization of particles (Manovic and Anthony, 2011C), different kind of thermal treatments (Valverde et al., 2013A; Manovic et al., 2008; Manovic et al., 2011B), acoustic fields (Valverde et al., 2013B) and subjecting the particles to various kinds of atmospheres like extended carbonation or steam regeneration (Arias et al., 2011A; Arias et al., 2011B). Detailed descriptions of each method are not presented in this thesis, instead here it is only noted that this kind of research has great potential to reduce the costs of capture in the calcium looping process. However, each method has to be examined, whether they are feasible both technically and economically at the large scale.

2.4.2 Chemical sorbent enhancement

As in the case of physical sorbent enhancement, chemical enhancement tries to increase the residual carrying capacity of the sorbent by means of chemical additives and dopants. A wide range of dopants has been studied by several research groups (Florin and Fennell, 2011; Li et al., 2009; Sun et al., 2012; Al-Jeboori et al., 2012; Al-Jeboori et al., 2013) demonstrating that chemical enhancement also has a great potential to reduce efficiency penalties in calcium looping. The studied dopants ranged from inorganic and organic acids to manganese salts and lime combined with metallic compounds like calcium aluminate. Because this thesis is modelling oriented, a detailed analysis of each sorbent enhancement technique is not necessary here. The benefit gained from doping has to be weighted case by case against the costs and technical challenges.

2.5 Advances and drawbacks to other carbon capture techniques

It is very clear that decarbonising the energy sector will not happen without economic consequences. Each carbon capture technique will have an economical penalty that will increase the heat and power production costs. The development of CO_2 market prices, the technological advancement of clean heat and power production methods and the political restraints set by governments ultimately define which CO_2 free technologies will prevail in the future. In the case of power generation combined with carbon capture and sequestration, it boils down to the net costs of the energy conversion technology.

Applying CCS to a power plant should be viewed case by case considering the existing infrastructure, material flows and the surrounding industry. If a power plant is situated near limestone sources or cement factories, the possibility of the calcium looping capture process applied to the plant rather than oxy-combustion or amine capture has to be considered.

The post-combustion calcium looping process has several advances compared to more traditional CO_2 capture methods. Part of the advances relate to the utilization of well-known technologies like the circulating fluidized bed technology, oxy-combustion and limestone utilization in fluidized beds. With well-known processes and materials, the problems related with prototype technologies are partially avoided, speeding-up the industrial utilization of the process. This is especially important with CCS techniques because the CO_2 emission reductions are needed in the upcoming years to avoid the acceleration of the climate change.

Another advance of the calcium looping cycle is the use of an abundant resource. Natural limestone is found all over the world which makes it a cheap and abundant sorbent. The carrying capacity and fragmentation behaviour determine the suitability of the lime for CO_2 capture purposes. The use of limestone also enables above 95 % sulphur capture levels for the system which will lower pollutant removal costs. In addition to that, limestone is used in many industrial processes as mentioned in chapter 2.2.5. The limestone synergy with these industries increases the attractiveness of this technology. The post-combustion calcium looping unit itself does not affect the flue gas source combustor which makes it ideal for retrofitting if the footprint of the unit allows it.

Alongside the advances, several drawbacks of this technology are present. Because the thermal power of the post-combustion calcium loop will be equal or higher than that of the source combustor, the construction investment of the plant will be high, close to that for the original power plant. The calcium looping unit will require a constant flow of limestone alongside the fuel which will require new logistical solutions for the plant. Also, although the technology utilizes well-known concepts like the CFB reactor, some unresolved issues still cause uncertainty for the technology, for example the fragmentation and attrition of fine limestone particles in a circulating fluidized bed, control of solid circulation rates and overall thermal design of the system.

2.6 Experimental demonstration of the calcium looping process

Extensive testing of the calcium looping process has been done in small scale equipment by several research groups worldwide. Successful steady-state operation has also been demonstrated by this date in three pilot scale devices.

CSIC, Spain, has successfully operated a small 30 kW_{th} laboratory scale calcium loop for several years (Alonso et al., 2010; Rodríguez et al., 2011A; Rodríguez et al., 2011B). The equipment consists of two interconnected circulating fluidized bed reactors

with 6.5 m heights and 0.1 m diameters. The calciner is electrically heated. High CO_2 capture levels and several hours of stable operation have been demonstrated in this system. Sulphur capture and the development of carrying capacity have also been studied.

The University of Stuttgart IFK has also demonstrated small scale calcium looping process in a 10 kW_{th} unit (Rodríguez et al., 2011A; Charitos et al., 2010). The unit is a combination of a BFB and CFB reactors. The CFB reactor is 12.4 m high and 70 mm in diameter. The BFB reactor is 114 mm in diameter. Reactors can be assigned either way, for example CFB or BFB as carbonator. The laboratory scale unit has been successfully operated for several hours and moderate capture efficiencies, 70-80 %, have been achieved.

The University of Stuttgart IFK erected a small 200 kW_{th} pilot plant capable of calcium looping, chemical looping and gasification testing. The system consists of three interconnected fluidized bed reactors. In the calcium looping experiments one reactor will act as the combustor producing actual flue gases to the turbulent carbonator. The regenerator calciner operates in the fast fluidization mode in the rig. Hydrodynamic stability and several hours of successful CO_2 capture were achieved in the setup. Capture efficiencies were high, around 90%. An accurate description of the 200 kW pilot plant can be found in Dieter et al. (2013).

One of the first calcium looping lab scale units was built by CANMET, Ottawa. The dual fluidized mini-bed system can be broken down into two main mechanical systems and one solids transport system. The first mechanical system is a calciner/regenerator that can be operated as a bubbling or a circulating fluidized bed combustor. The second mechanical system is a carbonator that can be operated as a bubbling or moving bed reactor. Finally, the solids transport system can be divided into the solids riser, transfer cyclone, and carbonator return leg. The calciner is 4.5 m high and the carbonator is 2 m. Each reactor has an internal diameter of 0.1 m and is surrounded by three 4.5 kW electric heaters, which provide supplemental heating during start-up and can be switched on or off to control temperatures. The calciner can be fluidized with oxygen-enhanced air and/or oxygen and recycled gas from a blower to control the bed temperature. The system has been run successfully with high capture efficiencies and several calcining atmospheres. (Symonds et al., 2009; Rodríguez et al., 2011A; Lu et al., 2008)

The Technical University of Darmstadt built a 1MW_{th} pilot scale facility capable of both chemical looping and calcium looping operation. The unit is a dual-circulating fluidized bed loop with 0.4 and 0.6 m diameters. The larger diameter reactor is 8.66 m high. The smaller diameter reactor is 11.35 m high. The carbonator captures CO_2 from synthetic flue gases or from a separate combustor. The calciner can be run with propane or solid fuels in air or oxy-combustion modes. Several successful campaigns have been made with moderate CO_2 capture rates, around 80 %, with different fuel solutions (Ströhle, 2012).

The biggest calcium looping plant currently in operation is the 1.7 MW pilot plant in Asturias, Spain (Sánchez-Biezma et al., 2011; Sánchez-Biezma et al., 2013). The pilot plant comprises of two interconnected 15 m high circulating fluidized beds. The carbonator is 0.65 m in diameter and the calciner 0.75 m. Solid transfer between reactors is handled with dual loop seals able to divide solid circulation to both reactors. The pilot plant has accumulated 800 hours of operation with capture efficiencies close to 90%. Oxy-combustion of solid fuel has been demonstrated successfully.

In addition to the mentioned units other active demonstration projects of the calcium looping process might be on-going while the writing this thesis that have not been published or advertised.

2.7 Modelling of the calcium looping process

Building industrial scale power generation units is expensive and creates a significant economic risk to the builder. In the case of carbon capture and storage technologies the risk is even higher because the industrial utilization of CCS is still economically unattractive. This emphasizes the importance of pre-design and modelling of CCS processes because the feasibility of the process can be studied with small effort and financial strain. Of course, scientific modelling always relies on assumptions and simplifications but the knowledge gained from models can greatly improve the breakthrough possibilities of a prototype technology. Several modelling approaches have been applied to calcium looping process by several research organizations ranging from simple process models to CFD simulations.

2.7.1 Process scheme models

The process scheme model, 0D process model is the simplest mass and energy balance solver that can be made for a system. Calculation times are very short and parameter variation and investigation is easy. Using ready-made process modelling tools like Aspen HYSYS® or IPSEpro facilitate the modelling task even further. The downside of the process scheme modelling is the simplifications that have to be made to describe a complex process. The accuracy of the 0D process models can be improved to some limit by adding complexity but the phenomena linked to spatial behaviour are ignored.

Several process scheme models have been developed by different research groups. Approaches vary from single reactor models to interconnected reactors and comprehensive process models including steam cycle integrations. Alonso et al. (2009) modelled a circulating fluidized bed carbonator solving the carbon balance of the carbonator reactor assuming fully mixed solid phase and plug flow of gas. Solids coming from the calciner were assumed to be fully calcined. The carbon balance was coupled with a model predicting solid residual activity and a kinetic model for the carbonation reaction rate. The model was used to predict carbonation efficiency for different looping and make-up ratios.

Martinez et al. (2013a) presented a model for the calciner similar to the one presented by Alonso et al. (2009) for the carbonator. A simple fluid dynamic approach was combined with a kinetic model for calcination. This approach was then used to evaluate the performance of a calciner reactor with parameter variation. From the model standpoint, a calcium looping calciner could be operated in a large scale.

Diego et al. (2012) presented an approach solving the pressure balance of the calcium loop and predicting the actual solid circulation rate between reactors and coupling that to a kinetic model for carbonation. The work investigated the actual flow between reactors as a function of reactor inventories and gas velocities compared to the required flow determined by available carrying capacity.

Romano (2012) created a similar carbonator model to approach used by Alonso et al. (2009) including the effect of sulphur capture and inert accumulation in the system. The model also included empirical models to predict solid concentrations in the reactor. The model was validated using experimental data available from lab-scale equipment and parametric investigation was made varying reactor inventories, make-up flow and looping ratios. Romano has also simulated the calcium looping with a comprehensive process model. The first analysis was a coal fired power plant retrofitted with post-combustion calcium looping capture (Romano, 2009). The second one analysed an oxyfuel CFB fitted with the calcium looping process to reach ultrahigh CO_2 capture efficiencies (Romano, 2013).

Hawthorne et al. (2009) constructed a comprehensive calcium looping process model in the Aspen PLUS™ simulation environment coupling it to a steam cycle calculation program. Using this approach, the net efficiency of a large calcium looping unit was studied.

Experimental validation of kinetic models for carbonation was done by Duelli et al. (2013) in a 10 kW lab-scale unit. Kinetic models were validated by solving the carbon balance over the carbonator reactor including parameters like solid active space time and carbon dioxide concentration in the reactor.

Vorrias et al. (2013) used a process simulator to analyse a large scale-calcium looping unit retrofitted to a lignite fired boiler. A very low efficiency penalty was achieved by using low make-up flows and solid to solid heat exchangers between the reactor solid return systems. Tools in this analysis were Aspen PLUS™ and IPSEPro™.

Ströhle et al. (2009) used a process simulation tool to study the feasibility of a large scale calcium looping unit. Aspen PLUS™ was used to simulate the case with similar assumptions as other the 0D models. Very low efficiency penalties were achieved which confirms from this modelling standpoint the feasibility of large scale calcium looping units.

2.7.2 Calcium looping models incorporating spatial discretization

The next step from the 0D process model are modelling tools incorporating some kind of spatial discretization. This means that the domain of the existing modelling problem is divided into calculation cells enabling the analysis of phenomena occurring inside the domain to some extent. Different discretization stages can be applied to the domain ranging from 1D to 3D. The applicability of the discretization has to be considered case by case. For example 1D models can be valid for high and narrow pilot units. For large cross-section industrial units the lateral phenomena can require more dimensions to produce accurate results.

Spatially discretized models usually incorporate more complex models for chemical reactions, heat transfer and solid entrainment. The benefit from more accurate phenomenon description is obvious but alongside that, the possibility for error sources increases.

Lasheras et al. (2011) presented a 1D carbonator model including submodels predicting solid distribution along the reactor height and the core-wall layer effect. The approach was used alongside the Aspen HYSYS® process model. The study reported parametric investigation of variables associated with solid suspension density profile, reactor solid inventory and make-up flow.

Calcium looping models including spatial discretization have also been developed by Myöhänen (2011) and Ylätalo et al. (2012). The approach of Myöhänen was used to three-dimensionally model the calciner reactor operation (Ylätalo et al., 2013). The calcium looping 1D-model presented by Ylätalo et al. is the topic of this thesis. The contribution of this approach to the field of calcium looping modelling is the addition of the energy balance solution and the possibility to simulate interconnected reactors in dynamic states.

2.7.3 CFD-modelling of the calcium looping process

Initial computational fluid dynamics (CFD) calculations have been made to study the behaviour of a calcium looping process reactor by Nikolopoulos et al. (2013). CFD modelling of two-phase flows is computationally quite challenging and combining two reactors will push the current limits of computer calculation power. A simple calculation of two-phase flow dynamics using energy minimization multi scale (EMMS) scheme was made for a cold model carbonator. The cold model carbonator was built in IFK Stuttgart with a 30 mm inner diameter and 5279 mm height (Nikolopoulos et al., 2013). CFD results were compared with pressure balance measurements which matched very well. Besides this study, further CFD analysis of the calcium looping process has not been reported in recent publications.

3 Dynamic 1D calcium looping model framework

3.1 Overall model framework

One of the main objectives of this thesis is to present a model framework capable of simulating the behaviour of the post-combustion calcium looping process in different scales with sufficient accuracy. The modelling approach selected for this problem is a 1D dynamic model for circulating fluidized bed reactors. Both reactors of the calcium looping process have been discretized vertically into 1D control volumes with an interconnection for the solid circulation through simple cyclone-standpipe-loop seal models, Figure 3.1. Time-dependent balance equations for mass, energy and gas and solid material fractions have been written for each control volume using the first order difference methods, for convective flows the upwind method and for diffusion of energy the central difference method. Time derivatives for mass, energy and material balances are solved each time step in the Matlab® Simulink simulation environment using built-in ordinary differential equation solvers. Solvers include constant time step solvers ODE4 or ODE5 and a variable time step solver ODE45.

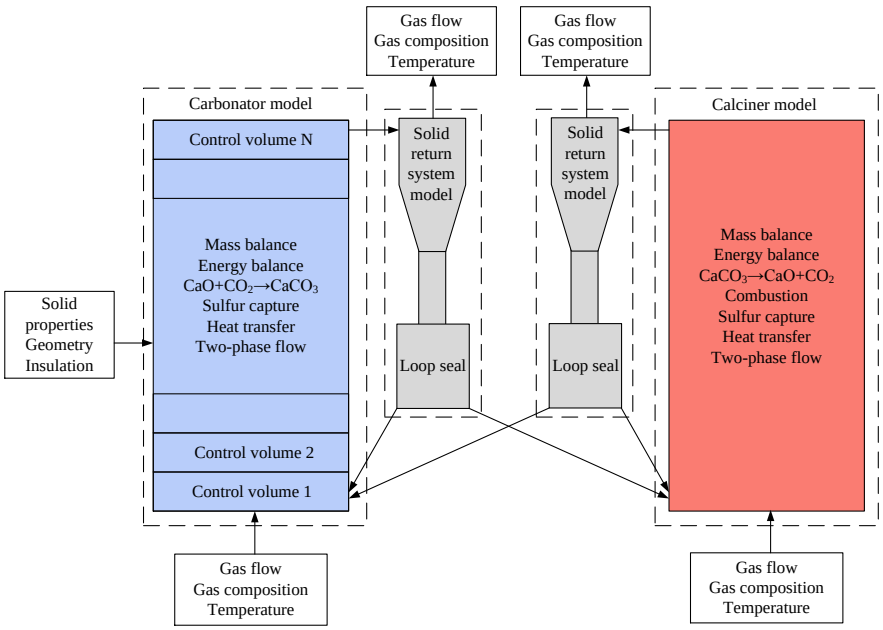

Figure 3.1. Overall 1D dynamic model framework.

The calcium looping model framework incorporates several fluidized bed phenomena alongside the mass and energy balance solvers. Solid behaviour in the circulating

fluidized bed reactor has been approximated with a modified density profile correlation. Heat transfer in the entrained bed is modelled using an empirical correlation devised from industrial CFB measurements. Mixing in the fluidized bed is modelled using two approaches: turbulent mixing of energy is modelled by means of dispersion between adjacent control volumes. Mixing of materials and energy can also be modelled through the core-wall layer approach which is common in fluidized bed modelling. Combustion and chemical reactions are modelled with correlations based on the best available knowledge from the literature.

The following chapters explain the mathematical and physical principles behind the model.

3.2 Discretization of the reactor models

Both the carbonator and calciner reactor models can be discretized spatially to a limited number of 1D control volumes. These control volume slices ($\Delta z_{freeboard}$ and Δz_{sloped}) are perfectly mixed in terms of mass and energy. The control volume size can be several cubic meters at the industrial scale. Core and wall layer regions are calculated separately in each control volume. Dimensioning of the reactor models is done by defining the height of the reactor, width and depth. The depth is considered constant but a separate sloped section can be distinguished from the rest of the reactor by defining a lower width and a height for the slope. This kind of sloped section is common in large scale fluidized bed reactors and is included in the model framework. The purpose of this kind of dimensioning is to keep fluidizing velocity constant alongside the reactor height if the volumetric gas flow changes drastically. This ensures good mixing and gas solid contact in the lower bed. From the model standpoint, this enables also the use of smaller control volumes in the lower bed area where the majority of reactions and interesting phenomena occur. In addition to the above mentioned dimensioning, the height of the exit channel can be defined which determines the control volumes where the gas and solids exit, Figure 3.2.

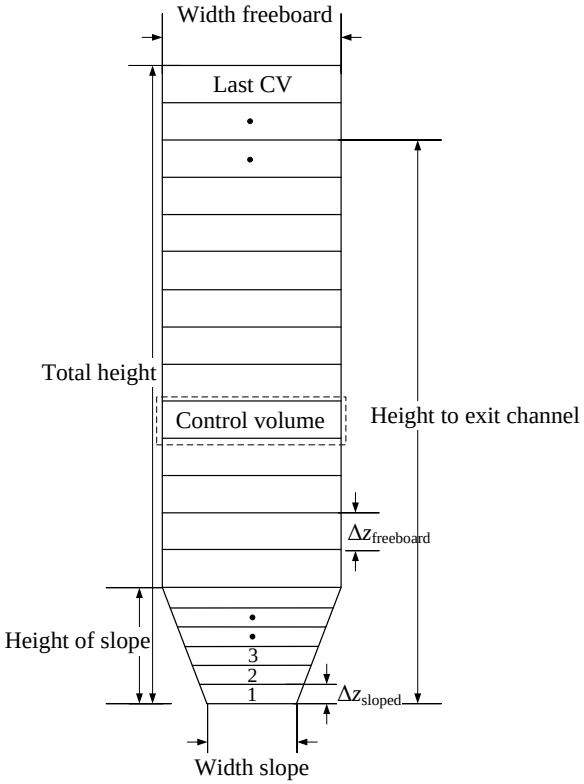

Figure 3.2. Discretization and dimensioning of the reactor models.

Mass boundary conditions of the reactor model have been defined in the following manner: gas inputs with arbitrary properties can be inserted to the first element as primary gas or as secondary gas inputs to any control volumes based on height coordinates. The amount of gas exiting the last control volumes is linearly scaled based on the height of the elements located in the exit channel region. Solids always enter the first element and leave at the final element. Exiting solids and their properties are sent to the loop seal models. Fuel can be inserted from any height releasing volatiles and moisture at the insertion point but char will appear at the bottom of a cell as the solids, Figure 3.3.

Thermal boundary conditions allow the definition of constant temperature surfaces inside the reactor. These surfaces can be membrane wall evaporator surfaces or single heat transfer surfaces. These surfaces can be refractory protected or plain depending on the construction of the modelled case. The model allows the calculation of 1D heat transfer through the refractory protected wall. The heat transfer area of these surfaces

can be freely defined. Energy transported alongside with gas and solids flows is considered by calculating the heat capacity of the flows based on the composition and temperature.

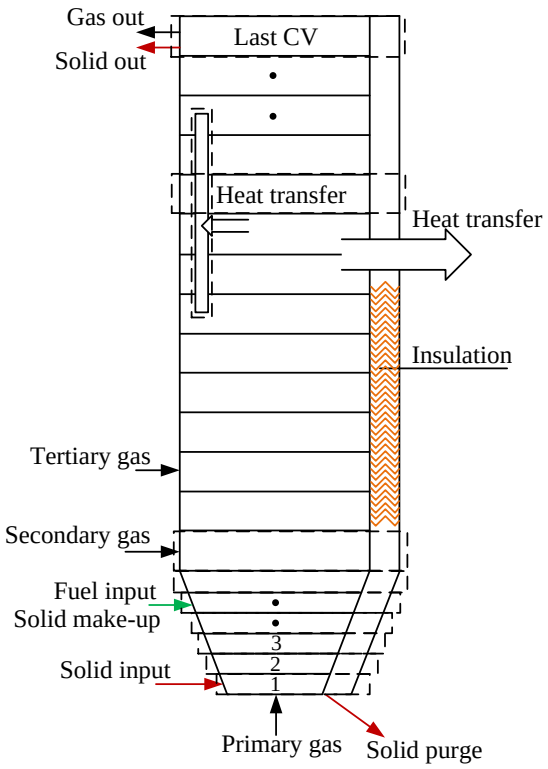

Figure 3.3. Reactor model boundary conditions

Time discretization of the model is done by dividing the total simulation time by a constant time step or a variable time step determined by the Simulink algorithm, Δt. The variable time step solver adjusts the time step based on the sensitivity of calculations trying to limit the calculation time, Figure 3.4.

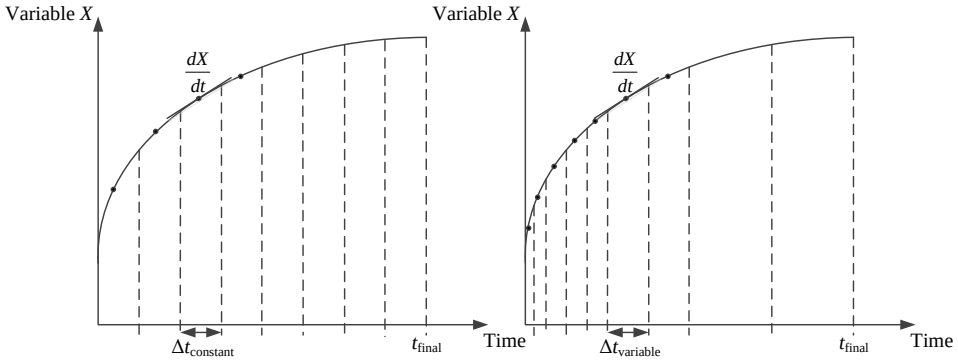

Figure 3.4. Time discretization scheme and the difference between constant (left) and variable time step discretization (right).

Figure 3.5 illustrates the essential simulation steps and procedures. The calculation sequence is repeated until the final time is reached advancing one time step at a time. Each calculation operation is a prerequisite for the next step, for example, the solid profile calculation requires the solution of gas mass flows and velocities beforehand. The Matlab Simulink solver incorporates a set of vector variables which are used to calculate the modelling case, Figure 3.5. The input vector **U** represents the inputs required for the model to initiate the calculation. The **U** vector can be changed during the simulation time in order to create a dynamic situation. The state value vector **X** represents the reactor model values like temperature or solid mass in the control volumes that change in time. State values are calculated in each time step based on the input vector and the previous time step values of **X**. A reasonable set of state values is required to initialize a simulation. The output vector **Y** contains important process parameters from the simulations. By adjusting sampling time in the Matlab workspace, the result vector can be updated during the simulations. Important information from the simulation can be printed in the **Y** vector like spatial time dependent variables or global variables.

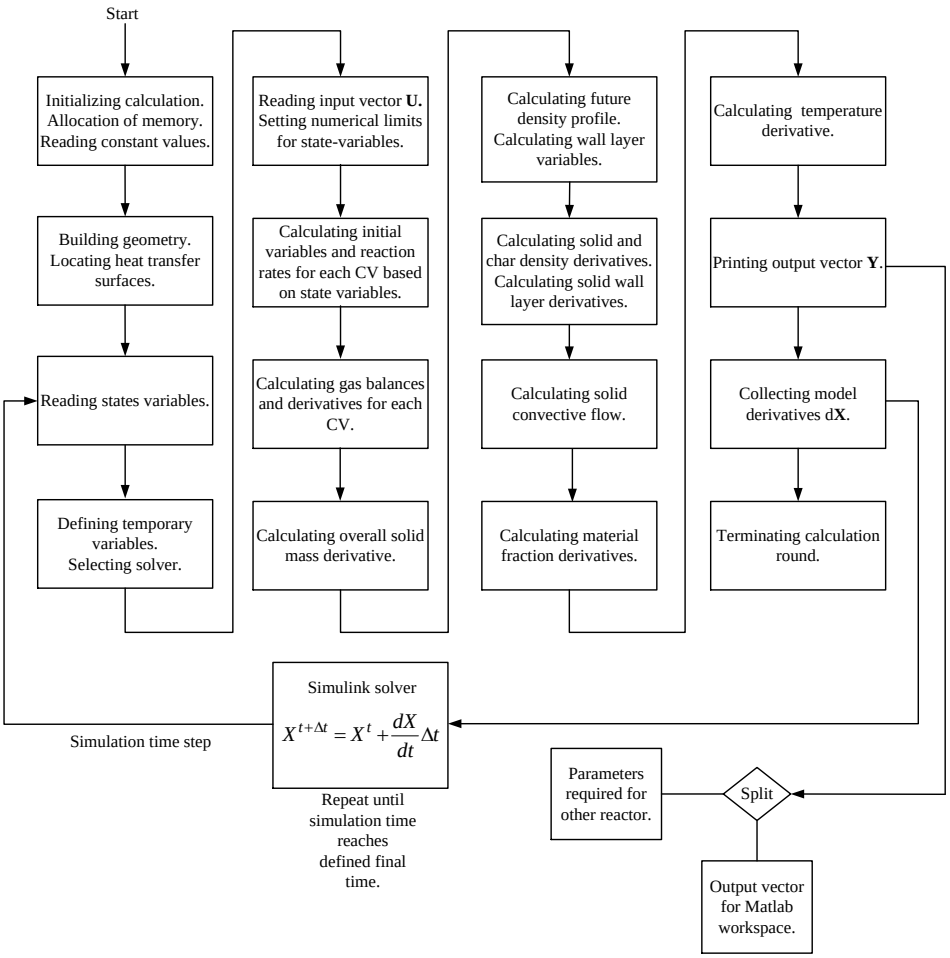

Figure 3.5. Calculation procedure of the reactor model. The set of time dependent state values is solved until the end time of the simulation is reached. Each calculation step is explained in the following chapters.

In addition to the mentioned vectors, the model incorporates constant variables defined in a configuration file including material properties, dimensions and experimental coefficients. For the solid material, thermal properties like heat conduction and solid heat capacity and fluidizing properties like particles sizes and apparent density are assumed constant. Thermal properties of gases are calculated based on the gas composition and gas property correlations.

3.3 Solving the mass balance

In the reactor model, several mass balances are solved during simulations. First of all, the total solid mass balance of the reactor is solved at each time step. In addition to that, the solid mass balance of each control volume is solved. The wall layer and core are considered separate solid regions interacting with each other within each control volume. Following the solid mass balance solution, the material fraction balances are solved for lime, limestone, ash and calcium sulphate. Also the overall gas mass balance of the system is solved including the gas mass balances of the control volumes.

3.3.1 Solid mass balance

The overall solid mass balance of the reactor includes all the solid flows entering and exiting the domain as seen in Figure 3.3. The general equation form for the balance is

$$\frac{dm_s}{dt} = \sum q_{m,s,in} - \sum q_{m,s,out} + \sum r_s \tag{3.1}$$

where m_s represents the total bed mass of the reactor [kg], $q_{m,s,i}$ is the term for solid mass flows in [kg/s], $q_{m,s,out}$ is the term for solid mass flows out [kg/s] and the sum of r_s describes the total change in solid mass due to heterogeneous chemical reactions [kg/s]. In the calcium looping process, the total solid mass changes due to carbonation, calcination and sulphation because gas is captured into the solid phase and incoming solid flows. Incoming solid flows can be from the make-up flow, ash accumulating from the fuel or just entering from the other reactor. Equation 3.1 includes only the mass situated in the core, the wall layer mass balance is calculated separately. Char is considered a separate solid phase and overall char mass balance is solved separately with a similar equation.

The solid flow through an element results from the local solid density change, element heterogeneous reactions and core-wall layer interactions applying the first order upwind method, Figure 3.6.

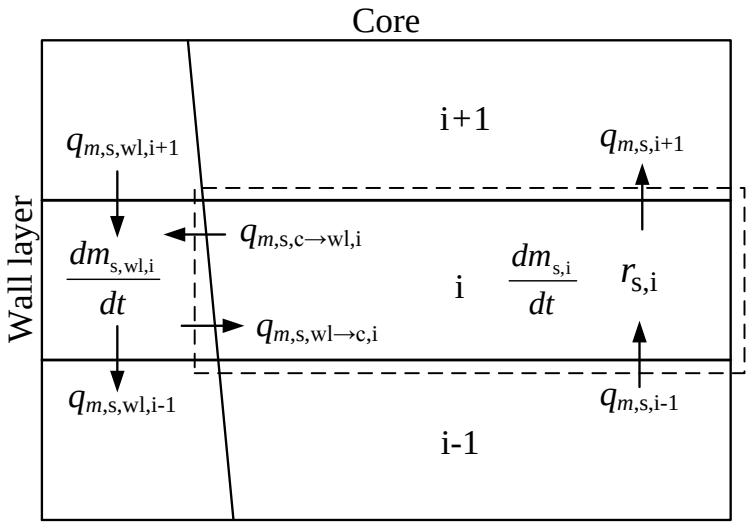

Figure 3.6. Solid mass flow balance of a single control volume.

A similar kind of solid mass flow equation can be written for a single control volume as the 0D mass balance.

$$\frac{dm_{s,i}}{dt} = \sum q_{m,s,in,i} - \sum q_{m,s,out,i} + r_{s,i} \tag{3.2}$$

where $m_{s,i}$ equals the control volume mass [kg], $q_{m,s,in,i}$ [kg/s] represents the collective solid mass flows into the element, $q_{m,s,out,i}$ describes the collective solid mass flows out of the element and $r_{s,i}$ is the collective mass change from heterogeneous reactions in the control volume. Subscript i represents the control volume element index. The essential variable is the solid mass flow to the subsequent element $q_{m,s,i+1}$. The sum of solid mass flows out of the element can be broken down into

$$\sum q_{m,s,out,i} = q_{m,s,i+1} + q_{m,s,c,\rightarrow wl,i} \tag{3.3}$$

where $q_{m,s,c\rightarrow wl,i}$ is the mass flow from the core to the wall layer [kg/s]. The sum of solid mass flows into the element can be broken down into

$$\sum q_{m,s,in,i} = q_{m,s,i-1} + q_{m,s,wl\rightarrow c,i} \tag{3.4}$$

where. Equation 3.2 can be rewritten

$$q_{\mathrm{m,s,i+1}} = q_{m,\mathrm{s,i-1}} + q_{m,\mathrm{s,wl\rightarrow c,i}} - q_{m,\mathrm{s,c\rightarrow wl,i}} - \frac{d\rho_{\mathrm{s,i}}}{dt} V_{\mathrm{i}} + r_{\mathrm{s,i}} \tag{3.5}$$

This kind of balance applies to all of the control volumes with the exception of the first and the last. In the first element there is no flow from the previous element but the flow from the return leg and the other reactor enters the balance. In addition to that, the wall layer downflow enters the first element. In the last element there is no flow to the succeeding element but everything flows out of the control volume core balance either from the exit or to the wall layer. Figure 3.7 describes the internal flow pattern of the 1D reactor model. The core-annulus model is a popular approach used to approximate the solid flow pattern in a circulating fluidized bed reactor (Adánez et al., 1995; Wang et al., 1999; Huilin et al., 2000).

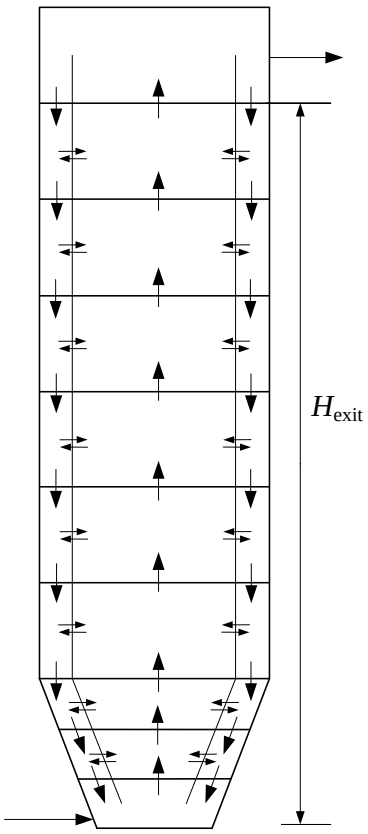

Figure 3.7. Reactor model internal solid flow pattern.

The wall layer solid mass balance can be devised the same way as the core balance, Figure 3.6. The difference compared to the core balance is the fact that the wall layer solid balance does not include gas-solid reactions. This is done to reduce the calculation time because the solid mass located in the wall layer is significantly smaller than in the core. The purpose of the wall layer model is to describe the wall layer phenomenon observed in fluidized bed experiments which reduces energy and material fraction gradients internally between the top and bottom part in a circulating fluidized bed. Equation for the wall layer solid flow is

$$\frac{dm_{\mathrm{s,wl,i}}}{dt} = \sum q_{m,\mathrm{s,wl,in,i}} - \sum q_{m,\mathrm{s,wl,out,i}} \tag{3.6}$$

here $m_{\mathrm{s,wl,i}}$ is the solid mass located in the control volume wall layer [kg], $q_{m,\mathrm{s,wl,in,i}}$ represents the solid mass flows in the wall layer element and $q_{m,\mathrm{s,wl,out,i}}$ is the solid mass flow out of the wall layer element [kg/s]. Similarly to the core solid mass flow the, wall layer downflow is defined from the mass balance. The solid mass flow out of the wall layer element includes the following terms

$$\sum q_{m,\mathrm{s,wl,out,i}} = q_{m,\mathrm{s,wl,i-1}} + q_{m,\mathrm{s,wl\rightarrow c,i}} \tag{3.7}$$

Equation 3.6 can be rearranged to solve the wall layer downflow

$$q_{m,\mathrm{s,wl,i-1}} = \sum q_{m,\mathrm{s,wl,in,i}} - q_{m,\mathrm{s,wl\rightarrow c,i}} - \frac{dm_{\mathrm{s,wl,i}}}{dt} \tag{3.8}$$

The derivate of the wall layer solid mass can be solved from the wall layer suspension density and wall layer volume.

$$\frac{dm_{\mathrm{s,wl,i}}}{dt} = \frac{dV_{\mathrm{wl,i}}}{dt}\rho_{\mathrm{s,wl,i}} + \frac{d\rho_{\mathrm{s,wl,i}}}{dt}V_{\mathrm{wl,i}} \tag{3.9}$$

Where $V_{\mathrm{wl,i}}$ signifies the wall layer volume [m^3] and $\rho_{\mathrm{s,wl,i}}$ the wall layer suspension density [$\mathrm{kg/m}^3$]. The wall layer volume does not change over time in this approach and thus Equation 3.9 is simplified

$$\frac{dm_{\mathrm{s,wl,i}}}{dt} = \frac{d\rho_{\mathrm{s,wl,i}}}{dt}V_{\mathrm{i}} \tag{3.10}$$

The wall layer suspension density is physically dependent on the core density. In this approach the wall layer suspension density is evaluated based experiments done by Zhang et al. (1993). Wall layer suspension density cannot exceed the theoretical packing density of the material in motion which is 50-60 % of the solid material density. The wall layer suspension density is always assumed to be higher in density than the core.

$$\rho_{\mathrm{s,wl,i}} = \begin{cases} 3\rho_{\mathrm{s,i}} \text{ if } \rho_{\mathrm{s,wl,i}} < 0.5\rho_{\mathrm{solid}} \\ \text{else } 0.5\rho_{\mathrm{solid}} \end{cases} \tag{3.11}$$

The derivative of the wall layer suspension density is updated each calculation step based on the core density change. The density in the wall layer changes only when the core density changes. In steady state situations, the wall layer flow is only affected by the net flows over the balance. The storing of mass and energy in the wall layer elements has meaning only in dynamic calculations. The wall layer does not affect heat transfer to the walls in this approach.

The volume of the wall layer in the control volume is determined based on the dimensions of the reactor and an empirical correlation proposed by Zhang et al. (1995). Thickness of the solid wall layer s_{wl} [m] in a circulating fluidized reactor is approximated as a function of reactor hydraulic diameter D_{e} [m]

$$s_{\mathrm{wl}} = 0.05 D_{\mathrm{e}}^{0.74} \tag{3.12}$$

The net flow of solids from the core to the wall layer is determined by setting a modelling parameter, η_{s2wl} [m/s]. This is purely a modelling parameter and has to be considered case by case and validated using empirical data. The equation for the core-wall layer flow is

$$q''_{m,\mathrm{s,c}\rightarrow\mathrm{wl,i}} = \eta_{\mathrm{s2wl}}\rho_{\mathrm{s,i}} \tag{3.13}$$

where $q''_{m,\mathrm{s,c}\rightarrow\mathrm{wl,i}}$ represents the core-wall layer flux [kg/(s m^2)]. A rate for the solids returning from the wall layer to the core $q''_{m,\mathrm{s,wl}\rightarrow\mathrm{c,i}}$ can be defined but it has not been utilized in the model. Core-wall layer mass flow can be calculated based on the control volume perimeter area and core wall layer flux.

Two separate solid balances are solved in the reactor model. Bed material mass balance is solved including CaO, $CaCO_3$, $CaSO_4$ and ash using steps described in Equations 3.1 – 3.21. The char mass balance and solid profile is solved similarly to the bed material excluding wall layer calculation.

3.3.2 Vertical distribution of solid material in the reactor model

Because the momentum equation is not solved in this modelling approach, a semi-empirical correlation is required to describe the behaviour of solids in the reactor. In this approach the division of the total reactor mass to different 1D control volumes is done based on a semi-empirical equation developed by Johnsson and Leckner (1995). The correlation gives an approximate value for the solid suspension density at a certain height for a circulating fluidized bed unit based on the fluidization properties of the particles. The original form of the equation is

$$\rho_s(z) = \left(\rho_{s,bed} - \rho_{s,exit} e^{KH_{exit}}\right) e^{-a(z-H_{bed})} + \rho_{s,exit} e^{K(H_{exit}-z)} \quad (3.14)$$

where ρ_s represents the local solid suspension density [kg/m^3], $\rho_{s,bed}$ is the grid bed density and $\rho_{s,exit}$ is the density around the exit channel. Coefficient K represents the transport zone solid decay constant [1/m] and H_{exit} is the height to the exit channel [m]. The local height coordinate is described with z [m] and the splash zone decay constant is a [1/m]. The height of the grid solid bed height is H_{bed} [m] which together with $\rho_{s,bed}$ defines the total solid inventory in the bed region. In the analyses of this study, solid inventories have been rather low which enables the modelling of the solid suspension density by setting the grid solid bed height to zero. This means that a solid column is not forming at the bottom of the reactor. The decay coefficients a and K describe the behaviour of the solids in different stages of the fluidized bed. Figure 3.8 illustrates the principles behind the Johnsson and Leckner equation. The decay coefficient of the splash zone a describes the formation of solid clusters over the dense bed area as a function of the grid velocity and particle terminal velocity. The transport zone decay coefficient K describes the entrainment of solid particles and clusters towards the exit area as a function of the particle terminal velocity and gas velocity in the dilute zone.

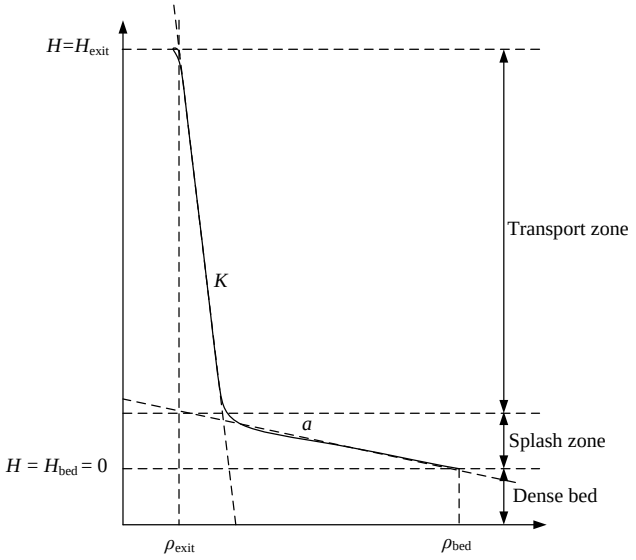

Figure 3.8. Johnsson and Leckner correlation principles. The mathematical slopes of the curve develop as a function of the fluidising velocity.

The transport zone decay coefficient K was defined by Johnsson and Leckner as

$$K = \frac{4\kappa}{D_e\left(v - v_t\right)} \approx \frac{0.23}{v - v_t} \tag{3.15}$$

where κ describes the net mass transfer coefficient [m/s], D_e is the hydraulic diameter of the unit [m], v is the superficial velocity of gas in the transport zone [m/s] and v_t is the approximate terminal velocity of the particles [m/s]. Similarly the decay coefficient for the splash zone is defined as

$$a = \frac{4v_t}{v_0} \tag{3.16}$$

where v_0 is the grid inlet superficial gas velocity [m/s].

The total solid inventory affects the solid suspension density profile. By integrating vertically the Johnsson and Leckner correlation over the whole domain, the total mass can be taken into account in the calculation of local density values.

$$m_s = \int_0^H A\left(\left(\rho_{s,bed} - \rho_{s,exit} e^{KH_{exit}}\right) e^{-a(z)} + \rho_{s,exit} e^{K(H_{exit} - z)}\right) dz \tag{3.17}$$

Where A represents the cross section of the domain [m^2]. Bed density was selected to be the most suitable free parameter in terms of numerical solution in the semi-empirical correlation of the density profile to be changed according to the total mass. Solving solid bed density from Equation 3.17 results in

$$\rho_{s,bed} = \frac{m_s - \int_0^H A\left(\rho_{s,exit} e^{K(H_{exit} - z)} - \rho_{s,exit} e^{KH_{exit}} e^{-a(z)}\right) dz}{\int_0^H A e^{-a(z)} dz} \tag{3.18}$$

The use of the Johnsson and Leckner correlation requires defining an exit density for the system. The solid exit density is dependent of the total solid mass of the system and the fluidization properties of the particles. This is why the exit density has been calculated using a simple approach including the effect of total solid mass and particle properties in the variable. A linear function is defined for the exit density and fluidizing velocity

$$\rho_{s,exit} = \rho_{s,pn} \frac{v - v_t}{v_{pn} - v_t} \tag{3.19}$$

where $\rho_{s,pn}$ is the pneumatic transport solid density [kg/m^3] which describes a situation where all the solid mass is evenly distributed along the reactor height. The pneumatic

transport density can be calculated by dividing the total reactor solid mass with the reactor volume. Pneumatic transport velocity v_{pn} [m/s] represents the superficial velocity where all the particles are entrained in a fully developed flow. Kunii and Levenspiel (1991) stated that for small particles, the pneumatic transport velocity is usually twenty times the terminal velocity.

When the solid bed density and exit density are defined, the vertical profile of the solid suspension density is obtained. In the dynamic solution procedure, changes in the bed density are considered by using new values of the reactor solid mass in setting of the bed density and exit density.

To calculate the decay coefficients, the approximate average terminal velocity of the particles in the solids has to be defined. This was done by solving the force balance of a spherical particle in free suspension. In the model the small lime particles are assumed always spherical. The terminal velocity can be defined by solving Equation 3.20 iteratively (Kunii and Levenspiel, 1991)

$$v_t = \left(\frac{4gd_p}{3C_D} \left(\frac{\rho_{\text{solid}}}{\rho_{\text{gas}}} - 1 \right) \right)^{0.5} \tag{3.20}$$

where g is the gravitational acceleration constant [m/s^2], d_p is the average particle diameter [m], C_D is the particle drag coefficient [-], ρ_{solid} is the apparent density [kg/m^3] and ρ_{gas} is the average gas density in the domain [kg/m^3]. The apparent density is approximated to be constant and around 1800-2300 kg/m^3 depending on the lime compositions. The drag coefficient depends on the particle Reynolds number which in turn is a function of the terminal velocity. The drag coefficient is assigned in the following way (Howard, 1989)

$$C_D = \frac{a_1}{\text{Re}_t^b} \tag{3.21}$$

where the coefficients a_1 [-] and b [-] are set based on the Reynolds number range Re_t [–].

Table 3.1. Values of the coefficients a_1 and b for different particle Reynolds number ranges.

Re_t	a_1	b
< 0.4	24	1
< 500	10	0.5
else	0.43	0

This kind of density profile approach can be replicated in the model for different kind of particle populations with different kind of fluidization properties. In the current model framework two solid suspension density profiles are solved: the reacting material and

the fuel char. The average material properties for the reacting material and char are evaluated and the material density and particle size are assumed constant although in reality, particle densities change from reactions.

3.3.3 Gas mass balance

The general form for the 1D gas balance can be written based on Figure 3.9. The gas mass in the domain is assumed constant because the gas mass derivative is very small compared to the solid mass derivate. If the gas density in the calcium looping reactor conditions is close to 0.4 kg/m^3 and the solid apparent density is 1800 kg/m^3 the scale of solid mass changes is usually thousand times larger than of the gas mass changes. That is why the effect of the gas mass change to the element mass and energy balance is neglected. In reality, the gas mass will change locally due to the composition change, temperature and pressure fluctuations.

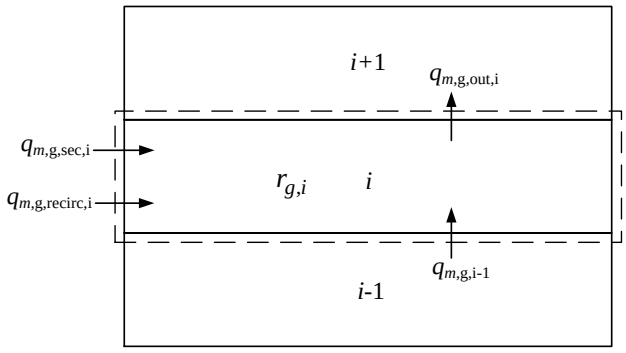

Figure 3.9. Gas mass balance of a single control volume. Gas is not stored in the control volume.

$$\begin{aligned} &\underbrace{\frac{dm_{g,i}}{dt}}_{0} = \sum q_{m,g,in,i} - q_{m,g,out,i} + r_{g,i} \\ &q_{m,g,out,i} = \sum q_{m,g,in,i} + r_{g,i} \\ &\sum q_{m,g,in,i} = q_{m,g,i-1} + q_{m,g,sec,i} + q_{m,g,recirc,i} \end{aligned} \tag{3.22}$$

where $m_{g,i}$ describes the total gas mass in the domain [kg], $q_{m,g,in,i}$ the gas flows in, $g_{m,g,out,i}$ the gas flow out [kg/s], $q_{m,g,sec,i}$ is a secondary or tertiary gas flow to the element [kg/s] and $q_{m,g,recirc,i}$ is a recirculation gas flow to the element [kg/s]. Incoming mass flows of gas can be from primary, secondary or tertiary gases or recirculation of flue gas, Figure 3.3. The leaving gas enters the subsequent element or exits the reactor if located in the exit channel area. The combined effect of the chemical reactions on the gas balance is marked as $r_{g,i}$ [kg/s]. These reactions can be carbonation, calcination,

sulphation, combustion of char and volatiles and the release of moisture from the fuel. The 1D control volume gas balance is similar for a single gas component

$$\frac{dm_{\mathrm{j,i}}}{dt} = \sum q_{m,\mathrm{j,in,i}} - q_{m,\mathrm{j,out,i}} + \sum r_{\mathrm{j,i}} = \sum q_{m,\mathrm{j,in,i}} - w_{\mathrm{j,i}} q_{m,\mathrm{g,out,i}} + \sum r_{\mathrm{j,i}} \tag{3.23}$$

where $m_{\mathrm{j,i}}$ is the gas component mass in the control volume [kg], $q_{\mathrm{m,j,in,i}}$ is the gas component flow to the control volume [kg/s], $q_{m,\mathrm{j,out,i}}$ is the gas component flow out of the control volume and $r_{\mathrm{j,i}}$ is the chemical reaction affecting the gas component in the control volume [kg/s]. The gas component mass fraction in the domain is marked as $w_{\mathrm{j,i}}$ [-]. Subscript j represents now the gas component. In the 1D reactor model the gas mass fraction derivatives are solved as

$$\frac{dw_{\mathrm{j,i}}}{dt} = \frac{d\left(\frac{m_{\mathrm{j,i}}}{m_{\mathrm{g,i}}}\right)}{dt} = \frac{1}{m_{\mathrm{g,i}}}\frac{dm_{\mathrm{j,i}}}{dt} - \underbrace{\frac{m_{\mathrm{j,i}}}{m_{\mathrm{g,i}}^2}\frac{dm_{\mathrm{g,i}}}{dt}}_{0} = \frac{\sum q_{m,\mathrm{j,in,i}} - w_{\mathrm{j,i}} q_{m,\mathrm{g,out,i}} + \sum r_{\mathrm{j,i}}}{m_{\mathrm{g,i}}} \tag{3.24}$$

Equation 3.24 is extendable to all control volumes and gas components. Depending on the reactor model, the derivatives of twelve gas components are solved including O_2, N_2, CO_2, H_2O, SO_2, NO, CO, CH_4, C_2H_4, H_2, NH_3 and H_2S. Combustion products and volatiles (CO, CH_4, C_2H_4, H_2, NH_3 and H_2S) are calculated in the calciner model where the combustion of solid fuel is present. The effect of combustion, volatile release and moisture to the gas balance is discussed more in Chapter 3.5.3. The recirculation of flue gas is possible in both reactor models which means that the determination of the recirculation gas composition is done in the exit.

The gas velocity is a critical parameter in calculating the solid behaviour in the reactor model. Gas velocities in the grid (v_0) and freeboard (v) have been defined in the following way.

$$v_0 = \frac{\left(q_{m,\mathrm{g,primary}} + q_{m,\mathrm{g,recirc}}\right) R T_1^*}{A_{\mathrm{grid}} M_{\mathrm{g,1}} \left(p + \Delta p_{\mathrm{bed}}\right)} \tag{3.25}$$

where $q_{m,\mathrm{g,primary}}$ is the primary gas flow in [kg/s], $q_{m,\mathrm{g,recirc}}$ is the recirculation of flue gas [kg/s], R is the ideal gas constant [J/(K mol)]. T^*_1 is the absolute temperature of the first element [K], A_{grid} is the average flow area of the grid [m^2] and $M_{\mathrm{g,1}}$ is the molar mass of gas in the first element [kg/kmol]. The pressure difference over the solid bed Δp_{bed} [Pa] is also taken into account in the grid velocity alongside the atmospheric pressure p [Pa]. Freeboard gas velocity is

$$v = \frac{q_{m,\mathrm{g,tot,out}} R T^*_{\mathrm{ave}}}{A_{\mathrm{n-1}} M_{\mathrm{n-1}} p} \tag{3.26}$$

where $q_{m,\mathrm{g,tot,out}}$ is the total flow of gas out of the last element [kg/s], T^*_{ave} is the average absolute temperature of the freeboard [K], $A_{\mathrm{n-1}}$ is the flow area of the second to last element [m^2] and $M_{\mathrm{n-1}}$ is the molar mass of the second to last element [kg/kmol].

3.3.4 **Material balance**

The composition of the solid material develops over time because of the capture of CO_2 and SO_2 and therefore, the solution of the solid material derivatives is required. The solid mass balance can be used to form the derivate for a solid material fraction in a 1D control volume. It has to be noted that the total mass change has to be taken into account in the calculation of material fractions.

$$\frac{dW_{k,i}}{dt} = \frac{d\left(\frac{m_{s,k,i}}{m_{s,i}}\right)}{dt} = \frac{1}{m_{s,i}}\left(\frac{dm_{s,k,i}}{dt} - \underbrace{\frac{m_{s,k,i}}{m_{s,i}}}_{W_{k,i}}\frac{dm_{s,i}}{dt}\right) \tag{3.27}$$

where $W_{\mathrm{k,i}}$ marks the material fraction [-] and $m_{\mathrm{s,k,i}}$ is the mass of the material k in the domain i [kg]. Subscript k represents material fractions from now on. The solid mass balance for a single material fraction in the 1D control volume is similar to the ones used before

$$\frac{dm_{\mathrm{s,k,i}}}{dt} = \sum q_{m,\mathrm{s,k,in,i}} - \sum q_{m,\mathrm{s,k,out,i}} + \sum r_{\mathrm{s,k,i}} \tag{3.28}$$

where $q_{m,\mathrm{s,k,in,i}}$ represents the material flows into the control volume and $q_{m,\mathrm{s,k,out,i}}$ describes the material flows out of it [kg/s]. Heterogeneous reactions affecting the material fraction are marked with $r_{\mathrm{s,k,i}}$ [kg/s]. Applying Equations 3.2 and 3.28 to Equation 3.27 the material fraction derivatives can be solved as a function of the incoming flows and chemical reactions

$$\frac{dW_{k,i}}{dt} = \frac{1}{m_{s,i}}\left(\sum q_{m,\mathrm{s,k,in,i}} + \sum r_{s,k,i} - W_{k,i}\left(\sum q_{m,\mathrm{s,in,i}} + \sum r_{\mathrm{s,i}}\right)\right) \tag{3.29}$$

Four material fractions are solved at each time step including CaO, $CaCO_3$, $CaSO_4$ and ash. The relation of CaO and $CaCO_3$ changes based on carbonation and calcination. $CaSO_4$ is formed from sulphation and considered a stable compound in the calcium looping conditions. Ash is considered inert and increases in the reactor based on the fuel flow. Fly ash is ignored in the current approach. The amount of fly ash exiting the

reactor cyclones can be evaluated when more information on the ash particle size distribution is available. The purge of solids affects all the fractions in the first element of the calciner reactor. The make-up to the calciner can be defined as CaO or $CaCO_3$.

Because solid components are transferred also in the wall layer, material fractions have to be solved also in the wall layer. Heterogeneous reactions in the wall layer are ignored. Hence Equation 3.29 is simplified to

$$\frac{dW_{\mathrm{k,wl,i}}}{dt} = \frac{1}{m_{\mathrm{s,wl,i}}}\left(\sum q_{m,\mathrm{s,k,wl,in,i}} - W_{\mathrm{k,wl,i}} \sum q_{m,\mathrm{s,wl,in,i}}\right) \tag{3.30}$$

where $W_{\mathrm{k,wl,i}}$ represents the wall layer material fractions [-] and $q_{m,\mathrm{s,k,wl,in,i}}$ incoming material flows to the wall layer control volume [kg/s].

3.4 Solving the energy balance

Solving the energy balance in the calcium looping process is a critical aspect in the modelling because of the temperature dependency of the relevant reactions and the high temperature solid flows travelling between reactors. The general equation form for the energy balance can be written abiding the laws of continuity. In the following subchapters the different terms of the energy equation are broken down and explained. After that the derivative of temperature can be solved from the energy equation. The core and wall layer are treated separately as in the mass balance solution. The 1D control volume is fully mixed and at constant temperature and the output flows have the element temperature. The energy equation includes several phenomena associated with energy transfer: convective flows in solids $q_{\mathrm{conv,s}}$ and gases $q_{\mathrm{conv,g}}$ [J/s], dispersion between elements q_{disp} [J/s], heat transfer q_{ht} [J/s] and chemical reactions q_{chem} [J/s].

$$\frac{dE_{\mathrm{i}}}{dt} = \sum q_{\mathrm{conv,s}} + \sum q_{\mathrm{conv,g}} + \sum q_{\mathrm{disp}} + \sum q_{\mathrm{ht}} + \sum q_{\mathrm{chem}} \tag{3.31}$$

where E_{i} represents the energy present in the control volume [J].The left side of the energy equation represents the change of energy in the control volume and can be broken down into derivates of internal energy in the solid phase and gas phase

$$\begin{aligned}
&\frac{dE_{\mathrm{i}}}{dt} = \frac{dU_{\mathrm{s,i}}}{dt} + \frac{dU_{\mathrm{g,i}}}{dt} = \frac{d\left(m_{\mathrm{s,i}}u_{\mathrm{s,i}}\right)}{dt} + \frac{d\left(m_{\mathrm{g,i}}u_{\mathrm{g,i}}\right)}{dt} = \\
&\frac{d\left(m_{\mathrm{s,i}}\left(h_{\mathrm{s,i}} - p_{\mathrm{i}}v_{\mathrm{i}}\right)\right)}{dt} + \frac{d\left(m_{\mathrm{g,i}}\left(h_{\mathrm{g,i}} - p_{\mathrm{i}}v_{\mathrm{i}}\right)\right)}{dt} = \frac{d\left(m_{\mathrm{s,i}}c_{p,\mathrm{s}}T_{\mathrm{i}}\right)}{dt} + \frac{\left(m_{\mathrm{g,i}}h_{\mathrm{g,i}}\right)}{dt} = \\
&\frac{dm_{\mathrm{s,i}}}{dt}\underbrace{c_{p,\mathrm{s}}}_{\text{constant}}T_{\mathrm{i}} + \frac{dT_{\mathrm{i}}}{dt}m_{\mathrm{s.i}}c_{\mathrm{p,s}} + \underbrace{\frac{dm_{\mathrm{g,i}}}{dt}h_{\mathrm{g,i}}}_{0} + \frac{dh_{\mathrm{g,i}}}{dt}m_{\mathrm{g,i}}
\end{aligned} \tag{3.32}$$

where $U_{s,i}$ is the internal energy of the solid phase [J] and $U_{g,i}$ is the internal energy of the gas phase [J]. Specific internal energies of the two phases $u_{s,i}$ and $u_{g,i}$ [J/kg] can be written as a sum of the phase enthalpy ($h_{s,i}$ and $h_{g,i}$ [J/kg]) and work done by the phase ($p_i v_i$). The work term is neglected in both phases in the equation because pressure is assumed constant. Specific heat capacity of the solids in constant pressure $c_{p,s}$ [J/kgK] is considered constant in the modelling approach. Gas entalphy $h_{g,i}$ [J/kg] can be determined based on the gas composition and temperature using correlations. As previously stated, the gas mass change is ignored in the modelling approach. Solving the temperature derivate from Equation 3.31 and 3.32 and results in

$$\frac{dT_i}{dt} = \frac{\sum q_{convs+g} + \sum q_{disp} + \sum q_{ht} + \sum q_{chem} - \frac{dm_{s,i}}{dt} c_{p,s} T_i - \frac{dh_{g,i}}{dt} m_{g,i}}{m_{s,i} c_{p,s}} \tag{3.33}$$

3.4.1 Convective flows of the solid phase

Using the mass balance of solids the convective flow of energy alongside solids to the control volume can be written.

$$\begin{aligned} &\sum q_{convs} = \sum q_{convs,in} - \sum q_{convs,out} = \\ &\sum q_{m,s,in,i} c_{p,s} \left(T_{s,in} - T_{NTP}\right) + \sum q_{m,s,out,i} c_{p,s} \left(T_i - T_{NTP}\right) \end{aligned} \tag{3.34}$$

where $q_{conv,s,in}$ and $q_{conv,s,out}$ represent the convective flows of energy in and out of the control volume balance [J/s]. $T_{s,in}$ is the temperature of the incoming mass flows [°C] and T_{NTP} is the reference temperature of the system [°C]. Including the derivative of mass term from Equation 3.33 to Equation 3.34 and taking the solid heat capacity as a common denominator the equation is

$$\sum q_{convs} - \frac{dm_{s,i}}{dt} c_{p,s} T_i = c_{p,s} \left(\sum q_{m,s,in,i} T_{s,in} - \sum q_{m,s,out,i} T_i - \frac{dm_{s,i}}{dt} T_i \right) \tag{3.35}$$

Because the incoming mass flows equal the mass change and mass flows out, the equation can be reduced to

$$\sum q_{convs} - \frac{dm_{s,i}}{dt} c_{p,s} T_i = c_{p,s} \sum q_{m,s,in,i} \left(T_{s,in} - T_i\right) \tag{3.36}$$

3.4.2 Convective flows of the gas phase

Equally to the convective flows in solids, the terms describing the convective flows in gases can be broken down to incoming flows and exiting flows. The incoming flows can include primary, secondary and recirculation gas flows.

$$\sum q_{\mathrm{conv\,g}} = \sum q_{\mathrm{conv\,g,in}} - \sum q_{\mathrm{conv\,g,out}} = \sum q_{m,\mathrm{g,in,i}} h_{\mathrm{g,in}} - \sum q_{m,\mathrm{g,out,i}} h_{\mathrm{g,i}} \tag{3.37}$$

where $q_{\mathrm{conv,g,in}}$ and $q_{\mathrm{conv,g,out}}$ describes the convective energy flows in gases in and out of the control volume [J/s]. Adding the gas enthalpy change due to species change from the general energy Equation 3.33 to the previous equation results in

$$\sum q_{\mathrm{conv,g}} - \frac{dh_{\mathrm{g,i}}}{dt} m_{\mathrm{g,i}} = \sum q_{m,\mathrm{g,in,i}} h_{\mathrm{g,in}} - \sum q_{m,\mathrm{g,out,i}} h_{\mathrm{g,i}} - \frac{dh_{\mathrm{g,i}}}{dt} m_{\mathrm{g,i}} \tag{3.38}$$

where $h_{\mathrm{g,in}}$ is the enthalpy of the incoming flows [J/kg]. Gas enthalpies are defined in the model based on gas composition and temperature in the control volumes. Each gas component enthalpy is calculated in a subprogram with correlations acquired from literature (Barin, 1989). Correlations for gas enthalpies are fourth degree polynomials assuming all the flue gases behave like ideal gases. The enthalpy change in time can be defined as a function of the gas composition derivates

$$\frac{dh_{\mathrm{g,i}}}{dt} m_{\mathrm{g,i}} = m_{\mathrm{g,i}} \sum \frac{dw_{\mathrm{j}}}{dt} h_{\mathrm{j,i}} \tag{3.39}$$

where $h_{\mathrm{j,i}}$ is the gas component enthalpy [J/kg].

3.4.3 Energy transfer in chemical reactions

A significant term in the energy equation is the energy transfer due to chemical reactions. Chemical reactions taken into account in the energy equation include the combustion of char and volatiles, evaporation of moisture, carbonation, calcination and sulphation.

$$\sum q_{\mathrm{chem}} = \sum r_{\mathrm{c,i}} Q_i \tag{3.40}$$

where $r_{\mathrm{c,i}}$ is the chemical reaction term in the control volume [kg/s] and Q_i is the general reaction enthalpy [J/kg].
Table 3.2 lists all the chemical reaction terms and associated mass based reaction enthalpies. Diverting from standard marking, endothermic reaction enthalpies are marked now with the negative sign.

Table 3.2. Chemical reaction terms and associated reaction enthalpies.

Reaction	r_c [kg/s]	Q_i [MJ/kg]
Carbonation	$r_{carb,i}$	3.179
Calcination	$r_{calc,i}$	-1.780
Sulphation	$r_{sulp,i}$	8.966
Char	$r_{char,i}$	32.792
Evaporation	$r_{H2O,i}$	-2.501
CO	$r_{CO,i}$	10.106
CH_4	$r_{CH4,i}$	50.143
C_2H_4	$r_{C2H4,i}$	47.255
H_2	$r_{H2,i}$	120.913
NH_3	$r_{NH3,i}$	13.324
H_2S	$r_{H2S,i}$	15.239

The evaporation of inherent moisture and formed water through combustion is taken into account in the energy balance. The rates and effects of chemical reactions are discussed further in Chapters 3.5.2 and 3.5.3.

3.4.4 Energy transfer in turbulent dispersion

Because the 1D model cannot describe the details of a two-phase flow, a dispersion model has been incorporated into the model framework to model the mixing of energy between subsequent control volumes. Applying Fick's law of diffusion and the central difference method to the modelling approach, the results is the following equation pair

$$\sum q_{\text{disp}} = \underbrace{D_s c_{p,s} A_b \rho_{\text{ave}}^{-} \frac{dT_i^{-}}{dz}}_{\text{Dispersion with lower element}} + \underbrace{D_s c_{p,s} A_t \rho_{\text{ave}}^{+} \frac{dT_i^{+}}{dz}}_{\text{Dispersion with upper element}} \tag{3.41}$$

where D_s is the dispersion coefficient [m^2/s], $A_{b/t}$ is the cross section of the bottom/top element boundary [m^2] and $\rho_{ave}^{+/-}$ is the average density between calculation element and siding element [kg/m^3]. The dispersion coefficient is universal for the domain in this approach. The driving force for the dispersion of energy between elements is the temperature difference dT/dz and the average density between the control volumes.

3.4.5 Heat transfer

Heat transfer modelling is required when thermal power is extracted from the calcium loop. As mentioned in Chapter 3.2, heat can be extracted by several means from the reactor model boundary. Wall heat transfer can happen via refractory protected constant temperature wall $q_{ref,i}$ [J/s] or plain constant temperature wall $q_{plainw,i}$ [J/s] depending on the reactor internal structure. The model can also be defined as an insulated reactor.

Separate constant temperature heat transfer surfaces $q_{sh,i}$ [J/s] can be defined inside the reactor if necessary. The wall layer does not affect the wall heat transfer in this approach. The term for heat transfer in the energy equation is

$$\begin{aligned}&\sum q_{ht} = q_{ref,i} + q_{plainw,i} + q_{sh,i} = \\ &x_{ref,i} A_i \alpha_{tot,ref,i} \left(T_i - T_{ref,i}\right) + \left(1 - x_{ref,i}\right) A_i \alpha_{tot,plainw,i} \left(T_i - T_{plainw,i}\right) \\ &+ A_{sh,i} \alpha_{tot,sh,i} \left(T_i - T_{sh,i}\right)\end{aligned} \tag{3.42}$$

where $x_{ref,i}$ is the fraction of refractory in the wall area, A_i is the element wall area [m^2], $\alpha_{tot,ref,i}$ is the heat transfer coefficient into the refractory [W/m^2K], $T_{ref,i}$ is the refractory surface temperature [°C], $\alpha_{tot,plainw,i}$ is the plain wall heat transfer coefficient [W/m^2K] and $T_{plainw,i}$ is the plain wall temperature [°C]. The separate heat transfer surface has its own heat transfer area $A_{sh,i}$, heat transfer coefficient $\alpha_{tot,sh,i}$ [W/m^2K] and surface temperature $T_{sh,i}$ [°C]. In the current model the heat transfer is a secondary modelling objective and a simple model (Dutta and Basu, 2002) is used for all heat transfer coefficients

$$\alpha_{tot,ref,i} = \alpha_{tot,plainw,i} = \alpha_{tot,sh,i} = 5\rho_{s,i}^{0.391} T_i^{0.408} \tag{3.43}$$

Heat can be stored in the refractory protected wall, which requires that the derivatives for the local wall temperatures are solved. One-dimensional transient heat conduction through the refractory protected wall can be approximated by

$$\frac{\partial T}{\partial t} \rho_{ref} c_{p,ref} = \lambda_{ref} \frac{\partial^2 T}{\partial x^2} \tag{3.44}$$

where ρ_{ref} is the density [kg/m^3], $c_{p,ref}$ is the heat capacity [J/(kgK)] and λ_{ref} the heat conductivity of the refractory [W/(mK)]. The wall structure was discretized into four elements which allows the solution of four temperature gradients in the wall, Figure 3.10.

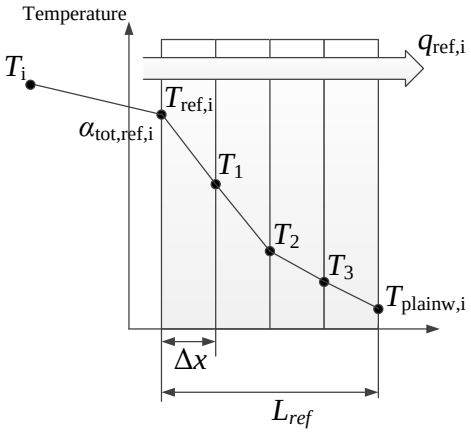

Figure 3.10. Discretization of the one-dimensional heat conduction in the refractory. L_{ref} represents the total length of the refractory.

The explicit solution for the wall surface temperature becomes

$$\frac{dT_{\mathrm{ref,i}}}{dt} = \frac{2\alpha_{\mathrm{tot,ref,i}}}{\rho_{\mathrm{ref}} c_{p,\mathrm{ref}} \Delta x}\left(T_{\mathrm{i}} - T_{\mathrm{ref,i}}\right) + \frac{2\lambda_{\mathrm{ref}}}{\rho_{\mathrm{ref}} c_{p,\mathrm{ref}} \left(\Delta x\right)^2}\left(T_1 - T_{\mathrm{ref,i}}\right) \tag{3.45}$$

where Δx is the refractory slice thickness [m]. The explicit solution for the rest of the refractory slices is

$$\frac{dT_{\mathrm{m,i}}}{dt} = \frac{2\lambda_{\mathrm{ref}}}{\rho_{\mathrm{ref}} c_{p,\mathrm{ref}} \left(\Delta x\right)^2}\left(T_{\mathrm{m+1,i}} + T_{\mathrm{m-1,i}} - 2T_{\mathrm{m,i}}\right) \tag{3.46}$$

Where m represents the refractory slice index. The thermal properties of the refractory are assumed constant. The width of the slice can be freely defined within the limits so that numerical diffusion is avoided. The constant temperature outside of the refractory is defined in the model input.

3.4.6 **Wall layer energy balance**

The wall layer transfers heat from the top to the bottom control volumes which means that an energy balance is required. The wall layer energy balance is formed only from the solid convection and therefore the analogy with the core solid convection term can be applied

$$\frac{dE_{wl,i}}{dt} = c_{p,s}\left(\sum q_{m,s,wl,in,i} T_{in,wl} - \sum q_{m,s,wl,out,i} T_{wl,i}\right) \tag{3.47}$$

where $E_{wl,i}$ is the energy stored in a wall layer control volume [J] and $T_{in,wl}$ is the temperature of the incoming flows to the wall layer control volume [°C].

$$\frac{dE_{wl,i}}{dt} = \frac{dU_{wl,i}}{dt} \approx \frac{d\left(m_{wl,i} c_{p,s} T_{wl,i}\right)}{dt} = \frac{dm_{wl,i}}{dt} c_{p,s} T_{wl,i} + \frac{dT_{wl,i}}{dt} m_{wl,i} c_{p,s} \tag{3.48}$$

where $U_{wl,i}$ is the internal energy in the control volume wall layer [J]. Solving wall layer temperature derivative and using the analogy to the core solid convection term results in

$$\frac{dT_{wl,i}}{dt} = \frac{c_{p,s} \sum q_{m,s,wl,in,i} \left(T_{in,wl} - T_{wl,i}\right)}{m_{s,wl,i} c_{p,s}} \tag{3.49}$$

3.5 Additional modelling of fluidized bed phenomena

Because the reactor model framework does not include a momentum equation solution and incorporates several heterogeneous reactions, additional semi-empirical models are required to successfully describe the phenomena present in a fluidized bed reactor.

3.5.1 Modelling of solid circulation

The prediction of solid circulation is more critical in the calcium looping process than in conventional fluidized beds because the looping ratio between reactors strongly affects the CO_2 capture efficiency and thermal balance. The modelling of solid entrainment was addressed already in Chapter 3.3.1 explaining the division of solid material in a fluidized bed reactor. In addition to that, the rate of solid material leaving the reactor is needed for the solution. A semi-empirical correlation was devised to approximate the solid mass flow out of the reactor $q_{m,s,exit}$ [kg/s]. Because the model does not solve the two-phase momentum equation, the semi-empirical approach has to be used to evaluate the solid circulation rate out of the reactor.

$$q_{m,s,exit} = \bar{\rho}_{s,exit} \bar{v}_{s,exit} A_{exit} = \varepsilon v A_{exit} \rho_{s,exit}^{b} \tag{3.50}$$

where $\rho_{s,exit}$ describes the average solid suspension density near the exit channel [kg/m^3] and $v_{s,exit}$ is the solid velocity in the exit channel region [m/s]. The slip coefficient between the gas and the solid particles is ε [-], A_{exit} is the cross section of the last element [m^2] and b is an empirical coefficient [-]. The slip coefficient is the relation of solid velocity and gas velocity. The average solid velocity and density in the exit region vary based on particle properties and reactor dimensions. The slip coefficient and

empirical coefficient *b* are model fit parameters and have to be evaluated experimentally.

3.5.2 Lime reactions

As previously stated, three lime related reactions are considered in the reactor model: carbonation, calcination and sulphation. Reaction rate equations have been devised for each reaction.

The ability of the material to capture carbon dioxide decreases over repeated carbonation and calcination cycles which is caused by the structural change of particles as discussed in Chapter 2.3. This has to be taken into account in the carbonation reaction either by modelling both of the kinetic and diffusion reaction regimes or using a more simple approach which is the case here. An average maximum carrying capacity has been defined for the whole material which means that the carbonate content of the solids cannot exceed a certain limit. Figure 3.11 illustrates the carbonation modelling approach.

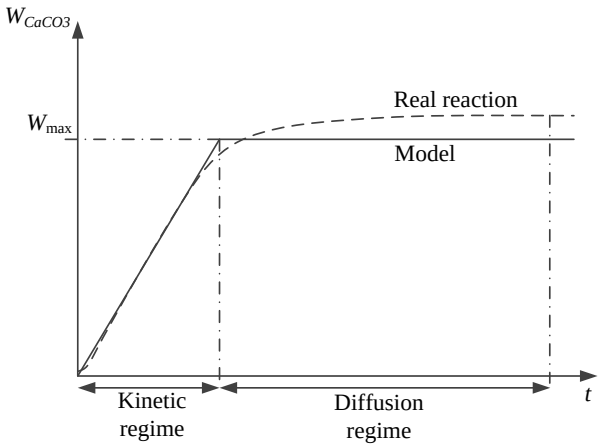

Figure 3.11. Modelling of the carbonation reaction. Reaction rate for carbonation is the slope of the model curve. After the maximum carbonation content is reached, the carbonation rate is zero. In reality the reaction will continue on with diffusion if residence time of the reactor is extended.

The carbonation model assumes the carbonation reaction to end after the maximum carbonate content is reached.

The carbonation reaction rate $r_{carb,i}$ [kg/s] equation has been modified from the approach of Shimizu et al. (1999) and Alonso et al. (2009)

$$r_{\mathrm{carb,i}} = m_{\mathrm{s,i}} k_{\mathrm{carb,i}} \left(W_{\max} - W_{\mathrm{CaCO3,i}}\right)\left(C_{\mathrm{CO2,i}} - C_{\mathrm{CO2,eq}}\right) \tag{3.51}$$

where $k_{\mathrm{carb,i}}$ is the kinetic coefficient for carbonation [m^3/(kmol s)], $W_{\max}$ is the maximum content of calcium carbonate in the solids [-], $W_{\mathrm{CaCO3,i}}$ is the carbonate content of the solids in the element [-], $C_{\mathrm{CO2,eq,i}}$ is the equilibrium CO_2 molar concentration in the element [kmol/m^3] and $C_{\mathrm{CO2,i}}$ is the molar concentration of CO_2 in the element [kmol/m^3]. The equilibrium molar concentration can be determined from the ideal gas law and Equation 2.2. The kinetic coefficient is determined based on the limestone type and surrounding temperature.

The maximum carbonate content in the solids is a transient variable depending on the history of the particles, Figure 2.9. In the current modelling approach, the parameter is given as an input but in the future, dynamic calculation of that variable as a function of the looping ratio and make-up flow is necessary.

Calcination is the opposite reaction of carbonation and in terms of reaction rate, much faster than the diffusion limited carbonation. Martínez et al. (2012a) stated that for particles sizes below 300 µm, thermal conduction and gas diffusion in the particles during calcination is negligible. This means that in calcium looping applications, calcination is fairly fast, and the only concern is the ambient temperature and CO_2 partial pressure. A calcination reaction rate $r_{\mathrm{calc,i}}$ [kg/s] equation was applied from the approach of Fang et al. (2009)

$$r_{\mathrm{calc,i}} = m_{\mathrm{s,i}} k_{\mathrm{calc,i}} W_{\mathrm{CaCO3,i}}^{2/3} \left(C_{\mathrm{eq,CO2,i}} - C_{\mathrm{CO2,i}}\right) \tag{3.52}$$

where $k_{\mathrm{calc,i}}$ is the kinetic coefficient for calcination [m^3/(kmol s)] which is determined based on temperature and limestone properties.

The sulphation reaction can happen via two mechanisms in the high temperature fluidized bed reactor: indirectly with CaO or directly with $CaCO_3$. Currently only indirect sulphation is considered in the reactor model. The indirect sulphation reaction rate equation $r_{\mathrm{sulf,i}}$ [kg/s] was fitted from de-Souza Santos (2010)

$$r_{\mathrm{sulf,i}} = m_{\mathrm{s,i}} W_{\mathrm{CaO,i}} k_{\mathrm{sulf,i}} w_{\mathrm{SO2,i}} w_{\mathrm{O2,i}} \tag{3.53}$$

Where $W_{\mathrm{CaO,i}}$ represents the calcium oxide material fraction in the solids [-], $k_{\mathrm{sulf,i}}$ is the kinetic coefficient of sulfation [1/s], $w_{\mathrm{SO2,i}}$ is the gas mass fraction of sulphur dioxide [-] and $w_{\mathrm{O2,i}}$ is the gas mass fraction of oxygen [-]. Sulphation is an equilibrium reaction but the reverse reaction is assumed negligible in the process.

3.5.3 Combustion

Combustion of solid fuels in fluidized beds is a fairly well researched area and the mechanisms are well known. In the case of the calcium looping process model, combustion is a secondary modelling objective. A simple combustion model was applied from the approach of Myöhänen (2011) to describe the oxy-combustion of solid fuels in the calciner reactor. The combustion model divides the fuel into combustible components, moisture and ash based on the ultimate and proximate analysis of the fuel. The base elements carbon, nitrogen, hydrogen, oxygen and sulphur are divided between char and volatiles of the fuel with correlations proposed by Myöhänen (2011). Oxygen in the fuel is assumed to be released with volatiles. When base elements in the volatiles are known, volatile gases can be formed based on the molar relations of carbon-oxygen and carbon-hydrogen. Carbon binds primarily oxygen forming carbon monoxide and carbon dioxide. Nitrogen and sulphur bind primarily hydrogen forming hydrogen sulphide and ammonia. Leftover carbon and hydrogen in the volatiles form methane and ethene. Any leftover hydrogen forms gaseous hydrogen. Volatile gases are assumed to follow the ideal gas law. Evaporation of moisture is assumed to be instantaneous. The general frame for the combustion model is illustrated in Figure 3.12.

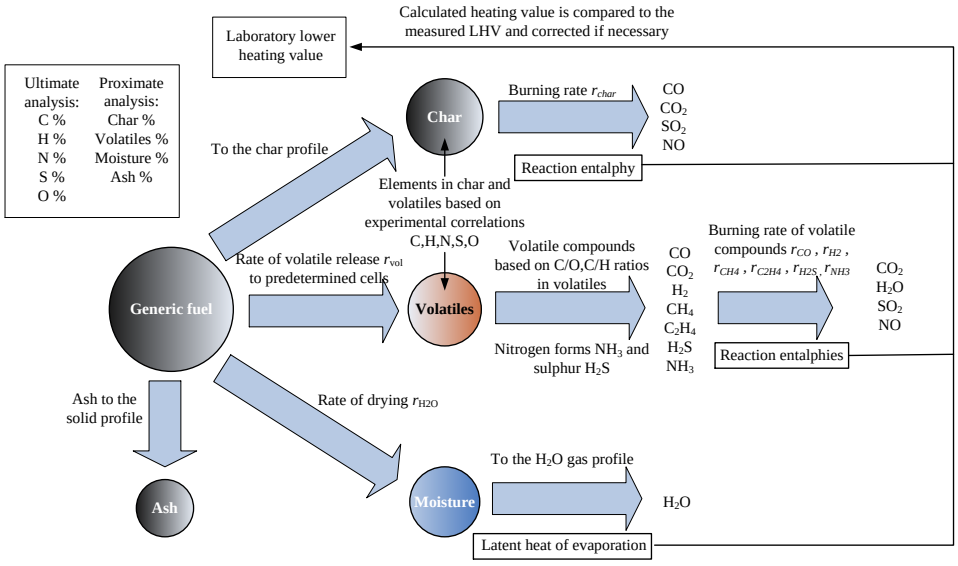

Figure 3.12. General frame for the combustion model.

The correlations for the division of elements H, N and S to char and volatiles are (Myöhänen, 2011)

$$\frac{H_{\text{char}}}{H} = 0.52 \cdot e^{-33\frac{H}{C}} \tag{3.54}$$

where H_{char} is the elemental hydrogen in char, H is the elemental hydrogen in the fuel and C is the elemental carbon in the fuel in mass fractions [-]; similarly

$$\frac{N_{\text{char}}}{N} = 0.088 \cdot w_{\text{char,daf}}^{0.6} \left(\frac{N}{C}\right)^{-0.6} \tag{3.55}$$

where N_{char} is the elemental nitrogen in char, N is the elemental nitrogen in the fuel in mass fractions [-] and $w_{\text{char,daf}}$ is the mass fraction of char in dry and ash free fuel [-] and

$$\frac{S_{\text{char}}}{S} = 0.14 \cdot w_{\text{char,daf}}^{0.2} \left(\frac{H}{C}\right)^{-0.6} \tag{3.56}$$

where S_{char} is the elemental sulphur in char and S is the elemental sulphur in the fuel in mass fractions [-]. Carbon in the char can be determined by assuming all the elemental oxygen forming volatiles and subtracting according to the char mass balance

$$C_{\text{char}} = 1 - S_{\text{char}} - N_{\text{char}} - H_{\text{char}} \tag{3.57}$$

where C_{char} is the elemental carbon in char in mass fractions [-].

Reaction rates for char and volatiles are acquired from literature. The reaction rate for char combustion $r_{\text{char,i}}$ [kg/s] in a fluidized bed unit was applied from the approach of Basu (2006)

$$r_{\text{char,i}} = m_{\text{char,i}} k_{\text{char,i}} p_{\text{O2,eff,i}}^{n} \tag{3.58}$$

where $m_{\text{char,i}}$ is the char mass in the control volume [kg], $k_{\text{char,i}}$ is the kinetic coefficient of the char combustion [1/(Pa s)] and $p_{\text{O2,eff,i}}$ is the effective partial pressure of oxygen in the control volume [Pa]. The reaction order n is assumed to be 1. The effective partial pressure term has been applied because the mass transfer in the microscale of the char particle is limited. The effective partial pressure of oxygen has been defined in the model as a function of the oxygen partial pressure and the char-gas contact coefficient φ [-] which is a modelling parameter

$$p_{\text{O2,eff,i}} = \varphi p_{\text{O2,i}} \tag{3.59}$$

The general reaction rate equation for volatiles is applied from De-Souza Santos (2010) and parameters from various sources (Vilienskii and Hezmalian, 1978; Branch and Sawyer, 1973; Leveson, 1997; Quan et al., 1973)

$$r_{\mathrm{g,vol,i}} = m_{\mathrm{g,vol,i}} k_{\mathrm{g,vol,i}} \frac{1}{T_{\mathrm{i}}^{d}} C_{\mathrm{vol,i}}^{a} C_{\mathrm{O2,i}}^{b} C_{\mathrm{x,i}}^{c} \tag{3.60}$$

where $r_{\mathrm{g,vol,i}}$ describes the general reaction of a volatile [kg/s], $k_{\mathrm{g,vol,i}}$ is the kinetic coefficient of a volatile [$\mathrm{m^3K^d/(kmol\ s)}$], $C_{\mathrm{vol,i}}$ is the molar concentration of the reacting gas [$\mathrm{kmol/m^3}$], $C_{\mathrm{O2,i}}$ is the molar concentration of oxygen and $C_{\mathrm{x,i}}$ is the molar concentration of a participating gas. The effect of participating gases is taken into account in some reactions for example in the combustion carbon monoxide where steam partial pressure has some effect. Empirical coefficients and reaction order variables are listed as a, b, c, and d [-]. A time derivate for the release of volatiles is solved at each time step. The time constant of the volatile release τ_{vol} is set as input and is dependent on the fuel properties.

$$\frac{dr_{\mathrm{vol}}}{dt} = \frac{q_{\mathrm{m,fuel}} w_{\mathrm{vol}} - r_{\mathrm{vol}}}{\tau_{\mathrm{vol}}} \tag{3.61}$$

where $q_{\mathrm{m,fuel}}$ is the fuel mass flow [kg/s], w_{vol} is the mass fraction of volatiles in the fuel [-] and r_{vol} is the general volatile release rate [kg/s]. In practise, the release rate of volatiles changes only if the fuel mass flow is changing over time.

The effect of combustion to the energy balance was discussed in Chapter 3.4.3. The local effect of volatile and char combustion is calculated based on the reaction rates and reaction enthalpies. The combined heat generated from the combustion is compared to the laboratory measured lower heating value of the fuel times the fuel flow and if the values differ, a normalization factor is applied.

3.6 Modelling of the solid return system

In addition to the reactor models, carbonator and calciner, the calcium looping process requires a solid return system to successfully separate gas from solid and ensure solid circulation between the reactors. Simple models of the solid return system have been built to the Matlab Simulink model. The purpose of the solid return system models is to represent the transient effect of the return system on the whole loop, Figure 3.13.

Reactions and fluidized bed behaviour in the cyclone, standpipe and loop seals are ignored. Heat transfer through a refractory protected wall is included in the return system modelling similarly to the reactor model. This is done due to the fact that industrial sized cyclones and loop seals might include heat transfer surfaces or cooling. Equations 3.45 and 3.46 are applied in the return system heat transfer modelling. Limited spatial discretization is possible in order to describe temperature differences in the solid return system.

The time delay of solids in the return system during transient states can be modelled by defining a time constant for the solid return system. However, only steady-state cases have been modelled in this thesis and this feature has not been utilized.

Simulation parameter γ_{return} for the solid recirculation defines the ratio of solids returning to the originating reactor. The design and operation of the loop seals will have a great effect on the efficiency of calcium looping system as described in later chapters.

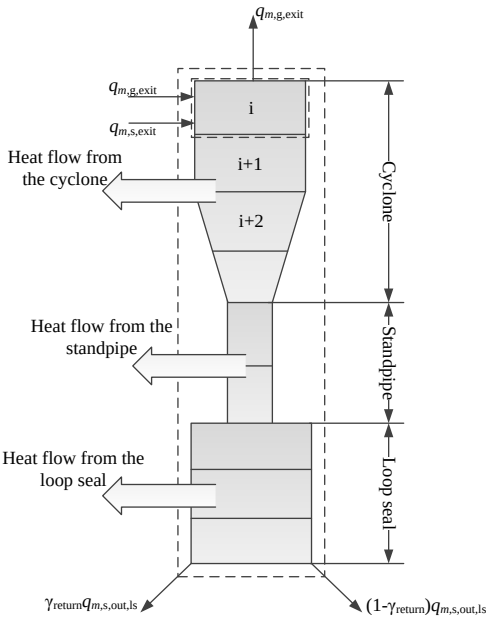

Figure 3.13. The overall model for the solid return system.

The cyclone model is assumed to operate at 100 % efficiency in the current approach but the separation efficiency can be evaluated with experimentally determined fit parameters if needed.

4 Applying the model to a laboratory scale calcium looping unit

In this section the essential results from Ylätalo et al. (2012) are presented. The simulation case was based on the 30 kW calcium looping test rig of INCAR-CSIC situated in Oviedo, Spain. The rig consists of two circulating fluidized bed reactors with the heights of 6500 mm and diameters of 100 mm, Figure 4.1.

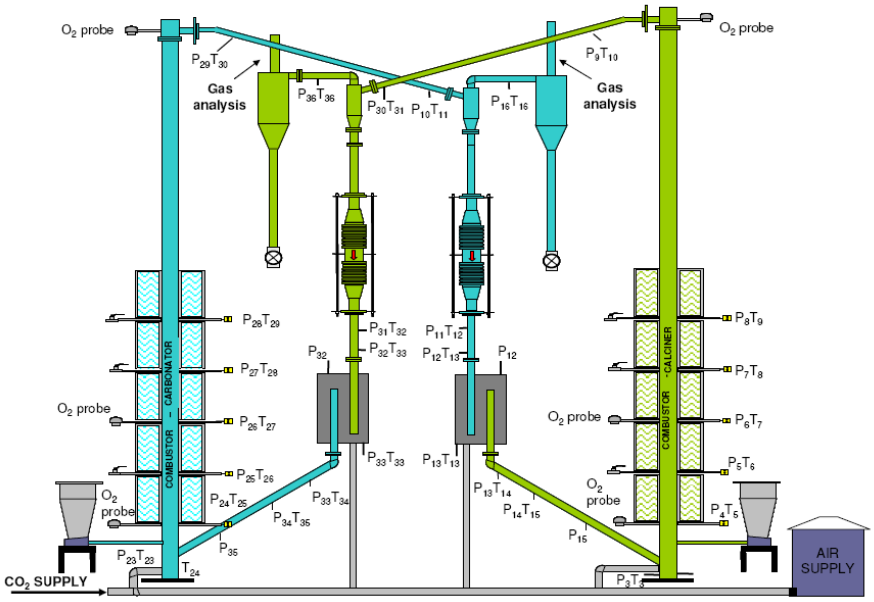

Figure 4.1. Illustration of the INCAR-CSIC 30 kW calcium looping rig (courtesy of D.Sc. Carlos Abanades, INCAR-CSIC Spain)

The operating temperatures of the reactors were 650 ºC in the carbonator and 700–800 ºC in the calciner in a nitrogen atmosphere. An accurate description of this test facility and test setup is given by Alonso et al. (2010). An early version of the 1D dynamic model was simulated and the results compared to the laboratory scale unit results. The comparison was done by selecting points from the measurements where the system operated at steady-state and operational parameters remained nearly constant for extended periods of time. Operational parameters from the experiments were introduced into the model and the system was simulated to a steady-state. The main parameters of the simulation are presented in Table 4.1.

Table 4.1. Input parameters for the laboratory scale simulation case

Parameter	Value
Input gas mass flow [kg/s]	0.0068
Input gas temperature [ºC]	20
Input gas CO_2 [w-%]	18.1
Input gas O_2 [w-%]	17.2
Input gas N_2 [w-%]	64.7
Input gas H_2O [w-%]	0.0
Solid mass in the reactor [kg]	1.2-2.0
Average particle diameter [µm]	100
Apparent solid density [kg/m^3]	1800
Maximum carrying capacity [w-%]	13.4
Calciner temperature [ºC]	800
Height of the carbonator [m]	6.5
Diameter of the carbonator [m]	0.1

The parameters not available from the experiments were evaluated based on literature and previous knowledge of the fluidized bed processes. The study of the results concentrated on the carbonator reactor since most of the experimental work examined its behaviour at that time (Rodriguez et al., 2011). With the experimental data available, the study of the capture efficiency and carbonator reactor temperature profile was conducted. Fluidizing gas mass flow rate and properties were set based on the experiments and were kept constant during the simulations. Particle diameter and density were assigned from the publication describing the experimental setup (Alonso et al., 2010). Solid slip coefficient and experimental exponent from Equation 3.50 were adjusted to match with the average solid circulation rate observed in the experiments. The maximum carrying capacity of the solid material was set to 13.4 w-% which is a typical value for material that has undergone several carbonation calcination cycles determined from the sample analysis of the solid material. Heat losses from the reactor were estimated by having a thick insulation around the unit and setting a surface temperature for the outside surface. The calciner was not simulated during the carbonator model validation. The carbonator content of the solids and temperature of the circulated material coming from the calciner were set as inputs. These values were received from the experiments. Internal circulation and dispersion parameters were selected by comparing the model temperature profile shape to the experimental profile. It was confirmed that the modelled temperature profile agrees with the experimental one, when the dispersion coefficient and wall layer flow are very low and consequently the horizontal backflow from the wall layer to the central core was also set zero. Because of the high aspect ratio of the experimental unit, it is reasonable to assume that the lateral effects are minimal. The validity of the reaction rate model was tested by comparing the capture efficiency as a function of solid inventory between the simulations and experiments for the given inputs, Figure 4.2.

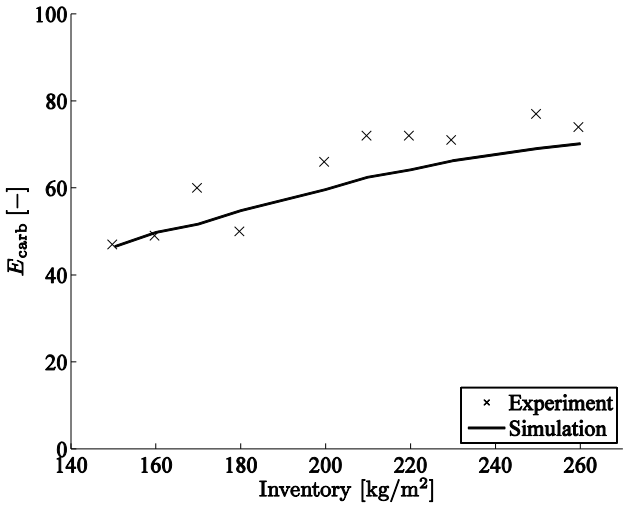

Figure 4.2. Capture efficiency as a function of carbonator reactor inventory per unit area. Model results compared to the laboratory scale unit results.

As expected, the capture efficiency increases steadily when solid inventory is added for a given CO_2 feed. The simulated capture efficiencies show good agreement with the experiments. Although the capture efficiencies are well predicted, the temperature of the lower bed is over-predicted in the simulations when the inventory increases, Figure 4.3.

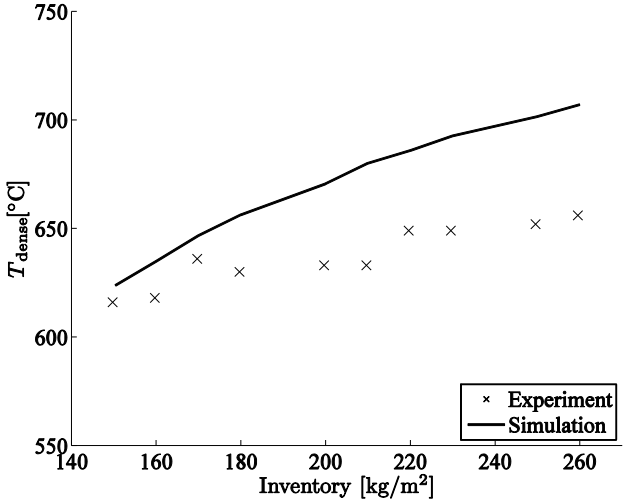

Figure 4.3. Carbonator average dense bed temperature from the experiments and simulations plotted as a function of solid inventory per unit area.

This discrepancy is mainly caused by the fact that the cooling of the experimental carbonator was done in practise by removing the insulation, when the temperature of the reactor increased. These changes were not included in the model calculations. The lower bed temperature has a considerable effect on the carbonator performance because the majority of the active material is situated there. If the temperature rises over the equilibrium condition, a sharp decrease in the capture efficiency will be experienced. This will eventually happen if inventory is added and no cooling is introduced to the reactor. In larger scales, evaporator surfaces or internal heat exchangers will be necessary to control the carbonator temperature in the desired region. In Figure 4.4 the vertical temperature profile of the carbonator is presented with two different inventories.

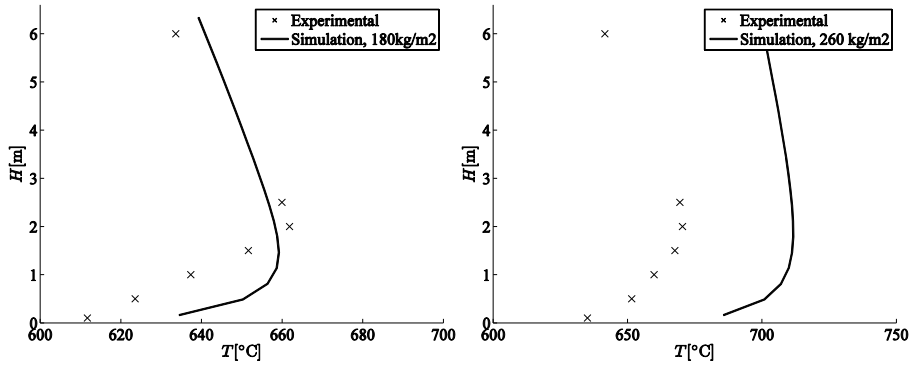

Figure 4.4. Vertical temperature profile of the carbonator with different solid inventories. Heat generated by carbonation increases with higher inventory which should be compensated by cooling.

The lower inventory profile agrees well with the temperature measurements from the experimental rig. With the higher inventory, the simulated temperature profile moves away from the ideal region, but preserves the similar shape as in the experiment. In the experiments, the insulation was removed, which lowered the temperature. Better agreement could have been seen, if the insulation properties of the model would have been changed accordingly. In the model, the details of changes in the insulation materials were not considered in the thermal boundary conditions and that is why the simulated temperature curve is higher than the measured. In Figure 4.5, the vertical $CaCO_3$ profile is presented for the 180 kg/m^2 inventory simulation. In the dense lower region, $CaCO_3$ content reaches quickly the theoretical limit defined by the active solids in the system. With no experimental information on the $CaCO_3$ content of solids, the intensity of the solid mixing had to be determined from the incoming and leaving $CaCO_3$ fractions in the solids with the help of pressure, and temperature profiles. Ultimately, the construction and fluidization mode of the reactor will determine how the core-wall layer flow is formed. The role of the wall layer-core phenomenon needs to be

studied in larger units, where the aspect ratio allows more solid movement in the horizontal direction.

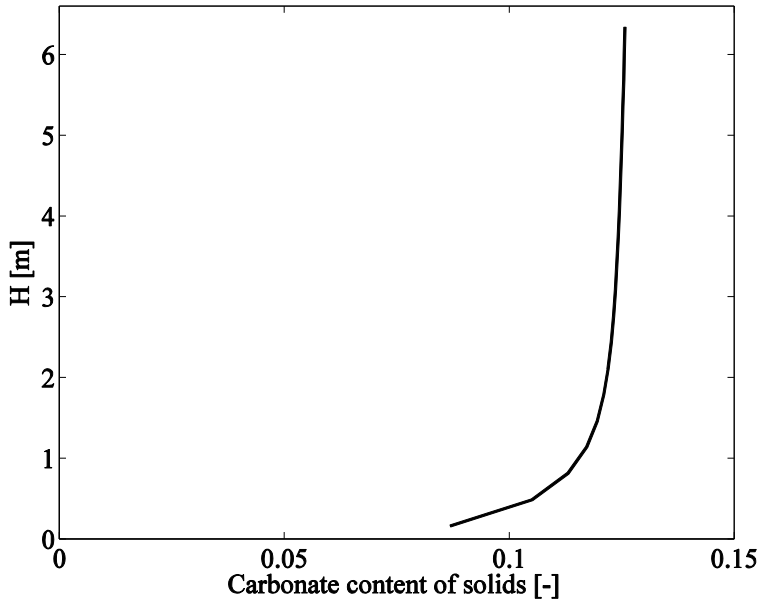

Figure 4.5. Fraction of calcium carbonate in the solids as a function of height. The majority of the carbonation occurs in the bottom bed region where active solids are plentiful.

Overall, the first attempt to validate the 1D model framework resulted in good information on the carbonator and small laboratory scale unit behaviour. Although the model includes experience based correlations, the model was able to calculate a small high-aspect ratio carbonator. The relevant phenomena and new development areas for the model were identified.

5 Modelling of a pilot scale calcium looping unit

The second modelling study presented in Ylätalo et al. (2013) concentrated on a calcium looping pilot plant. The calciner reactor of the pilot plant was analysed with two modelling approaches. After that, the interconnected behaviour of the carbonator and calciner was examined. The analysis was concerned the 1.7 MW calcium looping pilot plant located in Spain, Figure 5.1 (Sánchez-Biezma et al., 2011).

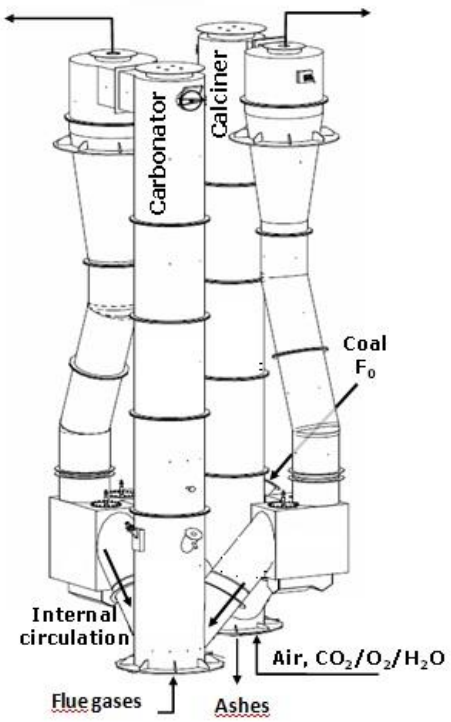

Figure 5.1. 3D isometric view of the 1.7 MW_{th} pilot plant courtesy of the CaOling project coordinator Andres Sánchez-Biezma Sacristian. Reactors are 15 m high with interconnected dual loop seals.

The main operating parameters used in this calculation case are listed in Table 5.1.

Table 5.1. Pilot plant operational and calculation parameters.

Parameter	Carbonator	Calciner
Height [m]	15	15
Diameter [m]	0.65	0.75
Solid inventory [kg]	~450	~350
Gas mass flow [kg/s]	0.35	0.4
Input gas O_2 [w-%]	6	40
Input gas CO_2 [w-%]	23	60
Input gas N_2 [w-%]	63	0
Input gas H_2O [w-%]	9	0
Input gas temperature [ºC]	120	50
Fuel flow [kg/s]	0	0.01-0.07
Fuel LVH [MJ/kg]	29	29
Average solid diameter [µm]	100	100
Average solid density [kg/m^3]	1800	1800
Carbonator cooling [kW]	0-800	-
Maximum carrying capacity [w-%]	15	15
Solid slip coefficient of the reactor [-]	0.8	0.8
Recirculation percentage [%]	0-100	0-100

The whole process is simulated with the 1D model, whereas in the 3D model only the calciner is modelled. The simulated solid circulation rate, fraction of $CaCO_3$ in the solid material and the solid temperature acquired from the 1D carbonator are used in the 3D calciner as inputs. One reasonable operation point was selected and the operation of the calciner was studied using both models. The simulation results were compared and validity of the models was studied. After that the recirculation of solids was adjusted gradually in the 1D model to find the optimal operation conditions which will minimize the fuel and oxygen consumption of the calciner and still keep the capture efficiency of the process on a reasonably high level. In Chapter 5.1 in the reference case calculation 60 % of the exiting material was recirculated back to the originating reactor and 40 % was circulated to the other reactor. In Chapter 5.2 the effect of recirculation on the process is examined more closely.

A detailed description of the 3D model can be found from Myöhänen (2011). The CFB3D model code combines fundamental balance equations with empirical correlations. CFB3D has been developed to model industrial scale CFB units, and it can be used as a tool for optimization, trouble-shooting and risk assessment studies. The model frame includes a three-dimensional description of the furnace which is linked to sub-models describing the hot loop processes of the CFB boiler: separators return legs and possible external heat exchangers. In the model, the calculation mesh is structural with hexahedral calculation cells. The furnace is modelled three-dimensionally by applying a control volume method to discretize and solve the various balance equations

in a steady state condition. The first order upwind differencing scheme and the Gauss–Seidel method with successive overrelaxation are used to solve the balance equations which include total gas and total solids. Model framework also includes fuel reactions and species, sorbent reactions and species ($CaCO_3$, CaO, $CaSO_4$ and inert), homogeneous reactions and gaseous species. Energy equation includes heat transfer within the gas–solid suspension and to surfaces.

5.1 Comparison of the 1D and 3D simulation results for the calciner

In the comparison of the 1D and 3D models, the thermal power of the calciner was 1.58 MW, the recirculation percentage 60 % and the carbonator cooling power was 420 kW. Other operation conditions for the studied case are given in Table 5.1. The calculated solid circulation rate for this case was 4.54 kg/s for the 1D model and 4.56 kg/s for the 3D model with a 2.9 m/s superficial gas velocity. Solid inventories in the calciner reactors were 259 kg in the 1D and 262 kg in the 3D model.

Figure 5.2 (a) presents the vertical temperature profiles averaged over the calciner cross section calculated with both models. The trends of both reactors are close to each other and the values range between 5-10 ºC. Small differences in the temperature profiles can be explained mainly by the fundamental differences between the models. The 3D-model which has a more dense calculation mesh takes into account more physical phenomena and more initial variables need to be defined and also some lateral effects are present. Figure 5.2 (b) presents a 3D image of the temperature and horizontal temperature gradients can be observed near to the material feed points of the calciner, even though the overall behaviour of the reactor can be considered 1D. In larger units, the complexity of the 3D-model is expected to be more realistic, demonstrating the effect of local gradients on the whole process. The temperature of the calciner is in the bottom area below calcination conditions because of the cold flow solid coming from the carbonator. At the height of the fuel inlet, however the temperature rises quickly to the calcining conditions.

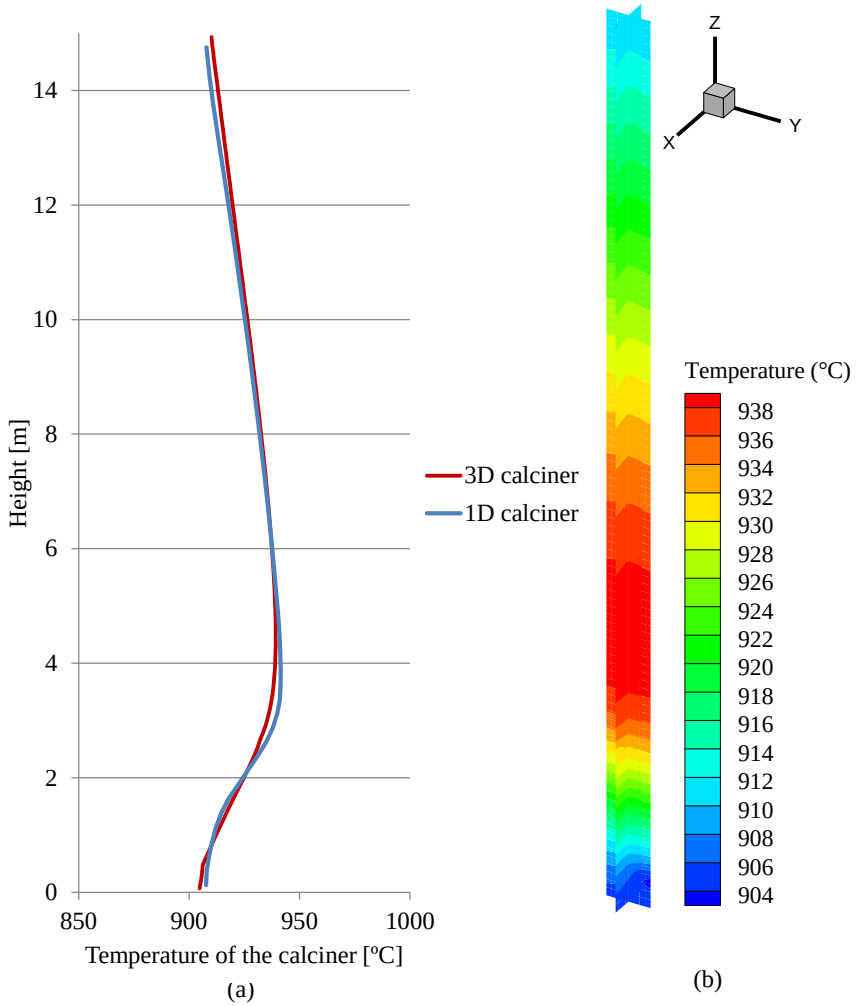

Figure 5.2. (a) Temperature profiles of the pilot plant calciner from 1D and 3D models and (b) 3D temperature contours of the calciner.

Figure 5.3 (a) presents the average vertical profile of the molar fraction of CO_2 in the gases in the 1D and 3D simulations. The adjacent Figure 5.3 (b) illustrates the 3D molar fraction of CO_2 in the gases. From the development of the CO_2 profile, it can be concluded that the calcination and combustion are very fast when the temperature reaches 890-900 ºC at the current oxy-fuel conditions. Maintaining high enough temperature is the most important factor in achieving full calcination if mixing is sufficient and particles are small enough that diffusion is not limiting calcination. The

vertical CO_2 profiles match quite well indicating that both the 1D and 3D models predict similar calcination behaviour in these conditions. Some differences can be noticed in the fuel inlet area which can be explained by the simplifications made in the 1D combustion model.

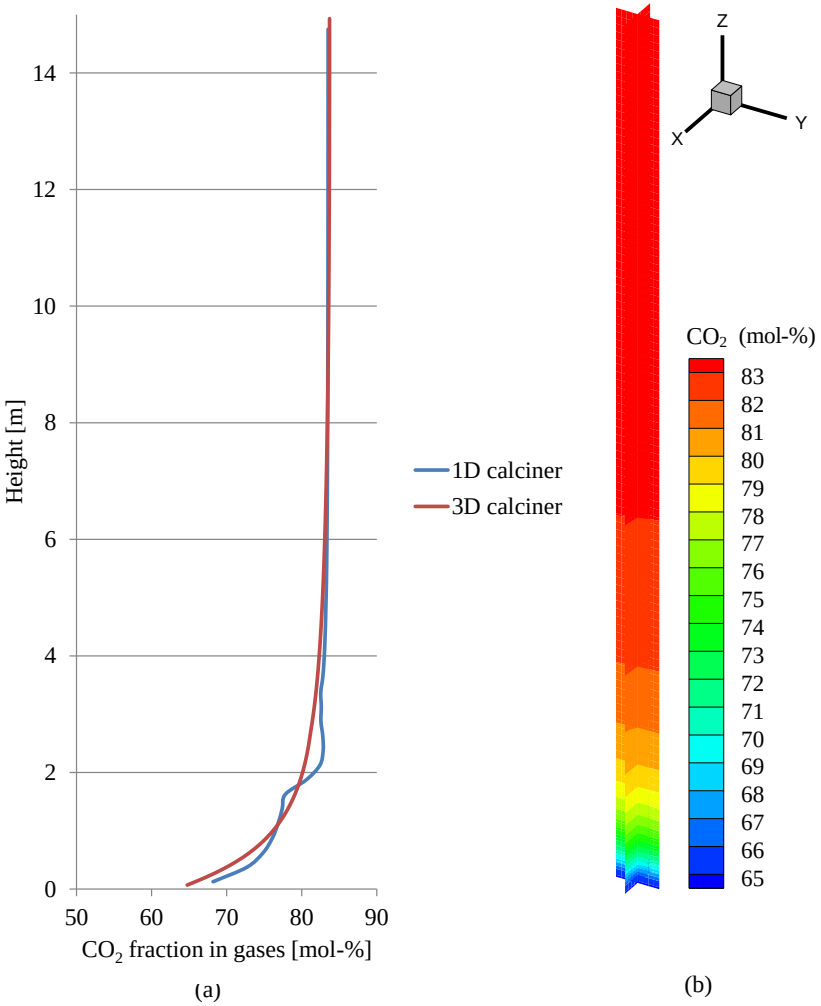

Figure 5.3. (a) CO_2 molar fraction in calciner flue gases in the 1D and 3D models and (b) 3D contours of the CO_2 molar fraction in flue gases.

Figure 5.4 (a) describes the vertical development of the fraction of $CaCO_3$ in the solids in both models. From the figure it can be concluded that the majority of the calciner

reactions occur within the first 3-4 m from the bottom. The depletion of $CaCO_3$ in the solids demonstrates the speed of the calcination reaction for solids. The 1D profile demonstrates that the calcination reaction and strong mixing in the fluidized bed drives the fraction of $CaCO_3$ close to zero; in other words full calcination is achieved. Differences between the models are small, but the gradients in the bottom area are higher in the 1D model because of the larger control volumes in the vertical direction. In Figure 5.4 (b) 3D contours of the $CaCO_3$ concentration are shown. Despite the asymmetry at the bottom where the inlet of $CaCO_3$ from the carbonator is clearly shown, the mixing is very intense and the overall behaviour of the studied calciner can be described using a 1D assumption.

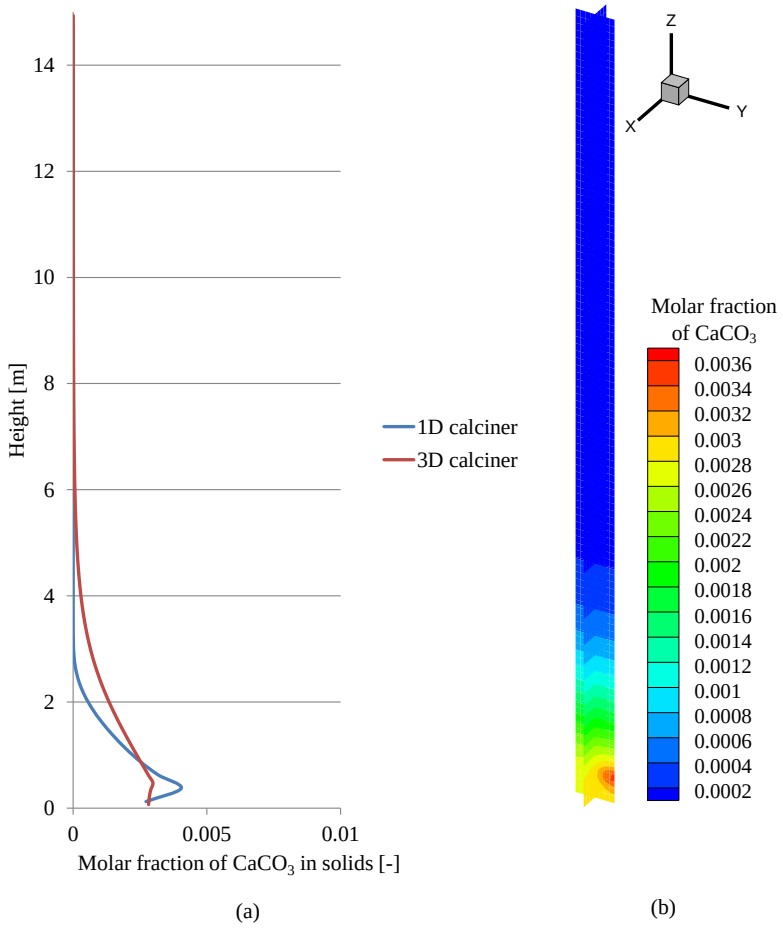

Figure 5.4. (a) 1D profile of the molar relation of calcium carbonate in the solids compared between the 1D and 3D models and (b) 3D contours of calcium carbonate molar fractions in the calciner reactor. The low $CaCO_3$ content suggests a very fast calcination rate.

5.2 The effect of solid circulation on capture efficiency

After the validation of the 1D model using the 3D model results, the 1D-model was used to simulate ten different recirculation values ranging from no recirculation to all the solid material being recirculated. The system parameters were the same as those previously presented for the 1D and 3D comparison case; only here, the calciner thermal power and carbonators cooling were modified. The fuel feed was adjusted to keep the calciner operating at the correct temperature. The oxygen to carbon dioxide molar ratio was kept constant although the need for oxygen decreased when fuel feed decreased. The carbonator reactor was simulated alongside the calciner to predict the carbonate content in the solids and temperature of the solids entering the calciner. Figure 5.5 presents the capture efficiency of the system, the calcination efficiency, the thermal power of the calciner and the carbonator cooling power as a function of solid recirculation.

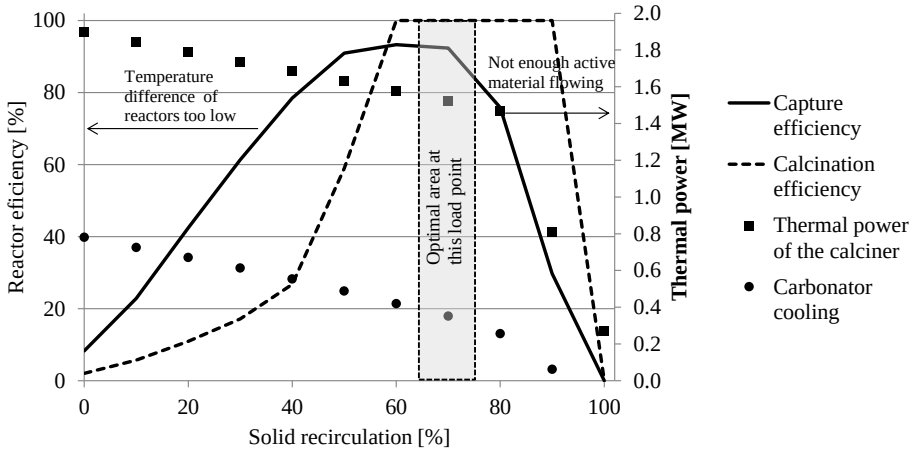

Figure 5.5. Carbonation and calcination efficiency plotted as a function of solid recirculation (left hand side axis). Thermal power and carbonator cooling requirement (right hand side axis) plotted also as a function of solid recirculation.

With no solid recirculation, achieving a high enough temperature difference between the reactors is difficult regardless of the extensive fuel feeding and carbonator cooling. When the recirculation is low the temperature of the calciner is too low and the temperature of the carbonator is too high for the carbonation conditions. In contrast, with very high recirculation, the amount of material traveling between reactors is lower so less active CaO is available for CO_2 capture. However, it is good to notice that the results presented here apply mainly to the construction used in the studied pilot plant. With a different construction and appropriately designed heat integration of the reactors,

it could be possible to operate the calcium looping process with good capture efficiency also without solid recirculation.

Figure 5.6 presents the values of solid fluxes out of the reactors in the different cases. It has to be noted that the solid fluxes start to change when the recirculation becomes very high. This is because the gas velocity in the calciner is decreasing due to the lower volumetric gas flow. In the same figure the molar flow of CaO is compared to the molar flow CO_2 arriving to the carbonator. The recirculation is taken into account when calculating the molar flow of CaO to the carbonator. It seems that although the flux of CaO the carbonator is high in the no recirculation case, the low calcination rate creates a lack of active CaO in the carbonator which can be seen also in Figure 5.5. Based on Figure 5.5, it can be determined that the optimal recirculation ratio in the studied case is around 60-70 % to achieve over 90 % capture efficiency for this operation point. It has to be noted that the solid circulation rate in the studied case is so high, around 3.0-4.6 kg/s, that the calcination efficiency does not have to be 100 % to achieve good capture efficiencies in the carbonator. Also the linear decrease of fuel feeding and cooling is not the best possible option in this case. With high recirculation ratios the calciner temperature starts rising rapidly which confirms that the calcium loop is not operating properly. With lower recirculation values the calcination efficiency could have been raised to 100 % with high thermal power but due to the fact that the practical cooling power is limited the temperature difference between the reactors would still have been too low for the carbonation process to take place. If the economy of the process is to be studied in more detail each point should be optimized case by case to find the lowest fuel consumption to cooling ratio. In addition, the optimal area of the recirculation will change depending on the capture load of the calcium looping process.

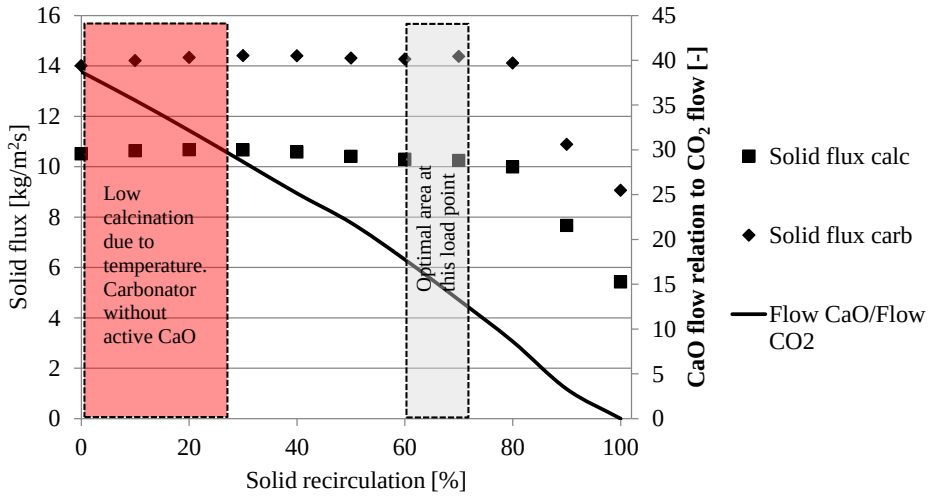

Figure 5.6. Solid flux out of the reactors plotted as a function of solid recirculation. Solid flux out of the reactors does not change until the calciner gas flow starts to drop after the fuel flow

drops. Flow of active CaO related to the flow CO_2 is also plotted as a function of solid recirculation. Flow of CaO drops steadily when recirculation increases. Active CaO flow between reactors is sufficient even when 70 % of the solids are recirculated.

The point of this exercise was to demonstrate that good solid circulation control is crucial in calcium looping to keep the process operation at the optimal level. The fine lime particles lead easily to high solid fluxes in the fast fluidization conditions and there are few options to control the flow. One way is to transfer the operation of the reactors to a different fluidization regime by adjusting the volumetric flow of the fluidizing gas, increasing the reactor size or particle size. Increasing reactor size won't benefit the process, with rising costs and losses. The particle size is difficult to maintain because of the inherent fragmentation of particles during calcination (Gonzáles et al., 2010). The calciner reactor gas flow and velocity are linked to the carbonator flue gas load which is defined by the requirement of CO_2 capture from the boiler. It is important to remember that the flue gas flow will change depending on the boiler load. In the current state, the most reasonable solution is to recirculate part of the solid material back to each reactor to reduce the thermal stress of the process and still maintain enough active material travelling between the reactors.

6 Scale-up study of an industrial scale calcium looping unit

Chapter 6 reports the essential results of Ylätalo et al. (2014). The study attempts to scale-up a calcium looping unit to an industrial size using 1D model framework and simple dimensioning rules.

A conceptual small power plant with a thermal power of 250 MW was selected as the scale-up case. Several factors affected the size of the selected case. The small industrial size poses less financial risk but can be successfully extrapolated to a larger scale. Also the retrofitting with the calcium loop doubles the thermal output of the plant. General operation parameters of the power plant and the calcium loop are listed in Table 6.1 as well as the composition of the primary fuel and some essential simulation parameters. Currently the model can handle only one fuel and therefore high quality coal was selected for the combustor and the calcium loop although power plants tend to use several fuels in combination. The calcium looping unit was modelled as a retrofit unit without the steam cycle or thermal integration to the 250 MW boiler.

Table 6.1. Essential simulation parameters of the scale-up case.

Parameter	Value
Combustor thermal power [MW]	250
Combustor fuel flow [kg/s]	8.333
Flue gas mass flow [kg/s]	115.92
Flue gas CO_2 [w-%]	21.16
Flue gas SO_2 [w-%]	0.17
Flue gas temperature [ºC]	120
Designed capture efficiency [%]	80
Calciner fuel flow [kg/s]	9.229
Fuel LHV [MJ/kg]	30
Calciner thermal power [MW]	277
Carbonator cooling need [MW]	58
Oxidant flow [kg/s]	26
Make-up flow [kg/s]	11.15
Estimated maximum carrying capacity [w-%]	41
Fuel char [w-%]	67.6
Fuel volatiles [w-%]	22.5
Fuel moisture [w-%]	2.4
Fuel ash [w-%]	7.5
Average particle size [µm]	200
Average particle density [kg/m^3]	1800
Turbulent dispersion coefficient [-]	0.3
Solid slip coefficient [-]	0.3
Wall layer flow speed [m/s]	0.01

6.1 Dimensioning and thermal design of the reactors

The flue gas flow rate of the carbonator can be used to dimension the carbonator reactor once the average particle size is determined for the system. For the selected fuel and air-ratio of 1.2, the flue gas flow is 116 kg/s. As previously stated, calcium looping systems tend to have a small particle size (<100 µm) due to fragmentation in the initial calcination. With this particle size, it is quite difficult to operate in the conventional CFB-region. That is why it is more practical to use a higher average particle size commonly found in CFB-units. If the average particle size is fixed to 200 µm, the maximum superficial gas velocity can be set to 6 m/s. Particle size 200 µm is in the Geldart B class depending on the density but the 100 µm particles approach the pneumatic transport region. A larger particle size could be achieved by using more durable limestone against fragmentation or increasing initial feed size. Calculating from the carbonator gas mass flow, approximate density and the maximum velocity, the cross section of the carbonator will be around 44 m^2. Because the gas velocity in the carbonator is decreasing due to the adsorption of CO_2 by CaO, the use of sloped bottom section, commonly found in CFB boilers, is not appropriate. Also, using secondary flue gas inputs is not necessary because that will only cause some of the flue gas CO_2 to bypass the dense, reactive part of the carbonator bed. The rectangle like cross section commonly used in CFB-boilers is not necessary but to maintain structural integrity with the calciner, the carbonator width is determined to be the same as that of the calciner. The height of both reactors could be defined to maximize the residence time of gas and solids but in practice, the height of the cyclone, standpipe and loop seal combination sets the maximum height of the system. In this case, a value of 35 m could be close to the reality when examining the existing CFB boilers.

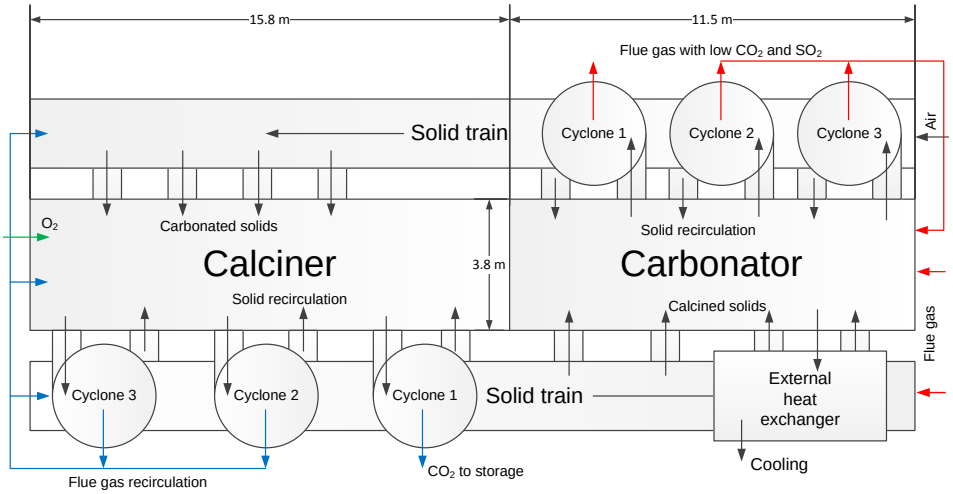

Figure 6.1. Concept image of the industrial calcium looping unit. External heat exchanger cools down the solid entering the carbonator reactor.

In the thermal design it was determined that an external heat exchanger with water tubes would be the best solution to remove heat from the incoming solids from the calciner and carbonation reaction. An evaporator surface in the carbonator would be inflexible in terms of cooling in lower loads. Initial simulations also pointed out that, if the carbonator bed is refractory protected due to the very high erosion rate of the dense bed, the heat transfer rate in the bed is not enough to cool the solids to 650 °C. Using in-bed heat transfer tubes would quickly cool the solids but it would also lead to fast erosion of the tubes. The most reactive bed part would be outside of the equilibrium which would cause trouble in the capture. It was determined that cooling the solids before feeding them into the carbonator would ease the heat transfer load in the carbonator bottom part. In addition, the equipment feeding the solids is also under great thermal stress and cooling is necessary. The location of external heat exchanger in the solid train feeding the carbonator is presented in Figure 6.1. In the model the external heat exchanger is executed by cooling the incoming solids to a low temperature (550-600 ºC). In an actual unit, the external heat exchanger could receive solids from the carbonator to cool the reactor more efficiently. The flue gas flows exiting the cyclones of the reactors are cooled down to 180 ºC but this is outside the model boundary and is only considered in the efficiency calculations.

Calciner dimensions can be evaluated similarly keeping in mind that the calciner gas flow consists of the oxygen required for combustion, CO_2 from the recirculation gas and the CO_2 released from the calcination of $CaCO_3$ in the circulated material and make-up flow. A superficial velocity of 6 m/s in the freeboard was selected as a boundary condition and the fuel flow was defined from a simple 0-D balance. With these assumptions the gas flow out of the calciner is around 108 kg/s. When the operation temperature is around 950 °C, the freeboard cross section is 60 m^2. The primary gas flow can be adjusted by reducing the amount of recirculation gas but it has to be kept in mind that the amount of oxygen in the gas should not rise over 40 vol-%, which could lead to too high combustion temperatures. In the calciner, a sloped section is necessary because the difference between the freeboard and grid gas mass flows is significant. By evaluating the ratio of grid gas mass flow and the exiting gas flow and estimating the height where most of the reactions have occurred, it was determined that the sloped section will be 5 m high and the grid cross section will be 43 m^2. With this dimensioning, the calciner velocity should remain constant along the reactor height. The width of the calciner was set to 3.8 m to keep the fuel, gas and solid penetration sufficient. Rectangular cross section commonly used in large CFB-units was also selected for the calciner. This will set the length of the reactor to 15.8 m and the width of the grid section to 2.7 m, because the length is not changed in the grid. The carbonator width will be 3.8 m and depth 11.5 m and both reactors will be structurally connected at the ends, Figure 6.1. This structural connection enables the construction of the solid return system alongside the reactor and the feeding of a portion of the solids back to the original reactor and transferring the remaining solids to the next reactor. The wall between the reactors is insulated to prevent heat transfer between the reactors. Also this solid train type of solution enables the division of solid feeding along the reactor length to even out the active solid concentration in the reactor. This kind of solution can

be modularized: larger units could be built by adding consecutive carbonator and calciner blocks, increasing the length. The main dimensions of the reactors and the thermal solutions are listed in Table 6.2.

Table 6.2. Rough dimensions of the industrial concept calcium loop.

Dimension (inner)	Carbonator	Calciner
Height of reactor [m]	35	35
Cross section of grid [m^2]	44	43
Cross section of freeboard [m^2]	44	60
Width of grid [m]	3.8	2.7
Width of freeboard [m]	3.8	3.8
Length [m]	11.5	15.8
End of sloped section height [m]	none	5
Elevation to exit channels [m]	33	33
Thermal design	External HE	Insulated

Both reactors are fitted with the ability to recirculate solids and gas. The reason for this is explained in the following sections. The calciner is fluidized with the mixture of recirculation gas and oxygen. The carbonator can be fluidized solely with flue gas from the combustor, with a combination of recirculation gas from the carbonator or just with air.

A simple pre-built Matlab PID-controller was assigned to the calciner reactor to control the purge of the calciner. The controller follows the calciner inventory and changes the purge if it deviates from the desired value. The purpose of the PID-controller was to facilitate calculations and remove unnecessary iterative calculations by hand.

6.2 Full load results

The simulation results for the full load case and design point of the plant can be seen in Figure 6.2 to Figure 6.5. Figure 6.2 describes the overall balance of the system.

The performance of the system is higher than originally intended. The capture efficiency is 85 %, when the design value was 80 %. The sulphur capture is also almost 100% in both reactors. The fuel flow of the calciner has been evaluated to 9.23 kg/s which is equal to 277 MW thermal power. The ratio of the calciner thermal power of the total thermal power, $q_{calciner}/(q_{calciner}+q_{combustor})$, is around 53% in the full load.

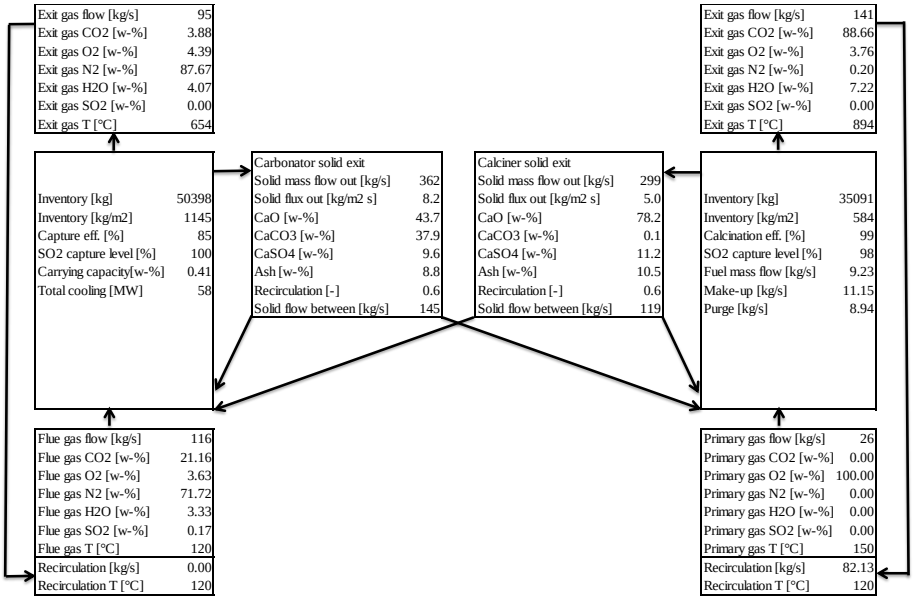

Figure 6.2. Overall balance of the full load calculation case.

The make-up flow for the case was determined based on the fuel ash and sulphur content, achieving an average carrying capacity of 41 w-% in the system. With the 6 m/s fluidization velocity, the solid mass flow out of the reactors is much larger than needed for moderate capture, and therefore 60 % of the solids is recirculated in both reactors. The fluidization velocity of the calciner is set to lower value than the carbonator velocity because it helps to control the overall solid inventory of the system. If the calciner velocity becomes higher and solids start to move to the carbonator, there is a danger that the whole reactor will be drained from solids. When the purge and solid control is on the calciner side, it is beneficial to keep the velocity difference favouring the calciner in other words higher velocity in the carbonator, Figure 6.3.

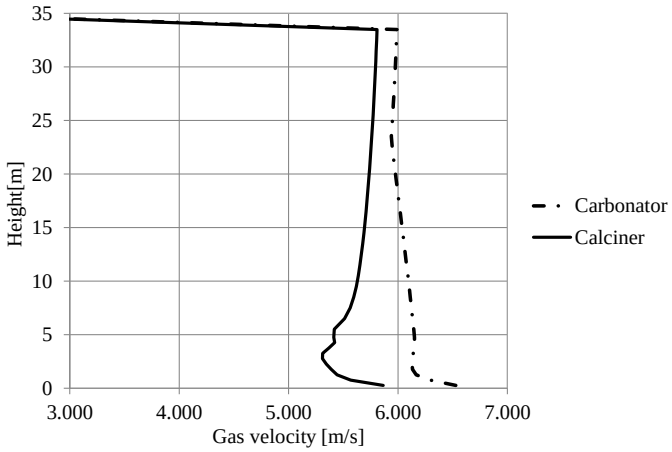

Figure 6.3. 1D velocity profiles of the reactors from full load calculation case.

Figure 6.4 displays the solid volume fraction profile and temperature profile of the carbonator. Especially from the temperature profile we can see that the temperature conditions are far from ideal even in the 1-D model. The entering solids are cooler than the objective temperature of the reactor. The total thermal power removed from the external heat exchanger and solid train is 58 MW.

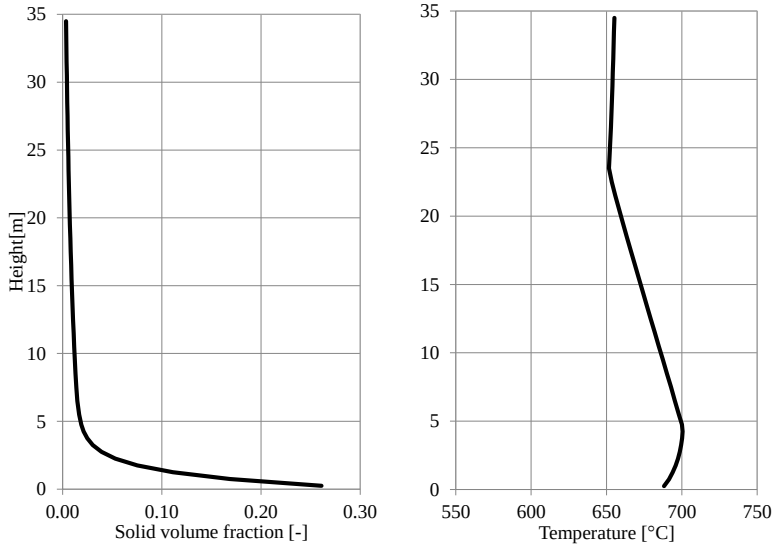

Figure 6.4. 1D solid volume fraction profile and temperature profile of the carbonator.

Figure 6.5 presents the corresponding solid volume fraction and temperature profiles for the calciner. Comparing the solid volume fraction profiles and calculated total masses of reactors Figure 6.2, it can be seen that the carbonator has a higher inventory than the calciner which could be a result of the higher $CaCO_3$ content in the carbonator. The average $CaCO_3$ concentration in the solids is quite close to the average activity achievable because recirculation increases the residence time of the solids in the reactor, displayed in Figure 6.2.

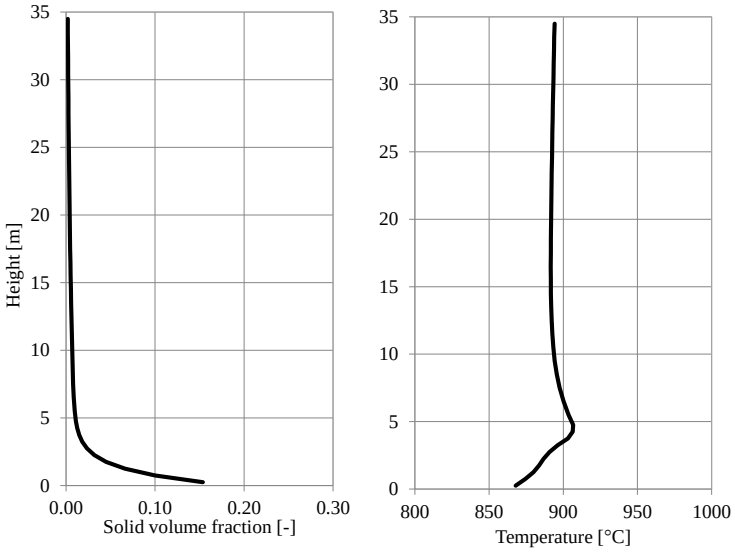

Figure 6.5. 1D solid volume fraction profile and temperature profile of the calciner.

Another interesting observation is that the calciner is running lower temperatures than the literature suggests. However, very good calcination efficiency is achieved. This could be a result of the lower CO_2 partial pressure in the calciner due to the flue gas recirculation, which increases the grid steam and oxygen partial pressures. The calcination model could overpredict the calcination reaction rate in the large-scale reactor. The average temperature in the 1D control volumes is quite close to the equilibrium temperature of the calcination reaction, which could cause some problems in a real unit because of the lateral temperature profiles present in a real large scale unit. In the temperature profile the insertion point of the cold solids can be seen as a drop of the temperature in the bottom region. Also the fuel insertion point close to the height of 5 m increases the local temperature by 50 ºC. The calcination reaction is dominated by heat transfer because mass transfer effects are not significant with particles smaller than 300 µm (Martínez et al., 2013a), which means that in the calciner the solid material has a long time to react compared to the carbonator, in which it is critical to achieve good gas-solid contact in the dense bottom region of the reactor. In other words, the calciner

operation is not so sensitive to local areas of temperatures below the calcination temperature in the lower part of the reactor.

6.3 Partial load results

In this section, the performance and behaviour of the large scale calcium looping unit is analysed in lower loads. In this context, the lower load means that the flue gas flow is lowered based on the power of the combustor where it is originating from. For example, the 75 % load means that the combustor is running at 75 % thermal power and the carbonator flue gas flow is updated based on that. The zero load scenario means that the power plant is shut down and no flue gas is available for the carbonator. The purpose of this zero load simulation is to demonstrate that the calcium looping unit can be run as an independent oxy-combustion power generation unit or a back-up power plant if the calcium looping unit is independent from the original combustor. Table 6.3 lists the input changes in different load scenarios.

All the other parameters were kept constant including the gas compositions and gas temperatures although they might change due to the changes in the combustor. The control scenarios have been devised based on the fluidizing conditions in the reactors. It was determined that achieving the CFB-mode becomes more difficult in the model when the fluidizing velocity drops below 4 m/s. From the 100 % to the 75 % load the adjustment can be done by means of lowering fluidizing velocities. Lower fluidizing velocity in the carbonator means a lower solid circulation rate and the calciner fuel and oxygen flow can be adjusted accordingly. When the CFB mode is not achievable anymore in the carbonator solely with the flue gas flow, the incorporation of the flue gas recirculation is necessary. In the calciner this is already present to dilute the oxygen flow. With both reactors equipped with the wet flue gas recirculation, a suitable fluidizing velocity can be achieved in different load scenarios. In the special case of the zero flue gas flow to the carbonator, the fluidization has to be handled with air. The flue gas recirculation has a positive side-effect, which is the increased CO_2 capture efficiency in the carbonator. However this comes with a price, because sustaining fluidization also requires maintaining some thermal power, which can be seen in Figure 6.6. This means that the relation of the calciner power to the combustor power increases in the lower loads, when in full power it is 53%, in the 30 % load it is 70%. The thermal efficiency of the loop increases a bit in the lower loads because less heat is needed for the make-up calcination or heating up the gas and solid flows. The thermal efficiency E_{thermal} of the system was approximated from equation

$$E_{\text{thermal}} = \frac{q_{\text{cooling}} + q_{\text{carb,gas}} + q_{\text{calc,gas}}}{q_{\text{fuel}}} \tag{6.1}$$

where q_{cooling} is the heat extracted from carbonator and solid train [W], $q_{\text{carb,gas}}$ is the heat captured from the gas stream leaving the carbonator and $q_{\text{calc,gas}}$ is the heat captured from gas stream leaving the calciner. The total thermal power of the calciner is q_{fuel}. The

exit temperature of the carbonator and calciner gas flows was selected to be 180 ºC after the backpass heat exchangers to account for the dew point of sulphuric acid. This approach does not consider the performance of the backpass in lower gas flows. It very likely that the heat captured in the backpass is less in lower loads and the actual thermal efficiency is not higher in lower loads.

Table 6.3. Input changes for different load scenarios.

Parameter	Full load	75 % load	50 % load	30 % load	0 % load
Calciner inventory set [kg]	35091	35067	35050	35064	35042
Carbonator inventory (calculated) [kg]	50398	49548	47039	29220	19135
Flue gas flow [kg/s]	116	87	58	35	0
Oxidant flow [kg/s]	26	19	18	16	15
Fuel flow [kg/s]	9.23	6.92	6.20	5.90	5.50
Calciner flue gas recirculation [kg/s]	82.13	59.00	58.00	60.00	59.00
Carbonator flue gas recirculation [kg/s]	0.0	0.0	28.90	52.09	85
Make-up flow [kg/s]	11.15	8.36	5.57	3.34	2.00
Calciner thermal power [MW]	277	208	186	177	165
Carbonator cooling [MW]	58	51	34	31	30
Heat extracted from carbonator backpass [MW]	54	37	35	38	39
Heat extracted from calciner backpass [MW]	142	102	106	98	89

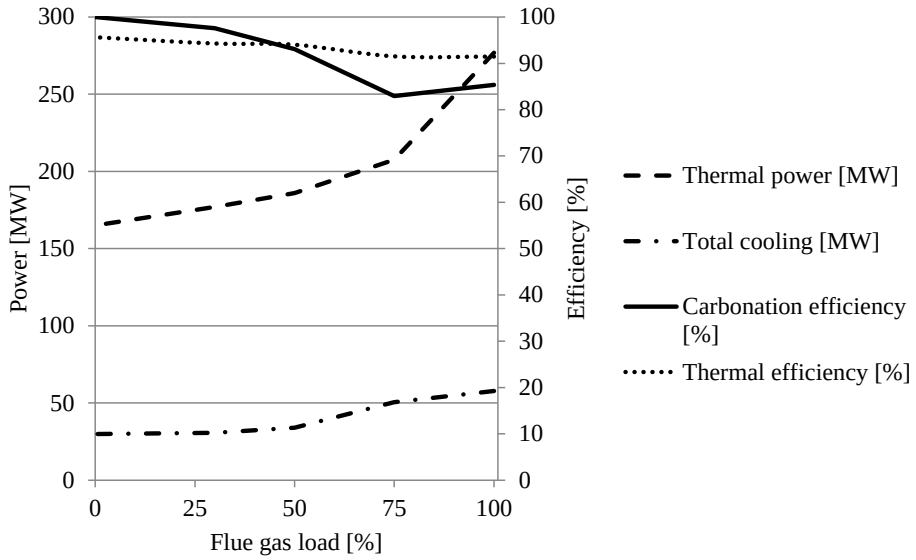

Figure 6.6. Thermal power of the calciner and total cooling of the carbonator plotted as a function of the flue gas load on the left hand side axis. In the same figure, carbonation efficiency and thermal efficiency of the calcium loop are plotted as a function of flue gas load (right hand axis).

The development of the flue gas recirculation is presented in Figure 6.7. Below the 75 % load the calciner flue gas recirculation is almost constant. In the carbonator the fuel gas recirculation increases linearly as the load is decreased until in the zero load scenario the whole reactor is fluidized with air. In addition to that, Figure 6.7 plots the average gas velocities in the reactors (left axis). The objective was to keep fluidization velocities constant in the reactors beyond 75 % load and use the solid material recirculation to adjust the flow of solids required for the CO_2 capture.

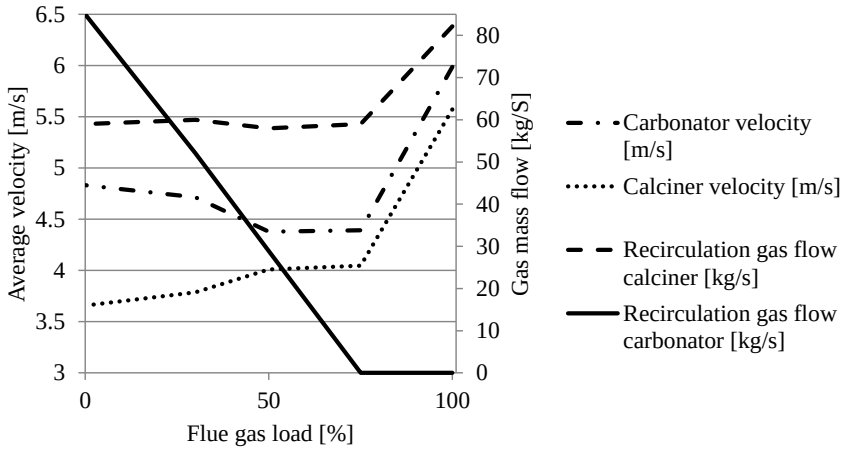

Figure 6.7. Recirculation gas flow to reactors in different load scenarios (right hand axis). Left hand axis presents the average velocity of the reactor in different load scenarios. Keeping average gas velocity close to the desired value becomes difficult in low flue gas loads.

However, maintaining gas velocities constant was not successful and the gas velocity drops in the calciner and increases in the carbonator due to the increase in the reactor temperature differences, Figure 6.8.

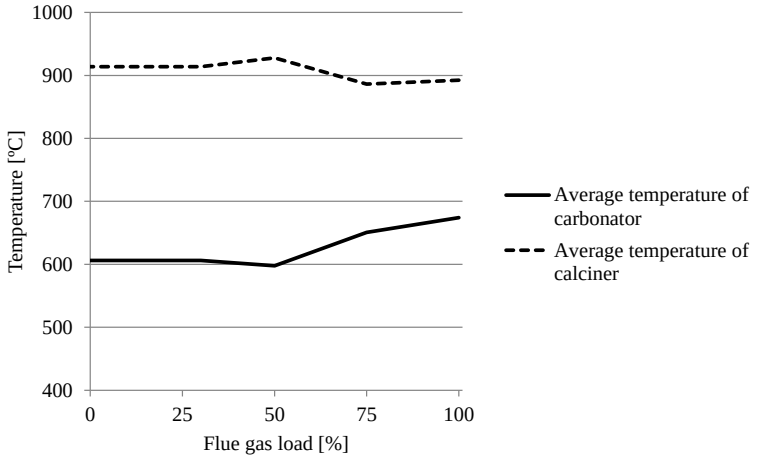

Figure 6.8. Average temperatures of the reactors in different loads. Several parameters affect the development temperatures in the reactors which in term have an effect on gas velocities. This creates a difficulty in controlling solid fluxes.

Figure 6.9 plots the adjustment of the make-up flow in different load scenarios and the control of solid flow between the reactors compared to the solid flow out of the carbonator. The make-up has been linearly controlled but it has a theoretical minimum set by the fuel ash and sulphur content. In the zero load case, the make-up flow does not have any significance for the CO_2 capture, but it is needed to compensate the purge needed for the ash and $CaSO_4$ removal. In the same plot the solid flow out of the carbonator is presented alongside the solid flow lead from carbonator to the calciner. Several factors affect the solid flow out of the carbonator. Below the 75 % load, the attempt was to keep the gas velocity at around 4 m/s although the temperature change increased the gas velocity. This did not increase the solid flow because the carbonate content of the solids and the inventory of the carbonator decrease in the lower loads resulting in lower solid flows. The solid flow from the carbonator to the calciner was adjusted with solid recirculation and the percentage of recirculation had to be controlled case by case because the solid circulation rate out of the reactors is changing as a function of solid inventory and fluidizing velocity.

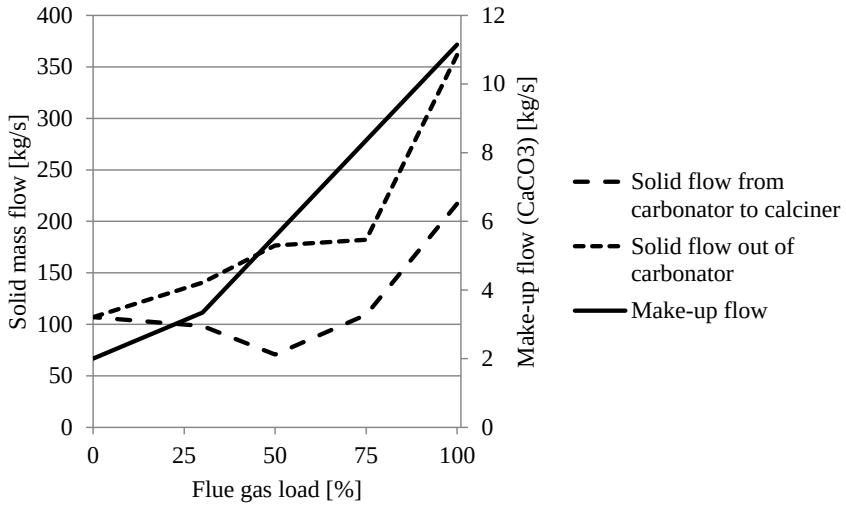

Figure 6.9. Solid flow out of the carbonator and solid allowed to the carbonator plotted as a function of flue gas load (left hand side axis). The solid mass flow has a lot of variation because it is dependent on several variables like gas velocity and reactor solid inventory and inventory composition.

An interesting observation is that in the zero load situation, fluidizing the carbonator with ambient air and running the calciner as an oxy-combustion circulating fluidized bed unit is also possible. Minimal heat was extracted from the external heat exchanger and solid train surfaces and the rest can be extracted in the backpasses of the reactors. If

the power plant is abruptly shut down, the calcium loop can provide back-up power for extended periods.

To summarize the different load scenario analysis, flexibility can be achieved using solid and flue gas recirculation and clever heat transfer design. The flue gas flow out of the calciner in the zero load case drops to 60% of the full load flow which will certainly have an effect on the backpass heat exchanger performance. The thermal efficiency in the partial loads will not be as good as predicted by the simplified approach used in this study. Also the performance of the turbulent bed external heat exchanger in lower loads is something that needs further investigation. Even if the flue gas load does not significantly change, several factors can affect the fluidization behaviour of the calcium looping unit. The particle population of the system can change in size or density during the runs due to agglomeration or attrition which requires a change in fluidization. Because the calcium looping process is sensitive to the solid circulation rates between the reactors, effective ways to control solid circulation are necessary. Even though there might be some error in the prediction of solid circulation rates and heat transfer, the general observations from the simulations are applicable to the operation of large scale calcium looping units.

7 Discussion

Modelling tools can be used to analyse a variety of phenomena in novel technologies. In this work, the analysis concentrated on features not included in earlier modelling work. These features include the coupling of the CFB reactor energy balance to the mass balance, the simulation of interconnected reactor behaviour and the analysis of spatial reactor phenomena. Model validation was also included in the research effort using the available data at that time.

The inclusion of the energy balance in the calcium looping model resulted in several conclusions. While it is clear that the essential chemical reactions of the calcium looping process are highly temperature dependent, the effect of local temperature gradients and local gas concentrations on the process performance was studied for the first time in this thesis. The traditional thermal design of circulating fluidized boilers can be applied to the calcium looping process with some reservations. In the carbonator design, where achieving high capture efficiency requires maintaining a temperature close to 650 ºC depending on the local CO_2 partial pressure, traditional membrane wall heat transfer might not be sufficient to achieve optimal operation conditions. Exothermic carbonation reactions and convective heat flow alongside high temperature solids from the calciner create high thermal stress in the carbonator bottom region. Of course, the turbulent mixing of the fluidized bed reactor evens out the temperature gradients but there is still the danger of exceeding the carbonation temperature in the bottom region. Also, the carbonation reaction is self-regulating, which decreases the heat load from reactions if the temperature exceeds the optimal conditions but the thermal strain of the calciner solid flow remains. The bottom region is also important because traditional circulating fluidized bed reactors have the majority of solids located in the lower reactor area and the rest of the height is usually dilute two-phase flow. In practise this means that a great deal of the capture occurs in the lower reactor region. The dilute phase can also contribute to the capture but for the most the optimal capture, suitable temperature has to be achieved in the lower reactor area. This is where problems occur if conventional membrane walls are used. A lot of heat transfer surface has to be installed in the lower bed area to achieve sufficient heat transfer due to the lower temperature than in normal circulating fluidized boilers. However, the bed area is subjected to high erosion due to the high volume fraction of solids and strong turbulent two-phase flow. The heat transfer surfaces have to be refractory shielded which in turn weakens heat transfer. This is why cooling down the solids before the carbonator is required which can be done in several ways, one method presented in Chapter 6.1.

The local temperature and gas concentration gradients of the calciner can also affect the process performance. A too low temperature in the calciner could result in only partial calcination which decreases the of amount active lime going to the carbonator. However, the process efficiency increases if the calciner temperature is as low as possible. The calciner operating temperature can be lowered by altering the reactor CO_2 concentration. Using fuels with high moisture content, high oxygen partial pressure in the grid gas and wet flue gas recirculation decreases the CO_2 partial pressure which in

terms allows the use of lower calciner temperatures. This was noticed in both studies presented in Chapters 5 and 6. Lower calciner temperature means smaller temperature difference between the reactors which in turn decreases the need for fuel and oxygen.

The interconnected reactor behaviour analysis revealed that the solid circulation rate between the reactors plays a key role in the process performance and behaviour. Rarely the flow of solids between the reactors is at optimal rate and the flow has to be limited by recirculating material to the reactors. The optimal rate of solid circulation between the reactors is a function of the maximum carrying capacity of the material and the thermal capacity of the system. High carrying capacity, which means large make-up flows, allows low solid circulation rates between the reactors which lowers the costs from combustion in the calciner. Low carrying capacity requires high solid circulation rates between the reactors which in turn increases fuel consumption. It can be determined that the maximum carrying capacity defines the minimum solid circulation rate between the reactors. The highest solid circulation rate between reactors is determined from the maximum thermal capacity of the system. The maximum thermal capacity in this context means the ability of the system to maintain the temperature difference between reactors by means of combustion and cooling. Keeping in mind the importance of the optimal solid circulation between reactors, the control of the solid circulation rate is especially critical in the calcium looping process. Solid circulation out of the reactor depends on the hydrodynamic properties of the particles, solid inventory and fluidizing gas velocity. A plant operator cannot control particle sizes and bed quality very effectively, and therefore the solid circulation rate has to be adjusted with gas velocities or by the limiting solid circulation rate between reactors. Adjusting the gas velocity is not a very flexible way of controlling solid circulation rates because the carbonator velocity is dictated from the gas flow from the originating combustor. Some adjustments can be done with secondary and tertiary fluidization. Effective control can be done with the combination of flue gas recirculation and solid recirculation which was discussed in Chapters 5 and 6. However, more detailed simulation of the behaviour of controllable solid return systems like dual loop seals has to be done to map out the flexibility and limits of the system. The development of particle size and hydrodynamic properties of solids is also coupled with this problem because particle fragmentation is an observed phenomenon in the calcium looping process (Gonzáles et al., 2010).

The analysis of the calcium looping process can be extended with the existing model framework. Dynamic calculations with calcium looping model have not been attempted. Most of the next generation calcium looping concepts could be studied with minor additions to the existing model. Further development of the model framework requires a wider validation of the model frame, increasing reliability and applicability. In addition to that, more complex models could be added if deemed necessary.

8 Conclusion

In this thesis a modelling approach was applied to the post-combustion CO_2 capture calcium looping process. A 1D dynamic process model was created to the Matlab Simulink environment using an in-house code and the best available knowledge from the literature on fluidized bed reactors and the calcium looping process.

Three modelling cases were analysed with the model. The first case was a comparison of simulation results to a laboratory scale 30 kW calcium looping unit. Considering the limited information available from the experiments and only the carbonator reactor simulated, the initial results were promising. The development of the reactor capture efficiency as a function of inventory showed a clear trend visible both in the model and experiments. Also the 1D temperature profile shape of the model and experimentally acquired temperature profile matched in most of the cases although with high inventories the temperature levels became higher than experimentally observed. This was explained by the removal of insulation from the reactor. Overall, the first attempt to validate the model framework was promising and showed the model's capabilities of reproducing the observed process behaviour.

The second modelling case was built around the 1.7 MW_{th} calcium looping pilot situated in Oviedo Spain. Two modelling approaches were applied to the studied case, a 3D steady-state reactor model (Myöhänen, 2011) and the 1D modelling approach presented in detail in this thesis. A model to model comparison of the calciner reactor was made by applying same boundary conditions and parameters to both models. The similarity of the results confirmed that the behaviour of the slim pilot reactor is quite one-dimensional. Also both models produced similar results although the modelling approach and reaction models are different. In addition to the model to model analysis of the calciner reactor, a general analysis of the overall system behaviour was made. It was determined that controlling the looping ratio between the reactors is one of the most critical aspects of the calcium looping process. The bed quality of the system can change during the operation or the fluidizing velocities can vary which increases or decreases the solid circulation rates. Solid circulation rates affect the energy and carbon balance of the system. This implies that the operator of the system can alter the amount of solids recirculating back to the reactor to minimize fuel consumption and maximize the capture efficiency.

The third modelling case attempted to scale-up the process to an industrial scale using simple dimensioning rules, experience gained from large CFB units and the model framework created in this thesis. Estimating the flue gas flows through the reactors, crude dimensions were assigned for the reactors assuming structural integration and solid looping arrangement. It was determined that solid cooling before the carbonator was necessary because otherwise the reactor would be running too hot in the lower region where the majority of the active solid is located. After dimensioning and thermal design, several load cases were analysed ranging from full flue gas load to zero flue gas flow to the carbonator. In the case of power plant shutdowns, the calcium loop can

continue operation as an oxy-combustion fluidized bed reactor. Using the flue gas recirculation and clever heat transfer design, the large scale calcium looping unit can be very flexible.

Overall, a robust and multifunctional model was created for the calcium looping process and presented in three modelling cases. The model development will continue onwards, several features require improvement, for example, the carrying capacity of the solids is a transient variable and an approach to describe that is required. The solid circulation rate prediction needs more validation as the size of the lime particles in the calcium looping units is not the same as in conventional fluidized bed boilers. More overall validation of the model framework is required to increase the reliability. The dynamic properties of the model have remained un-used for now, but they should be utilized in further analysis of the process.

References

Abanades, J.C. (2002). The maximum capture efficiency of CO2 using carbonation/calcination cycle of CaO/CaCO3. *Chemical Engineering Journal*, 90, pp. 303-306.

Abanades, J.C. and Alvarez, D. (2003). Conversion limits in the reaction of CO2 with lime. *Energy & Fuels*, 17, pp. 308-315.

Abanades, J., Grasa, G., Alonso, M., Rodriguez, N., Anthony, E., and Romeo, M. (2007). Cost structure of a postcombustion CO2 capture system using CaO. *Environ.Sci.Technol.*, 41, pp. 5523-5527.

Abanades, J., Murillo, R., Fernandez, R., Grasa, G., and Martínez, I. (2010). New CO2 capture process for hydrogen production combining Ca and Cu chemical loops. *Environmental Science & Technology*, 44, pp. 6901-6904.

Adánez, J., de Diego, L., Gayán, P., Armesto, L., and Cabanillas, A. (1995). A model for prediction of carbon combustion efficiency in circulating fluidized bed combustors. *Fuel*, 74, pp. 1049-1056.

Al-Jeboori, M., Fennell, P., Michaela, N., and Feng, K. (2012). Effects of different dopants and doping procedures on the reactivity of CaO-based sorbents for CO2 capture. *Energy & Fuels*, 26, pp. 6584-6594.

Al-Jeboori, M., Nguyen, M., Dean, C., and Fennell, P. (2013). Improvement of limestone based CO2 sorbents for Ca looping by HBr and other mineral acids. *Industrial & Engineering Chemistry Research*, 52, pp. 1426-1433.

Alonso, M., Rodríguez, N., Grasa, G., and Abanades, J.C. (2009). Modelling of a fluidized bed carbonator reactor to capture CO2 from combustion flue gas. *Chemical Engineering Science*, 64, pp. 883-891.

Alonso, M., Rodríguez, N., González, B., Grasa, G., Murillo, R., and Abanades, J.C. (2010). Carbon dioxide capture from combustion flue gases with calcium oxide chemical loop. Experimental results and process development. *International Journal of Greenhouse Gas Control*, 4, pp. 167-173.

Arias, B., Grasa, G., and Abanades, J.C. (2010). Effect of sorbent hydration on the average activity of CaO in a Ca-looping system. *Chemical Engineering Journal*, 163, pp. 324-330.

Arias, B., Abanades, J.C., and Grasa, G. (2011). An analysis of the effect of carbonation conditions on CaO deactivation curves. *Chemical Engineering Journal*, 167, pp. 255-261.

Arias, B., Grasa, G., Abanades, J.C., Manovic, V., and Anthony, E. (2011A). The effect of steam on the fast carbonation reaction rates of CaO. *Industrial & Engineering Chemistry Research*, 51, pp. 2478-2482.

Arias, B., Abanades, J.C., and Anthony, J.C. (2011B). Model for self-reactivation of highly sintered CaO particles during CO2 capture looping cycles. *Energy & Fuels*, 25, pp. 1926-1930.

Arias, B., Cordero, J., Alonso, M., and Abanades, J. (2012). Sulfation rates of cycled CaO particles in the carbonator of a Ca-looping cycle for post-combustion CO2 capture. *AIChE Journal*, 58, pp. 2262-2269.

Barin, I. (1989). *Thermochemical data of pure substances, Parts I and II*. ISBN 3-527-27812-5.

Barker, R. (1973). Reversibility of the reaction CaCO3 = CaO + CO2. *J. Appl. Chem. Biotechnol.*, 23, pp. 733-742.

Basu, P. (2006). *Combustion and gasification in fluidized beds*. Boca Raton, FL, USA: CRC Press.

Borgwardt, R. (1989). Sintering of nascent calcium oxide. *Chemical Engineering Science*, 44, pp. 53-60.

Branch, M. and Sawyer, R. (1973). Ammonia oxidation kinetics in an arc heated flow reactor. In: *Proceedings 14th international symposium on combustion*, pp. 967-974. Pittsburgh, USA.

Champagne, S., Lu, D., Macchi, A., Symonds, R., and Anthony, E. (2013). Influence of steam injection during calcination on the reactivity of CaO-based sorbent for carbon capture. *Industrial & Engineering Chemistry Research*, 52, pp. 2241-2246.

Charitos, A., Hawthorne, C., Bidwe, A., Sivalingam, S., Schuster, A., Spielhoff, H., and Scheffknect, G. (2010). Parametric investigation of the calcium looping process for CO2 capture in a 10 kWt dual fluidized bed. *International Journal of Greenhouse Gas Control*, 4, pp. 776-784.

de-Souza Santos, M. (2010). *Solid fuels combustion and gasification*. CRC Press. ISBN 9781420047493.

Diego, M., Arias, B., and Abanades, J.C. (2012). Modeling the solids circulation rates and solids inventories of an interconnected circulating fluidized bed reactor system for CO2 capture by calcium looping. *Chemical Engineering Journal*, 198-199, pp. 228-235.

Dieter, H., Hawthorne, C., Zieba, M., and Scheffknecht, G. (2013). Progress in calcium looping post-combustion CO2 capture: successful pilot scale demonstration. *Energy Procedia*, 37, pp. 48-56.

Donat, F., Florin, N., Anthony, E., and Fennell, P. (2010). Influence of high-temperature steam on the reactivity of CaO sorbent for CO2 capture. *Environmental Science & Technology*, 46, pp. 1262-1269.

du Motay, T. and Maréchal (1868). Industrial Preparation of Hydrogen. *Bull Mensuel de La Société Chimique de Paris*, pp. 334-334.

Duelli, V., Bernard, L., Bidwe, A., Stack-Lara, V., Hawthorne, G., Zieba, M., and Scheffknect, G. (2013). Calcium looping process: experimental investigation of limestone performance regenerated under high CO2 partial pressure and validation of a carbonator model. *Energy Procedia*, 37, pp. 190-198.

Dutta, A. and Basu, P. (2002). Overall heat transfer to water walls and wing walls of commercial circulating fluidized bed boilers. *Journal of Institute of Energy*, 75, pp. 85-90.

Fang, F., Li, Z.-S., and Cai, N.-S. (2009). Experiment and modeling of CO2 capture from flue gases at high temperature in a fluidized bed reactor with Ca-based sorbents. *Energy & Fuels*, 23, pp. 207-216.

Florin, N. and Fennell, P. (2011). Synthetic CaO-based sorbent for CO2 capture. *Energy Procedia*, 4, pp. 830-838.

German, R. and Munir, Z. (1976). Surface area reduction during isothermal sintering. *Journal of American Ceramic Society*, 59, pp. 379-383.

Gonzáles, B., Alonso, M., and Abanades, J.C. (2010). Sorbent attrition in a carbonation/calcination pilot plant for capturing CO2 from flue gases. *Fuel*, 89, pp. 2918-2924.

Grasa, G. and Abanades, J.C. (2006). CO2 capture capacity of CaO in long series of carbonation calcination cycles. *Industrial & Engineering Chemistry Research*, 45, pp. 8846-8851.

Grasa, G., Murillo, R., Alonso, M., and Abanades, J.C. (2009). Application of the the random pore model to the carbonation cyclic reaction. *AIChE Journal*, 55, pp. 1246-1255.

Hawthorne, C., Trossman, M., Galindo Cifre, P., Schuster, A., and Scheffknecht, G. (2009). Simulation of the carbonate looping power cycle. *Energy procedia*, 1, pp. 1387-1394.

Howard, J. (1989). *Fluidized Bed Technology: Principles and Applications*. Bristol UK: Taylor and Adams.

Huilin, L., Guangbo, Z., Rushan, B., Yongjin, C., and Gidaspow, D. (2000). A coal combustion model for circulating fluidized bed boilers. *Fuel*, 79, pp. 165-172.

Johnsson, F. and Leckner, B. (1995). Vertical distribution of solids in a CFB-furnace. In: *Proceedings of the 13th International Conference on Fluidized Bed Combustion*, pp. 671-679. Orlando, USA: ASME.

Kunii, D. and Levenspiel, O. (1991). *Fluidization Engineering*, 2nd edn. Butterworth-Heineman. ISBN 0-409-90233-0.

Lasheras, A., Ströhle, J., Galloy, A., and Epple, B. (2011). Carbonate looping process simulation using a 1D fluidzed bed model for the carbonator. *International Journal of Greenhouse Gas Control*, 5, pp. 686-693.

Leveson, P. (1997). *Kinetic studies to determine the rates of ammonia and hydrogen sulphide destruction under claus plant operating conditions*. Sheffield, UK: Department of Chemical Engineering and Fuel Technology. PhD thesis.

Li, Y., Zhao, C., Chen, H., Liang, C., Duan, L., and Zhou, W. (2009). Modified CaO-based sorbent looping cycle for CO2 mitigation. *Fuel*, 88, pp. 697-704.

Li, Y., Liu, C., Sun, R., Liu, H., Wu, S., and Lu, C. (2012). Sequential SO2/CO2 capture of calcium-based solid waste from the paper industry in the calcium looping process. *Industrial & Engineering Chemistry Research*, 51, pp. 16042-16048.

Lu, D., Hughes, R., and Anthony, E. (2008). Ca-based sorbent looping combustion for CO2 capture in pilot-scale dual fluidized beds. *Fuel Processing Technology*, 89, pp. 1386-1395.

Manovic, V., Anthony, E., Grasa, G., and Abanades, J.C. (2008). CO2 looping cycle performance of a high purity limestone after thermal activation/doping. *Energy & Fuels*, 22, pp. 3258-3264.

Manovic, V. and Anthony, E. (2010). Carbonation of CaO-based sorbents enhanced by steam addition. *Industria &l Engineering Chemistry Research*, 49, pp. 9105-9110.

Manovic, V., Wu, Y., and Anthony, E. (2011A). Core-in-shell CaO/CuO-based composite for CO2 capture. *Industrial & Engineering Chemistry Research*, 50, pp. 12384-12391.

Manovic, V. and Anthony, E. (2011A). Integration of calcium and chemical looping combustion using composite CaO/CuO based materials. *Environmental Science & Technology*, 45, pp. 10750-10756.

Manovic, V. and Anthony, E. (2011B). CaO-based pellets with oxygen carriers and catalysts. *Energy & Fuels*, 25, pp. 4846-4853.

Manovic, V., Anthony, E., and Loncarevic, D. (2011B). Improving stability of a CaO-based sorbent for CO2 by thermal pretreatment. *Industrial & Engineering Chemistry Research*, 50, pp. 6933-6942.

Manovic, V. and Anthony, E. (2011C). Reactivation and remaking of calcium aluminate pellets for CO2 capture. *Fuel*, 90, pp. 233-239.

Martínez, I., Murillo, R., Grasa, G., Rodríguez, N., and Abanades, J.C. (2011a). Conceptual design of a three fluidised beds combustion system capturing CO2 with CaO. *International Journal of Greenhouse Gas Control*, 5, pp. 498-504.

Martínez, I., Grasa, G., Murillo, R., Arias, B., and Abanades, J.C. (2012a). Kinetics of calcination of partially carbonated particles in a Ca-looping system for CO2 capture. *Energy & Fuels*, 26, pp. 1432-1440.

Martínez, A., Lara, Y., Lisbona, P., and Romeo, L. (2012b). Energy penalty reduction in the calcium looping cycle. *International Journal of Greenhouse Gas Control*, 7, pp. 74-81.

Martínez, I., Grasa, G., Murillo, R., Arias, B., and Abanades, J.C. (2013a). Modelling the continuous calcination of CaCO3 in a Ca-looping system. *Chemical Engineering Journal*, 215-216, pp. 174-181.

Metz, B., Davidson, O., de Coninck, H., Loos, M., and Meyer, L. (2005). *Special report on carbon dioxide capture*. Cambridge, UK: Intergovernmental panel on climate change.

Myöhänen, K. (2011). *Modelling of combustion and sorbent reactions in three-dimensional flow environment of a circulating fluidized bed furnace*. Lappeenranta, Finland: Acta Universitatis Lappeenrantaensis. ISBN 978-952-265-160-0. PhD thesis.

Nikolopoulos, A., Nikolopoulos, N., Charitos, A., Grammelis, P., Kakaras, E., Bidwe, A.R., and Varela, G. (2013). High-resolution 3-D full-loop simulation of a CFB carbonator cold model. *Chemical Engineering Science*, 90, pp. 137-150.

Quan, V., Marble, F., and Klingel, J. (1973). *Proceedings of 14th international symposium on combustion*, pp. 851-860. Pittsburgh, USA.

Ramkumar, S. and Fan, L.-S. (2010). Thermodynamic and experimental analyses of the three-stage calcium looping process. *Industrial & Engineering Chemistry Research*, 49, pp. 7563-7573.

Rodríguez, N., Alonso, M., Abanades, J.C., Charitos, A., Hawthorne, C., Scheffknect, G., Lu, D., and Anthony, E. (2011A). Comparison of experimental results from three fluidized bed test facilities capturing CO2 with CaO. *Energy Procedia*, 4, pp. 393-401.

Rodríguez, N., Alonso, M., and Abanades, J.C. (2011B). Experimental investigation of a circulating fluidized-bed reactor to capture CO2 with CaO. *AIChE Journal*, 57, pp. 1547-5905.

Rodríguez, N., Murillo, R., and Abanades, J.C. (2012). CO2 capture from cement plants using oxyfired precalcination and/or calcium looping. *Environmental Science and Technology*, 46, pp. 2460-2466.

Romano, M. (2009). Coal-fired power plant with calcium oxide carbonation for post-combustion CO2 capture. *Energy Procedia*, 1, pp. 1099-1106.

Romano, M. (2012). Modeling the carbonator of a Ca-looping process for CO2 capture from power plant flue gas. *Chemical Engineering Science*, 69, pp. 257-269.

Romano, M. (2013). Ultra-high CO2 capture efficieny in CFB oxyfuel power plants by calcium looping process for CO2 recovery from purification units vent gas. *International Journal of Greenhouse Gas Control*, 18, pp. 57-67.

Sánchez-Biezma, A., Ballesteros, J.C., Diaz, L., de Zárraga, E., Álvarez, F., and Lopez, J. (2011). Post-combustion CO2 capture with CaO. Status of the technology and next steps towards large scale demonstration. *Energy Procedia*, 4, pp. 852-859.

Sánchez-Biezma, A., Paniagua, J., Diaz, L., Lorenzo, M., Alvarez, J., Martínez, D., Arias, B., Diego, M.E., and Abanades, J.C. (2013). Testing postcombustion CO2 capture with CaO in a 1.7 MWt pilot faciltiy. *Energy Procedia*, 37, pp. 1-8.

Shimizu, T., Hirama, T., Hosoda, H., Kitano, K., Inagaki, M., and Tejima, K. (1999). A twin fluid-bed reactor for removal of CO2 from combustion processes. *Trans IChemE*, 77, pp. 62-68.

Silcox, G., Kramlich, J., and Pershing, W. (1989). A mathematical model for the flash calcination of dispersed CaCO3 and Ca(OH)2 particles. *Industrial & Engineering Chemistry Research* , 28, pp. 155-160.

Stanmore, B. and Gilot, P. (2005). Review - calcination and carbonation of limestone during thermal cycling for CO2 sequestration. *Fuel Processing Technology*, 86, pp. 1707-1743.

Ströhle, J., Galloy, A., and Epple, B. (2009). Feasibility study on the carbonate looping process for post-combustion CO2 capture from coal fired plants. *Energy Procedia*, 1, pp. 1313-1320.

Ströhle, J. (2012). Carbonate looping experiments in 1 MWth scale sing a CFB calciner fired with coal and oxygen-enriched air. In: *2nd International Workshop on Oxyfuel FBC Technology*. Stuttgart, Germany. http://oxyfbc.eu-projects.de/Portals/29/OxyFBC/12_Str%C3%B6hle_TUD%20-%20Oxy-CFB-Workshop_2012-06-28.pdf.

Sun, R., Li, Y., Liu, H., Wu, S., and Lu, C. (2012). CO2 capture performance of calcium-based sorbent doped with manganese salts during calcium looping cycle. *Applied Energy*, 89, pp. 368-373.

Sun, R., Li, Y., Liu, C., Xie, X., and Lu, C. (2013). Utilization of lime mud from paper mill as CO2 sorbent in calcium looping process. *Chemical Engineering Journal*, 221, pp. 124-132.

Symonds, R., Lu, D., Hughes, R., Anthony, E., and Macchi, A. (2009). CO2 capture from simulated syngas via cyclic carbonation/calcination for a naturally occurring limestone: pilot plant testing. *Industrial & Engineering Chemistry Research*, 48, pp. 8431-8440.

Valverde, J. (2013). A model on the CaO multicyclic conversion in the Ca-looping process. *Chemical Engineering Journal*, 228, pp. 1195-1206.

Valverde, J., Sanchez-Jimenez, P., Perejon, A., and Maqueda, L. (2013A). Constant rate thermal analysis for enhancing the long-term CO2 capture of CaO at Ca-looping conditions. *Applied Energy*, 108, pp. 108-120.

Valverde, J., Raganati, F., Quintanilla, M., Ebri, J., Ammendola, P., and Chirone, R. (2013B). Enhancement of CO2 capture at Ca-looping conditions by high-intensity acoustic fields. *Applied Energy*, 111, pp. 538-549.

Wang, Q., Luo, Z., Li, X., Fang, M., Ni, M., and Cen, K. (1999). A mathematical model for a circulating fluidized bed boiler. *Energy*, 24, pp. 633-653.

Wang, J. and Anthony, E. (2005). On the decay behaviour of the CO2 absoprtion capacity of CaO-based sorbents. *Insdustrial & Engineering Chemistry Research*, pp. 627-629.

Wang, A., Wang, D., Deshpande, N., Phalak, N., Wang, W., and Fan, L.S. (2013). Design and operation of a fluidized bed hydrator for steam reactivation of calcium sorbent. *Industrial & Engineering Chemistry Research*, 52, pp. 2793-2802.

Vilienskii, T. and Hezmalian, D. (1978). Dynamics of the combustion of pulverized fuel. *Energia*, 11, pp. 246-251.

Vorrias, I., Atsonios, K., Nikolopoulos, A., Nikolopoulos, N., Grammelis, P., and Kakaras, E. (2013). Calcium looping for CO2 capture from lignite fired power plant. *Fuel*. In press. http://dx.doi.org/10.1016/j.fuel.2012.12.087.

Ylätalo, J., Ritvanen, J., Arias, B., Tynjälä, T., and Hyppänen, T. (2012). 1-Dimensional modelling and simulation of the calcium looping process. *International Journal of Greenhouse Gas Control*, 9, pp. 130-135.

Ylätalo, J., Parkkinen, J., Ritvanen, J., Tynjälä, T., and Hyppänen, T. (2013). Modeling of the oxy-combustion calciner in the post-combustion calcium looping process. *Fuel*, 113, pp. 770-779.

Ylätalo, J., Ritvanen, J., Tynjälä, T., and Hyppänen, T. (2014). Model based scale-up study of the calcium looping process. *Fuel*, 115, pp. 329-337.

Zhang, W., Johnsson, F., and Leckner, B. (1993). Characteristics of the lateral particle distribution in circulating fluidized bed boilers. In: *Proc. 4th Int. Conf. on Circulating Fluidized Beds*. Somerset PA, USA.

Zhang, W., Johnsson, F., and Leckner, B. (1995). Fluid-dynamic boundary layers in CFB boilers. *Chemical Engineering Science*, 50, pp. 201-210.

ACTA UNIVERSITATIS LAPPEENRANTAENSIS

511. JÄRVI, KATI. Ecosystem architecture design: endogenous and exogenous structural properties. 2013. Diss.

512. PIILI, HEIDI. Characterisation of laser beam and paper material interaction. 2013. Diss.

513. MONTO, SARI. Towards inter-organizational working capital management. 2013. Diss.

514. PIRINEN, MARKKU. The effects of welding heat input usability of high strength steels in welded structures. 2013. Diss.

515. SARKKINEN, MINNA. Strategic innovation management based on three dimensions diagnosing innovation development needs in a peripheral region. 2013. Diss.

516. MAGLYAS, ANDREY. Overcoming the complexity of software product management. 2013. Diss.

517. MOISIO, SAMI. A soft contact collision method for real-time simulation of triangularized geometries in multibody dynamics. 2013. Diss.

518. IMMONEN, PAULA. Energy efficiency of a diesel-electric mobile working machine. 2013. Diss.

519. ELORANTA, LEENA. Innovation in a non-formal adult education organisation – multi-case study in four education centres. 2013. Diss.

520. ZAKHARCHUK, IVAN. Manifestation of the pairing symmetry in the vortex core structure in iron-based superconductors. 2013. Diss.

521. KÄÄRIÄINEN, MARJA-LEENA. Atomic layer deposited titanium and zinc oxides; structure and doping effects on their photoactivity, photocatalytic activity and bioactivity. 2013. Diss.

522. KURONEN, JUHANI. Jatkuvan äänitehojakautuman algoritmi pitkien käytävien äänikenttien mallintamiseen. 2013. Diss.

523. HÄMÄLÄINEN, HENRY. Identification of some additional loss components in high-power low-voltage permanent magnet generators. 2013. Diss.

524. SÄRKKÄ, HEIKKI. Electro-oxidation treatment of pulp and paper mill circulating waters and wastewaters. 2013. Diss.

525. HEIKKINEN, JANI. Virtual technology and haptic interface solutions for design and control of mobile working machines. 2013. Diss.

526. SOININEN, JUHA. Entrepreneurial orientation in small and medium-sized enterprises during economic crisis. 2013. Diss.

527. JÄPPINEN, EERO. The effects of location, feedstock availability, and supply-chain logistics on the greenhouse gas emissions of forest-biomass energy utilization in Finland. 2013. Diss.

528. SÖDERHOLM, KRISTIINA. Licensing model development for small modular reactors (SMRs) – focusing on the Finnish regulatory framework. 2013. Diss.

529. LAISI, MILLA. Deregulation’s impact on the railway freight transport sector’s future in the Baltic Sea region. 2013. Diss.

530. VORONIN, SERGEY. Price spike forecasting in a competitive day-ahead energy market. 2013. Diss.

531. PONOMAREV, PAVEL. Tooth-coil permanent magnet synchronous machine design for special applications. 2013. Diss.

532. HIETANEN, TOMI. Magnesium hydroxide-based peroxide bleaching of high-brightness mechanical pulps. 2013. Diss.

533. TYKKÄLÄ, TOMMI M. Real-time image-based RGB-D camera motion tracking and environment mapping. 2013. Diss.

534. PEKKOLA, SANNA. Performance measurement and management in a collaborative network. 2013. Diss.

535. PANOREL, IRIS CHERRY. Pulsed corona discharge as an advanced oxidation process for the degradation of organic compounds in water. 2013. Diss.

536. TORKKELI, LASSE. The influence of network competence of internationalization of SMEs. 2013. Diss.

537. MOLANDER, SOLE. Productivity and services – safety telephone services for the elderly. 2013. Diss.

538. SITARZ, ROBERT. Identification of research trends in the field of separation processes. Application of epidemiological model, citation analysis, text mining, and technical analysis of the financial markets. 2013. Diss.

539. KATTEDEN, KAMIEV. Design and testing of an armature-reaction-compensated permanent magnet synchronous generator for island operation. 2013. Diss.

540. HÄMÄLÄINEN, HARRI. Integration of learning supportive applications to development of e-portfolio construction process. 2013. Diss.

541. RATCHANANUSORN, WARIN. Development of a process for the direct synthesis of hydrogen peroxide in a novel microstructured reactor. 2013. Diss.

542. PERFILEV, DANIIL. Methodology for wind turbine blade geometry optimization. 2013. Diss.

543. STROKINA, NATALIYA. Machine vision methods for process measurements in pulping. 2013. Diss.

544. MARTTONEN, SALLA. Modelling flexible asset management in industrial maintenance companies and networks. 2013. Diss.

545. HAKKARAINEN, JANNE. On state and parameter estimation in chaotic systems. 2013. Diss.

546. HYYPIÄ, MIRVA. Roles of leadership in complex environments
Enhancing knowledge flows in organisational constellations through practice-based innovation processes. 2013. Diss.

547. HAAKANA, JUHA. Impact of reliability of supply on long-term development approaches to electricity distribution networks. 2013. Diss.

548. TUOMINEN, TERHI. Accumulation of financial and social capital as means to achieve a sustained competitive advantage of consumer co-operatives. 2013. Diss.

549. VOLCHEK, DARIA. Internationalization of small and medium-sized enterprises and impact of institutions on international entrepreneurship in emerging economies: the case of Russia. 2013. Diss.

550. PEKKARINEN, OLLI. Industrial solution business – transition from product to solution offering. 2013. Diss.

551. KINNUNEN, JYRI. Risk-return trade-off and autocorrelation. 2013. Diss.